MODELING AND CONTROL OF GRID-CONNECTED PV SYSTEM WITH LINEAR AND NON-LINEAR LOADS

2022
MASTER THESIS
ELECTRICAL AND ELECTRONICS

ENGINEERING

MUSTAFA HASHIM MUTTALEB MUTTALEB

Thesis Advisor

Assist. Prof. Dr. Mohammad Abdullah Mohammad ALMOKHTAR

MODELING AND CONTROL OF GRID-CONNECTED PV SYSTEM WITH LINEAR AND NON-LINEAR LOADS

Mustafa Hashim Muttaleb MUTTALEB

T.C.
Karabuk University
Institute of Graduate Programs
Department of Electrical and Electronics Engineering

Prepared as

Master Thesis

Assist. Prof. Dr. Mohammad Abdullah Mohammad ALMOKHTAR

KARABUK
May 2022

I certify that in my opinion the thesis submitted by Mustafa Hashim Muttaleb MUTTALEB titled "MODELING AND CONTROL OF GRID-CONNECTED PV SYSTEM WITH LINEAR AND NON-LINEAR LOADS" is fully adequate in scope and quality as a thesis for the degree of Master of Science.

Assist. Prof. Dr. Mohammad Abdullah Mohammad ALMOKHTAR .....
Thesis Advisor, Department of Electrical and Electronics Engineering

This thesis is accepted by the examining committee with a unanimous vote in the Department of Electrical and Electronics Engineering as a Master of Science thesis. 08. 06, 2022

Examining Committee Members (Institutions)	Signature
Chairman : Assoc. Prof. Dr. Ziyodulla YUSUPOV (KBÜ)	.....
Member : Assist. Prof. Dr. Mohammad ALMOKHTAR (KBÜ)	.....
Member : Assist. Prof. Dr. Khalid O. Moh YAHYA (IGU)	.....

The degree of Master of Science by the thesis submitted is approved by the Administrative Board of the Institute of Graduate Programs, Karabuk University.

Prof. Dr. Hasan SOLMAZ..... .....
Director of the Institute of Graduate Programs

"I declare that all the information within this thesis has been gathered and presented in accordance with academic regulations and ethical principles and I have according to the requirements of these regulations and principles cited all those which do not originate in this work as well."

Mustafa Hashim Muttaleb MUTTALEB

ABSTRACT

M. Sc. Thesis

MODELING AND CONTROL OF GRID-CONNECTED PV SYSTEM WITH LINEAR AND NON-LINEAR LOADS

Mustafa Hashim Muttaleb MUTTALEB

Karabük University
Institute of Graduate Programs
The Department of Electrical and Electronics Engineering

Thesis Advisor:
Assist. Prof. Dr. Mohammad Abdullah Mohammad ALMOKHTAR
May 2022, 84 pages

Rising fuel costs, aged equipment, continuing increase of energy consumption, and integrating renewable energy (RE) supplies into the grid are the most challenging issues that electric utilities face. In recent years, photovoltaic (PV) penetration into power grid particularly the low/medium voltage network has increased dramatically. In this regard, meeting the continuing worldwide energy demand with PV technology necessitates integrating technological features with PV systems that allow them to respond intelligently. In this study, medium-sized PV system rated at 100 kW connected to the utility grid is modeled and analyzed. The system is made up of four sub-arrays, each with a capacity of 25 kW. A non-isolated DC/DC boost converter was used in the simulated system, utilizing a maximum power point tracking (MPPT) algorithm to extract the PV panel's maximum productivity. To track the MPPT point, one of the most common techniques namely the incremental conductance (Inc-Cond) was used. In addition, a three-phase voltage source inverter system namely neutral

point clamped (NPC), enabling the installed PV system to interact with the utility grid, was modeled. Both linear and non-linear loads were investigated. A phase-locked loop (PLL) was used to synchronize the solar PV inverter with the 60 Hz grid. The system was tested under various loading and irradiance conditions and the results demonstrated the effectiveness of the system to control the energy flow between the PV system, grid and the load. The modeled system was designed by using the MATLAB-Simulink environment.

Key Words : Grid-Connected Inverter, MPPT, DC-DC Converter, NPC, Phased Locked Loop, Photovoltaic.

Science Code : 90513

ÖZET

Yüksek Lisans Tezi

LİNEER VE LİNEER OLMAYAN YÜKLERLE ŞEBEKE BAĞLANTILI PV SİSTEMİNİN MODELLENMESİ VE KONTROLÜ

Mustafa Hashim Muttaleb MUTTALEB

Karabük Üniversitesi
Lisansüstü Eğitim Enstitüsü
Elektrik ve Elektronik Mühendisliği Anabilim Dalı

Tez Danışmanı:
Assist. Prof. Dr. Mohammad Abdullah Mohammad ALMOKHTAR
Mayıs 2022, 84 sayfa

Artan yakıt maliyetleri, eskimiş ekipman, enerji tüketiminde devam eden artış ve yenilenebilir enerji (RE) kaynaklarının şebekeye entegre edilmesi, elektrik şirketlerinin karşılaştığı en zorlu konulardır. Son yıllarda, elektrik şebekesine fotovoltaik (PV) penetrasyonu, özellikle düşük/orta gerilim şebekesi önemli ölçüde artmıştır. Bu bağlamda, dünya çapında devam eden enerji talebinin PV teknolojisi ile karşılanması, teknolojik özelliklerin akıllıca yanıt vermelerini sağlayan PV sistemleri ile entegre edilmesini gerektirmektedir. Bu çalışmada, şebekeye bağlı 100 kW gücündeki orta ölçekli PV sistem modellenmiş ve analiz edilmiştir. Sistem, her biri 25 kW kapasiteli dört alt diziden oluşmaktadır. Simüle edilen sistemde, PV panelinin maksimum üretkenliğini çıkarmak için bir maksimum güç noktası izleme (MPPT) algoritması kullanan, izole edilmemiş bir DC/DC yükseltici dönüştürücü kullanıldı. MPPT noktasını izlemek için en yaygın tekniklerden biri olan artımlı iletkenlik (Inc-Cond) kullanılmıştır. Ayrıca, kurulu PV sisteminin şebeke ile etkileşimini sağlayan,

nötr nokta kelepçeli (NPC) olarak adlandırılan üç fazlı bir gerilim kaynaklı evirici sistemi modellenmiştir. Hem doğrusal hem de doğrusal olmayan yükler incelenmiştir. Solar PV inverterini 60 Hz şebeke ile senkronize etmek için faz kilitli bir döngü (PLL) kullanıldı. Sistem, çeşitli yükleme ve ışınım koşulları altında test edildi ve sonuçlar, sistemin PV sistemi, şebeke ve yük arasındaki enerji akışını kontrol etmedeki etkinliğini gösterdi. Modellenen sistem MATLAB-Simulink ortamı kullanılarak tasarlanmıştır.

Anahtar Kelimeler : Şebeke-Bağlantılı İnvertör, MPPT, DC-DC Dönüştürücü, NPC, Paz Kilitli Döngü, Fotovoltaik.

Bilim Kodu **:** 90513

ACKNOWLEDGMENT

I would like to express my deepest gratitude to my advisor, Dr. Mohammad Almokhtar, whose sincerity and encouragement I will never forget. Dr. Almokhtar has been an inspiration as I hurdled through the path of this Master's degree. He is the true definition of a leader and the ultimate role model. This thesis would not have been possible without Dr. Almokhtar, whose guidance from the initial step of research enabled me to develop an understanding of the subject. I am thankful for the extraordinary experiences he arranged for me and for providing opportunities for me to grow professionally. It is an honor to learn from Dr. Almokhtar.

I am grateful for my parents whose constant love and support keep me motivated and confident. My accomplishments and success are because they believed in me. My Deepest thanks to my friends, who keep me grounded, remind me of what is important in life, and are always supportive of my adventures.

CONTENTS

Page

Page

Page

LIST OF FIGURES

Page

Page

Page

LIST OF TABLES

Page

SYMBOLS AND ABBREVIATIONS

SYMBOLS

I	:	The current output PV array
V	:	The voltage output PV array
I_S	:	The reverse saturation current of the diode
I_L	:	The photocurrent of PV cell
I_{Sh}	:	The short circuit current of the cell
T	:	The cell temperature
e	:	The charged electron
k	:	The Boltzmann's constant
m	:	The ideality factor
K_i	:	The short circuit current temperature co-efficient
G	:	The solar radiation in W/m^2
V_{in}	:	Boost converter's input voltage
V_O	:	Boost converter's output voltage
I_{in}	:	Boost converter's input current
I_o	:	Boost converter's output current
L_{boost}	:	Inductors for a boost converter
D	:	Duty ratio
C_f	:	Filter capacitor
L_f	:	Filter inductor
F_S	:	Switching frequency
F	:	Grid frequency
C_{dc}	:	Capacitance of DC link capacitor
Si	:	Silicon
P	:	Active power
Q	:	Reactive power
Kp	:	Proportional gain

Ki	:	Integral gain
Ig	:	Grid current
Vg	:	Grid voltage
I_{LL}	:	Linear load current
I_{NL}	:	Non-linear load current
Vdc	:	The DC bus voltage.
Δi	:	Inductor ripple current.
ΔVo	:	Allowable output ripple voltage.
S	:	Apparent power
dq	:	Axis Park transformation.
I_d	:	Active current component aligned along d-axis
I_q	:	Reactive current component aligned along q-axis
V_d	:	Grid phase voltage component aligned along d-axis
V_q	:	Grid phase voltage component aligned along q-axis
R/X	:	Line impedance ratio: ac system reactance to resistance ratio
Θ	:	Grid phase angle
Ia	:	Phase a current .
I_b	:	Phase b current
Ic	:	Phase c current
Va	:	Phase a voltage
V_b	:	Phase b voltage
V_C	:	Phase c voltage

ABBREVIATIONS

RE	:	Renewable Energy
PV	:	Photovoltaic
KW	:	Kilowatts
DC	:	Direct Current
NPC	:	Neutral Point Clamped
MPPT	:	Maximum Power Point Tracker
ICN-COND	:	Incremental-Conductance
PLL	:	Phased Locked Loop
THD	:	Total Harmonic Distortion

P&O	:	Perturbation and Observation
MPP	:	Maximum Power Point
AC	:	Alternating Current
DGs	:	Distributed Generations
PWM	:	Pulse Width Modulation
APFs	:	Active Power Filters
VSI	:	Voltage Source Inverter
DERs	:	Distributed Energy Resources
DCC	:	Direct Current Control
FO	:	Fractional Order
LVRT	:	Low Voltage Ride Through
SVPWM	:	Space Victor Pulse Width Modulation
DSP	:	Digital Signal Processors
CSI	:	Current Source Inverter
VSC	:	Voltage Source Converter
STATCOM	:	A Static Synchronous Compensator
PDPWM	:	Phase Disposition Pulse Width Modulation
PI	:	Proportional – Integral
PID	:	Proportional-Integral-Derivative
DCMLI	:	Diode Clamped Multi-Level Inverter
MPC	:	Model Predictive Control
CM	:	Common Mode
PBC	:	Passivity Based Control
EL	:	Euler Lagrange
KLMS	:	Kernel Least Mean Square
MW	:	Megawatts
IGBT	:	Insulated Gate Bipolar Transistor
IC	:	Inductor-Capacitor
MOSFET	:	Metal-Oxide-Semiconductor Field Effect Transistor
VOC	:	Voltage Oriented Control
RMS	:	Root Mean Square
DCM	:	Discontinuos Conduction mode
CCM	:	Continuos Conduction mode

FC	:	Flying Capacitor
CHB	:	Cascaded H-Bridge
SRF	:	Synchronized Revolving Frome
IEEE	:	Institute of Electrical and Electronics Engineers
P.F	:	Power Factor
FFT	:	Fast Fourier Transform

PART 1

INTRODUCTION

1.1. BACKGROUND

Global energy demand has become a major political and social issue in recent decades, as power generation has mostly relied on energy sources such as oil, gas, and coal, which were previously thought to be nearly unlimited [1]. As the world's energy demand rises at an alarming rate and fossil fuel stocks dwindle, a need for clean energy alternatives has become increasingly apparent [2]. The sun's rays hit the earth's surface and generate all non-renewable and renewable sources of energy. Sunlight is non-polluting energy that keeps life on Earth going, and while non-renewable energy supplies have taken a long time to develop, renewable energy resources are, in general, always accessible. Hydropower, wind power, and solar energy are examples of renewable energy sources. While hydropower has long been a well-known technology, there is currently a lot of study being conducted on solar and wind power [3].

A solar cell is a semiconductor diode with a light-exposed p–n junction. Photovoltaic cells are built from a variety of semiconductors and manufactured in a variety of ways. At the moment, mono-crystalline silicon solar cells are the only ones available on a commercial scale. Silicon photovoltaic cells are created by combining a thin Silicon film or a thin layer of bulk Silicon with electrodes. Doping one of Silicon layer's surfaces results in the formation of the p–n gap. On the semiconductor's Sun-facing surface, a thin metallic grid is put. A PV cell's physical structure is seen in Figure 1.1. When light strikes a short-circuited cell, it forms charged particles, which generate electrical current. Charges are produced when the received photon's energy is enough to separate the semiconductor's atomic electrons; this occurrence is dependent on the semiconductor and incoming light spectrum.

The PV phenomenon may be defined as the provided by the sun light, the formation and passage of charge carriers so at the p–n gap, and the collection of such electrically charged particles at the PV device's interfaces [4]. The incoming light flux and the semiconductor's absorption capacity influence the rate at which electric carriers are produced. The band gap of semiconductors, cell surface inversion (defined by surface structure and processing), inherent carrier accumulation in recombination rate, electronic mobility, temperature, semiconductors, and a variety of other parameters all contribute to adsorption capacity [5].

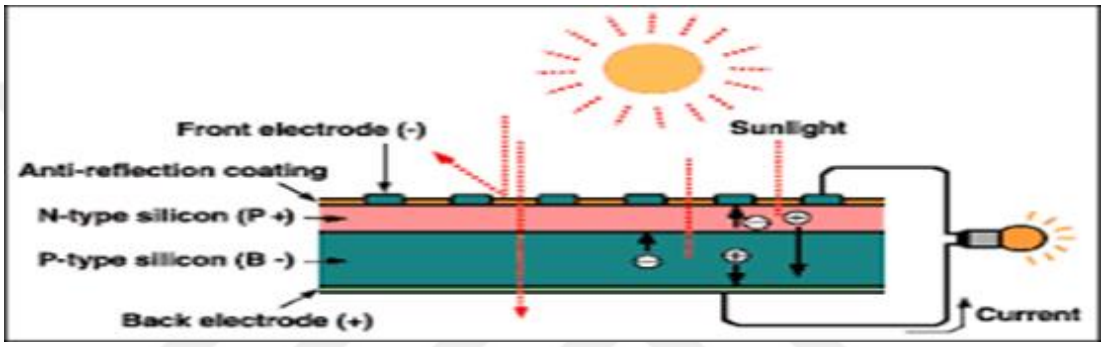

Figure 1.1. Physical structure of a PV cell.

In PV systems, proper maximum power point tracker (MPPT) controllers are integrated with power electronic circuits to achieve MPP functioning. Many MPPT algorithms for tracking maximum power (MP) under constant uniform irradiance, rapid step-changing irradiance, and part shade circumstances have recently been devised [6]. Direct and indirect MPPT algorithms are the two types of MPPT algorithms. Direct MPPT approaches, like incremental conductance (IncCond) and perturb and observe (P&O), identify the MPP using real-time system data (see Figure 1.2), also in table 1.1 notes the characteristics of several MPPT algorithms.

On the other hand, indirect approaches like fraction current short circuit, fraction open-circuit voltage, fuzzy logic control, and sliding mode control are dependent on system factors like short circuit current and open-circuit voltage. Because of the ease with which it may be used. When a bigger step size is employed, the controller reaches the MPP sooner, resulting in greater steady-state oscillations. Otherwise, reduced steady-state oscillations exist for tiny step-size applications. However, reaching the MPP takes longer, resulting in a larger power loss.

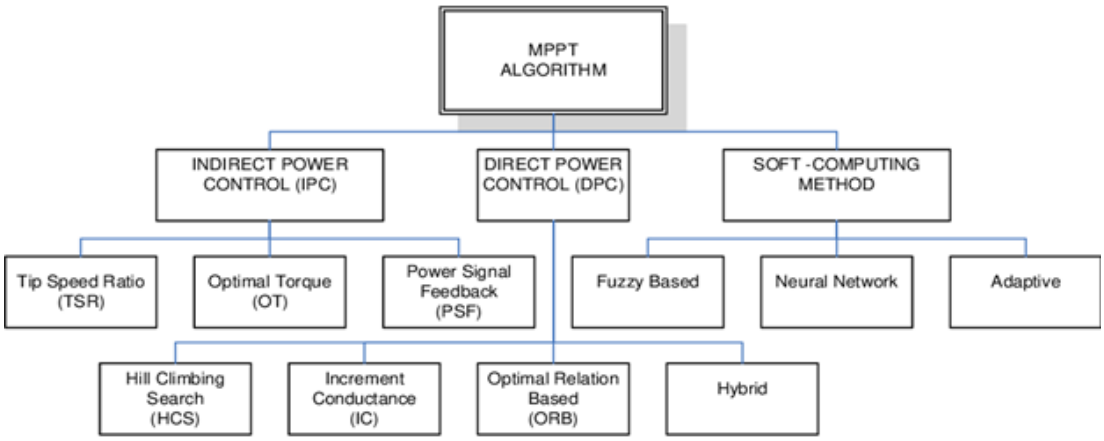

Figure 1.2. Direct MPPT algorithm.

Table 1.1. MPPT Algorithm Characteristics.

MPPT Methods	**INC**	**P&O**	**ANN**
Transient Fluctuation	Bad	Bad	Good
Dynamic response	Medium	Poor	High
Temperature characteristics	Poor	Poor	Good
Tracking speed	Slow	Slow	Moderate
Steady Oscillation	Moderate	Large	Zero
System complexity	Simple	Simple	Medium
Static Error	High	High	Low
Overall Efficiency	Medium	Medium	High
Control Accuracy	Accurate	Low	Accurate

To obtain the most feasible power from the PV array and ensure efficient operational effectiveness, the PV power condition system requires the method MPPT control strategy, and current regulation is required to manage the real power and reactive power. A phase-locked loop (PLL) must gather grid voltage and current, as also frequency, phase angle, and amplitude, to govern the entire system. Further, the photovoltaic array's full extreme power should be provided to the grid. The current commands for the q-axis and d-axis, respectively, are provided by started requiring reactive power and extreme power PV arrays. Controlling these currents is done via feedback and feedforward controllers. In the basic MPPT algorithm, the incremental conductance approach is utilized. Grid voltage and current information are also

received via the space vector phase-locked loop. The PLL is also discussed, as well as current controller design standards. A thorough analysis, design idea, and simulation are also included. Finally, simulation findings suggest that the control strategies provided are practical. A PV system can be single-stage or two-stage, with a DC/DC (isolated or non-isolated) or DC/AC converter as the second stage. Between the PV array and the grid system, the transformer works as a galvanic isolator. A high-frequency transformer can also provide isolation in a DC/DC converter. As a result, the system's entire size and volume have shrunk. As a result, grid-connected PV systems with separate DC/DC converters for low and medium power applications are becoming increasingly widespread. Because of their better efficiency, modularity, lower conductance, and reduced switching, multilevel topologies that have been proposed are commonly employed in Solar PV. The neutral point clamped (NPC) inverter is commonly employed in contrast to other inverter topologies because it delivers reduced current harmonics and lower voltage strains on the inverter parts [7]. If there is an unexpected voltage rise, the PV system's capacity may be lowered. During low load and high power generation, power curtailment, or restricting the capacity of distribution generators, can help to decrease reverse power flows. Active power curtailment involves minimal adjustments to distributed generator inverter control logic (DGs). Curtailed active power refers to the loss of power, whereas injected power reduces linearly as AC voltage rises. The authors described a grid-connected PV system with feed-forward current regulation [8]. On the other hand, the rate of solar irradiation is not taken into consideration in the published study. For partially shaded PV systems, a novel MPPT algorithm is suggested, which will allow the system to respond to changing solar radiations [9]. As a result, this study looks at a two-stage PV multilevel inverter with a non-isolated DC/DC boost converter and a three-phase NPC DC/AC inverter. An incremental-based MPPT algorithm is used to keep the dc-link voltage constant. The system is managed so that MPP follows the reference trajectory in a dispatched power operation, which is also recorded. The system's performance is also proved in unbalanced grid voltage settings, albeit the control of the imbalanced state is not covered in this work. The efficacy of the described work is evaluated using MATLAB/Simulink software. The described work is a viable solution for PV curtailment, with decreased current harmonics on the AC side, giving extra advantages in a grid-connected system, according to extensive simulation findings.

Grid-connected pulse width modulation (PWM) voltage source inverters are widespread in PV installations. The control strategy of grid-connected inverters is significantly responsible for the conversion power quality of an inverter-based PV system, which includes low THD, high power factor, and rapid dynamic response. Equipment linked to utility wires has been subjected to severe rules to protect grid security. Some of these restrictions were created in reaction to increasing harmonic distortion levels. As a result, planners and academics have had trouble reconciling solar energy's rapid integration with electrical transmission and distribution systems. The grid management can request a specified quantity of real and reactive power from the different generators in large-scale energy-producing sites.

Power quality is worsening daily as a result of the growing usage of power electronic-based devices with a non-linear connection between voltage and current. Non-linear household and industrial equipment are the main producers of harmonics in the power supply network. The harmonic is measured using some indicators, the most popular of which being Total Harmonic Distortion (THD). In this thesis, a comprehensive harmonic analysis of THD in the load current of non-linear devices is undertaken. The Power Harmonic Analyzer is used to assess and evaluate the THD levels of all the non-linear loads in the current spectrum. Excessive usage of non-linear loads in the supply system has exposed several features of growing harmonic contamination in the supply system, which is damaging the distribution network and causing poor power quality [10]. Most energy users are unaware of harmonic pollution, which might have a range of effects on energy conservation and economic crises shortly. In a periodic, steady-state situation, harmonics are the undesirable frequency that is overlaid on the fundamental frequency [11]. Harmonics are produced by household appliances with a non-linear connection between current and voltage waveforms. These harmonics in the power supply system can cause equipment failure, equipment heating, voltage instability, and swells, corruption of data in computers, and telephone line interference. In the household sector, harmonics analysis is crucial since it leads to enhanced inefficiency, cost reductions, and optimum appliance utilization. The harmonic spectrum acquired from different home and industrial appliances is displayed concerning the THD indicator of harmonics. The peak and RMS current values, as well as the THD value, of various appliances, are calculated. The high THD content

in the supply system shows significantly distorted current and voltage waveforms due to the presence of a power electronics-based circuit. The creation of harmonics and reactive power increases when the usage of non-linear loads such as power electronics switches, electrical drives, computers, furnaces, and electronic ballasts expands, resulting in the flow of load currents that are an integer multiple of odd harmonics [12]. Active power filters can be used to provide a harmonic less input current waveform to compensate for the aforementioned issues. In recent years, several research academics and publications about active power filters have indeed been published.

APFs cannot be used in high-voltage or high-potential applications due to the secure form of evaluation of electronic switching equipment. Combining VSI and APF circuits can help to overcome these limitations. The enormous size and resonance impact of passive filters are two of its major disadvantages. Active power filters are not affected by these limitations since inductors are not employed. An active power filter can remove unwanted current components by injecting a compensatory current in the opposite direction. APF has been implemented using a pre-owned VSI and is connected to the grid through an interface filter inductor. It's typically used to correct for low-power range unpredictable loads caused by semiconductor device constraints. The APF-based voltage source converter's output current and voltage must be capable of delivering almost harmonic less current. Furthermore, because it provides a harmonically lower current, the resultant voltage should not be able to support the low-frequency harmonic elements.

1.2. THE PROBLEM STATEMENT OF RESEARCH

Electric utilities are now dealing with many difficulties, including growing fuel costs, aging equipment, expanding energy consumption, frequency control, and the difficulty of integrating renewable energy supplies into the system. PV adoption on the electric grid has also expanded dramatically in recent years. With the recent surge in PV penetration and the progress of the worldwide PV industry, there is a critical need to add intelligent response elements into PV systems. Those elements include an efficient MPPT controller, a powerful inverter that serves as a master ie., regulating the energy

flow while ensuring synchronization between the PV system and utility grid. One more issue which needs to be considered in the modeled grid-connected PV system is the power quality.

1.3. OBJECTIVES OF THE RESEARCH

The thesis aims to explore the performance of solar PV energy connected to an electric power grid interfaced via a VSI power conditioning unit. The following is a summary of the research goals:

1. Mathematically modeling the system components using MATLAB/Simulink environment.
2. Using a multi-tasking modulator system consisting of a transistorized three-phase VSI.
3. Examining the system's performance and difficulties with power quality.

1.4. RESEARCH METHODOLOGY

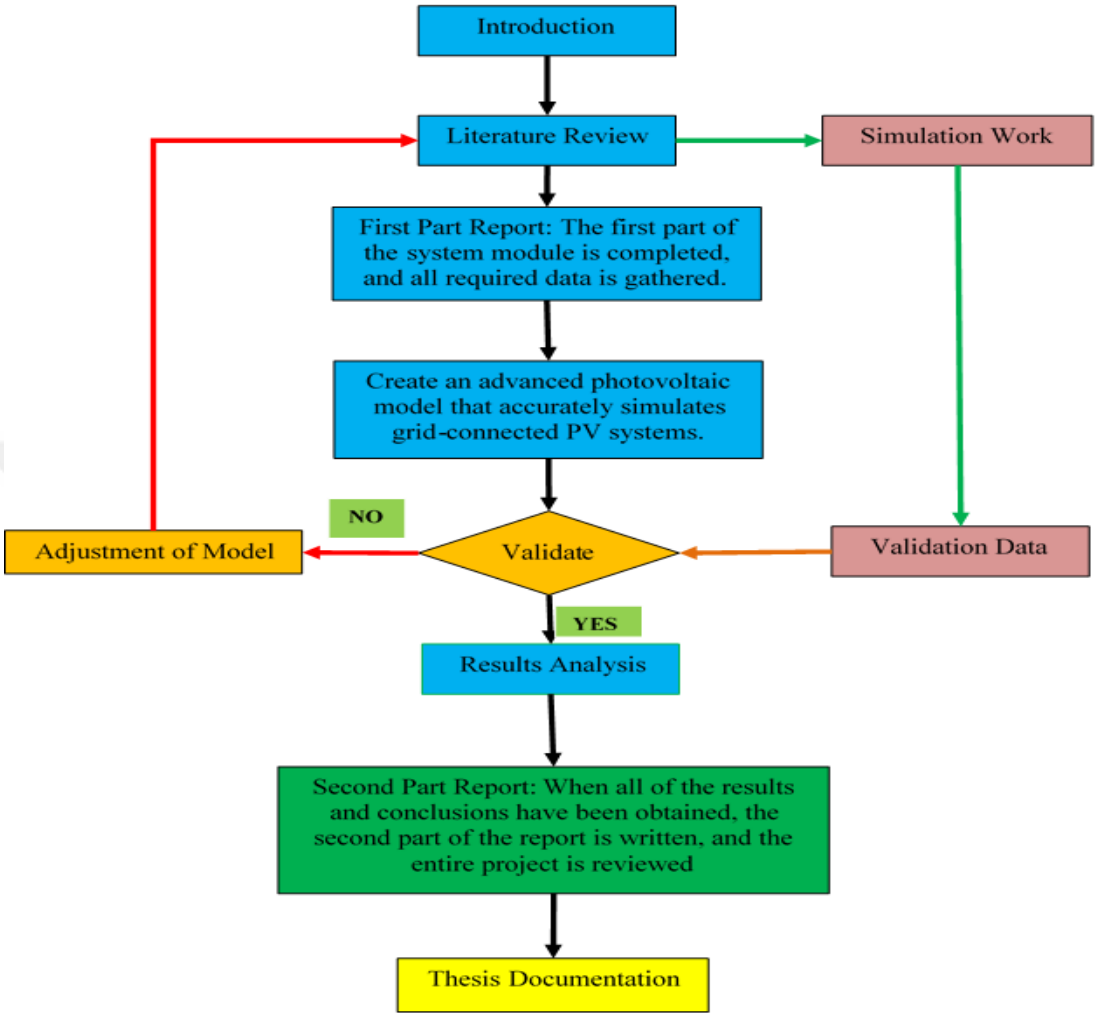

Figure 1.3. Flowchart of the Research Methodology.

1.5. SCOPE OF THESIS

This study focuses on the modeling of a three-phase PV grid connected with 100 kW rated capacity. While photons hit the photovoltaic cell and give energy to the electrons to produce electrical energy in the form of DC, the MPPT works to find the greatest point that the current and voltage of the cell can reach, and through it, the maximum value of energy is inputted to the inverter to convert the DC to AC. The PV system is composed of four subsystems each rated at 25 kW associated with a dc-dc boost converter equipped with MPPT control. The output voltage to the dc-link is 500 V which is an input to a DC-AC converter; a three-level type Neutral Point Clamp (NPC)

controlled by PWM. Furthermore, an LC filter and two types of loads; a linear load sized at 45 kW and a non-linear load rated at 7 kW.

1.6. SIGNIFICANCE OF THE RESEARCH

The integration of distributed energy resources (DERs) like PV generating into the utility grid has acquired a lot of impetus in recent years, thanks to increased power consumption, rapid depletion of fossil, and a growing preference for renewable energy resources. However, the capacity of these integrated generators must be correctly coupled to optimize the value of such integrated systems. The majority of distributed energy resources link to the utility grid via a power electronics interface, and with correct regulation of the inverter interaction, they may provide both real and reactive power. Recognizing the operational challenges involved in the implementation of PV systems, especially power fluctuations, this study will contribute to the enhancement of the PV system grid-connected by presenting methods to evaluate PV system performance as well as possible solutions to the operational issues encountered. It will also speed the adoption of PV systems into the electric grid. The projected model, on the other hand, is a smart and efficient system that will produce a complete result that will assist the system operator in better understanding the behavior of a Grid-connected PV system. Finally, the results of this study will assist either utility or PV system owners in selecting the most environmentally friendly option for leveling out PV output power.

1.7. ORGANIZATION OF THESIS

The following is a summary of the five chapters:

Chapter 1 Introduction: The introduction, goal, statement of the research, issue objectives, background, and purpose of doing this study are all covered in this chapter. Chapter 2 Literature Review: The literature-based information on PV grid-connected, kinds of PV systems (Grid-Connected, Standalone, and Hybrid), and Grid-Connected Inverter Technology are all discussed in this chapter.

Chapter 3: The grid design model, PV system, MPPT, boost DC-DC converter inverter, LC filter, loads, the utility grid, and Mathematical Modeling are all covered.

Chapter 4: shows the simulation results of the planned Grid-connected PV system. Previous research is summarized, and the findings of this study are assessed accordingly.

Chapter 5: provides the findings of this study, discusses the findings, and gives some suggestions for further studies.

PART 2

LITERATURE REVIEW

2.1. INTRODUCTION

Connecting solar PV systems to the electrical grid without using batteries to deliver surplus energy is considered one of the important ways to raise the RE share. This is advantageous in terms of improving power system performance and quality. Therefore, many researchers address this in their research studies, analyses, and designs.

2.2. PV SYSTEM CLASSIFICATIONS

Typically, PV systems are classified according to technological characteristics and component configuration. The main three types of PV systems are stand-alone systems, hybrid systems, and grid-connected systems. More information about the three configurations is provided in the following sections.

2.2.1. PV System with Grid-Connection

Grid-connected types of PV systems are often employed in improving the efficiency of the main electric grid by reducing energy losses and enhancing the network voltage level. However, this cannot always be the condition since those systems may have a detrimental influence on the grid, particularly if their saturation is significant [13]. Grid-tied systems are the basic solar installations that employ a conventional inverter but without energy storage, as illustrated in Figure 2.1. This may be ideal for clients who are currently being fed by the main grid and need to add a solar feeder to their existing houses. Those systems may be eligible for federal and provincial rewards to continue paying for the system. Grid-connected systems are simple to construct and

extremely cost-effective due to the small number of components in them [14]. The main purpose of a grid-connected system is to save money on power while still taking advantage of solar power. One of the drawbacks of this method, however, is that it fails in power cuts. This is because liners operating on electricity lines must be aware that the grid is without power. When grid-tied inverters are not aware of the grid, they must instantly disconnect. This guarantees that power is cut off in the event of a power failure or an emergency, and it is unable to store energy for future use [15]. When users utilize energy from batteries, including during high-demand times, users are not able to monitor it. If a customer has a simple grid-connected device, however, customers are able to increase capacity later if they wish. An AC-coupled device is used to connect the primary grid-coupled inverter to the battery charging inverter. This is a good choice for end-users that need to obtain solar immediately to benefit from incentives but are yet prepared to be invested in storage. When solar creates more energy than consumers use, the energy may be transferred to the grid, which benefits the customer. When the load exceeds the capacity of solar, energy is purchased from the main grid. Consumer do not rely entirely on solar power to meet their needs. The main message is that even when the system goes down, so does the sun, and there is no battery bank in the system.

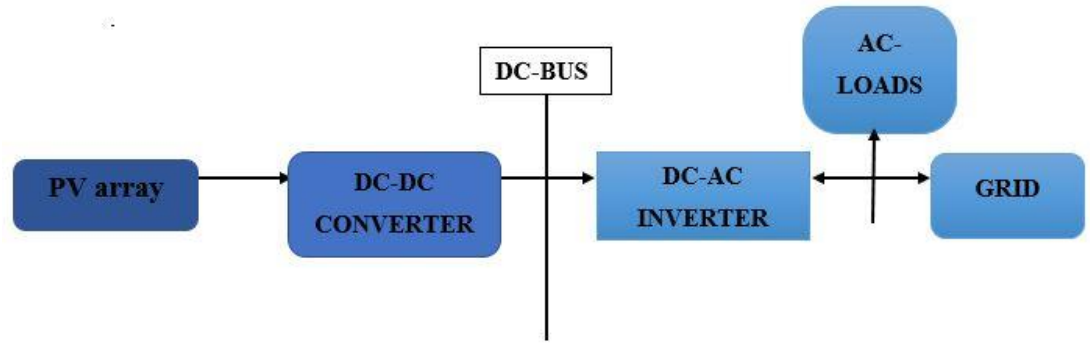

Figure 2.1. Grid-connected PV system depicted as a block diagram.

2.2.2. Stand-alone PV System

Consumers who are unable to access the network may benefit from off-grid technologies. This inability might be due to the remoteness of a location and the expense of obtaining electricity. In most cases, it is illogical for someone who is linked

to the system to disconnect totally and use an off-grid device. Figure 2.2 illustrates a block diagram of a stand-alone battery-storage. The advantages of a stand-alone system include energy self-sufficiency, being able to provide power to remote places that are not connected to the main grid and setting power tariffs and charging for power use. Another advantage of an off-grid system is that it is adaptable, allowing to extend power as demand for energy grows. Many off-grid systems contain many storage resources, including solar, wind and generators, because the unit is the only source of power. The weather and year-round circumstances are taken into consideration when constructing the device. Another way to keep the batteries charged is if the solar cells are buried in snow [16] and the need for a backup generator in case any of the renewable energy sources fail. One disadvantage is that off-grid type installations may be ineligible for some incentive schemes. should design gadgets to handle 100% of the energy demands, plus a bit extra Off-grid networks include more pieces and, as a result, are more expensive than grid-tied systems.

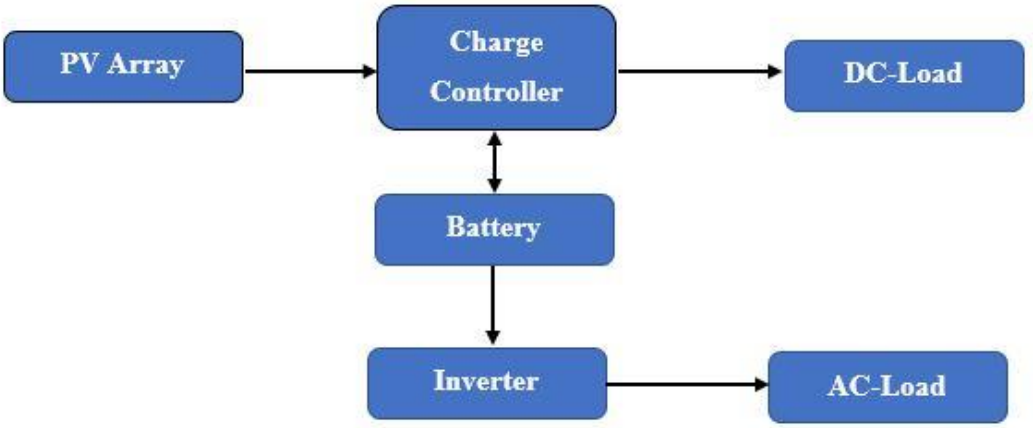

Figure 2.2. Block schematic of a stand-alone PV system with battery bank.

2.2.3. PV-Hybrid Systems

As illustrated in Figure 2.3, hybrid systems often relate to the integration of any two input sources. In this case, photovoltaic solar can be used with wind, diesel generators, turbines, or any other non-renewable and renewable power source. In general, solar systems would employ a charging station to save energy generated by panels for a preset time of insufficient sunlight. There would also be severe periods of poor weather

where an extra supply would be necessary to ensure power output. Photovoltaic-hybrid systems combine a PV system with other power sources, often a diesel generator and a renewable energy source such as a wind turbine [17]. Energy production will typically be sized to meet a baseload need with the backup supply being used only when necessary. This solution not only delivers all of the advantages of PV in terms of cheap operation and maintenance costs, it also guarantees a consistent power supply [18].

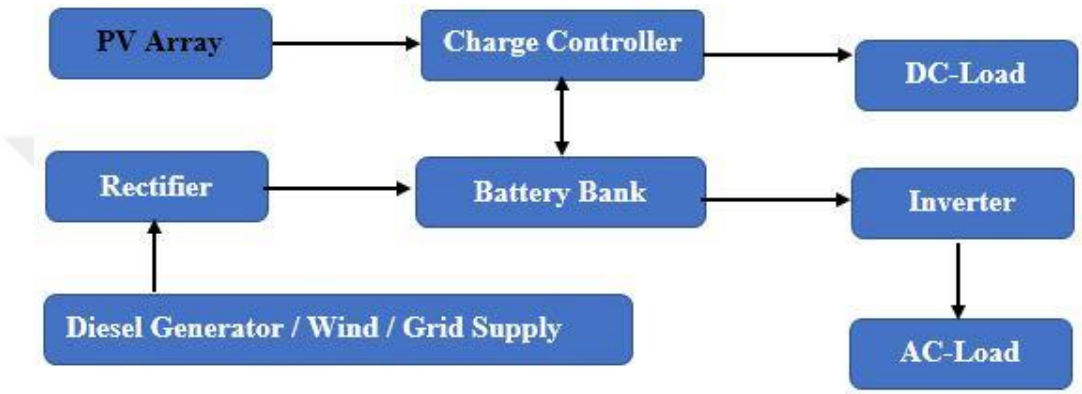

Figure 2.3. Block diagram of a photovoltaic hybrid system.

2.3. TECHNOLOGY OF GRID-CONNECTED INVERTERS

PV systems that are grid-connected are characterized by the number of power steps and are available in a wide range of technologies and topologies [19]. To link the PV system to the utility grid, many technological approaches are employed in PV plant applications. Each technique has its benefits and limitations when compared to others in terms of effectiveness and MPPT.

2.3.1. Centralized Inverters

This is the earlier technology, as illustrated in Figure 2.4. To link PV panels to the grid, the original method utilized centralized inverters. The PV panels were connected in a string, with each panel providing a high sufficient voltage to preclude further amplification. These series links were used in tandem with string diodes to produce large power outputs [20]. In this configuration, PV panels were linked in series to a

centrally located inverter. This arrangement is used in three-phase power plants ranging from 10 kW to 1000 kW. The main advantages of the multilevel inverter are their high accuracy (lower losses during power transmission) and low cost (due to the use of only one inverter). This design has several drawbacks, however, including the need for lengthy DC cables to link PV systems to the inverter, as well as losses incurred by string diodes, PV module incompatibilities, and centralized MPPTs [21].

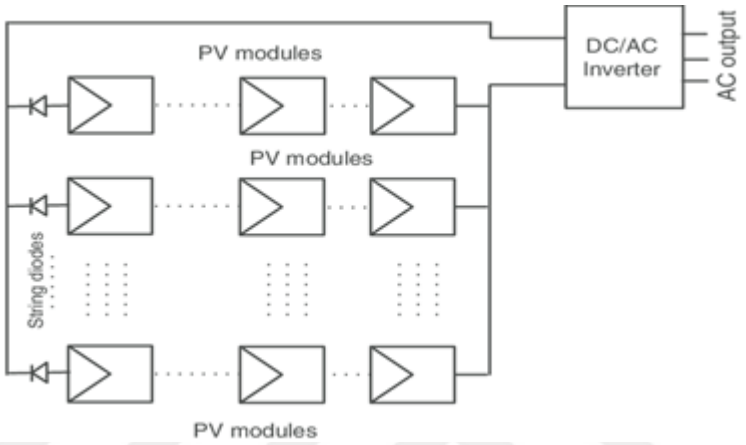

Figure 2.4. Centralized inverter.

2.3.2. String Inverters

The present technique consists of two components: string inverters and an AC module. In cases of only one string of PVs, panels are connected to the inverter using the string inverter, as shown in Figure 2.5, the centralized inverter may be downsized to a more reasonable amount. The input voltage should be sufficiently high to prevent the promotion of higher. This aims to address some of the drawbacks of central inverters. The PV strings in this architecture are connected to independent inverters rather than to central inverters, as compared to the multilevel inverter. If the DC supply before the inverter is too low, a type of DC-DC converter can be invested to enhance the voltage level. This is because the system is no longer dependent on a single inverter. A combination of behavioral losses is also minimized although they are not eliminated. This structure, when opposed to the centralized converter, enhances overall efficiency while also decreasing the price owing to the ability of mass production [22]. The solar modules in the specified topology are linked in such a way that they are put together to create a string. The PV array's voltage varies from 150 V to 450 V [23].

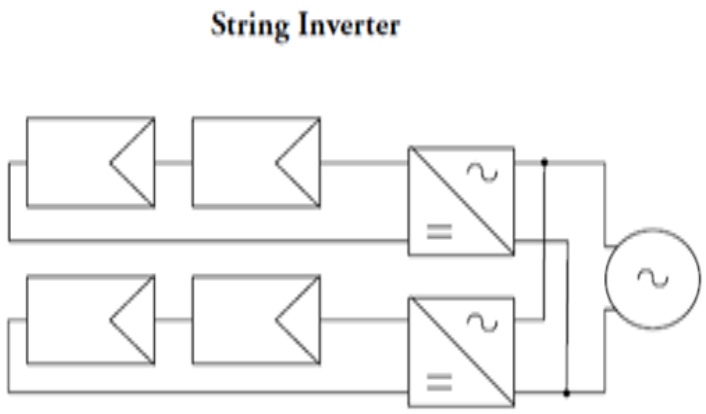

Figure 2.5. String inverters.

2.3.3. Multi-String Inverters

As a result of this current and future structure, multi-string inverter topologies, which are a mix of string and module inverters, have become accessible. The multi-string inverter, illustrated in Figure 2.6 as an expansion of the string inverter, connects numerous string types, each with its DC-DC converter to a common DC-AC inverter, as seen in Figure 2.6. This is preferable to a centralized system since each string may be managed independently [24]. With this setup, maximum energy ranges of 5 kW are feasible, and each string is followed by a separate DC-DC converter before even being linked to a single common inverter. The architecture enables the use of inverters with a variety of power ratings and PV modules with a variety of current-voltage (I-V) characteristics. It is feasible to enhance power efficiency by implementing MPPT for every string. This yields an architecture that is both versatile and economical, and it is expected to become the industry norm in areas where centralized and string conversions are currently utilized.

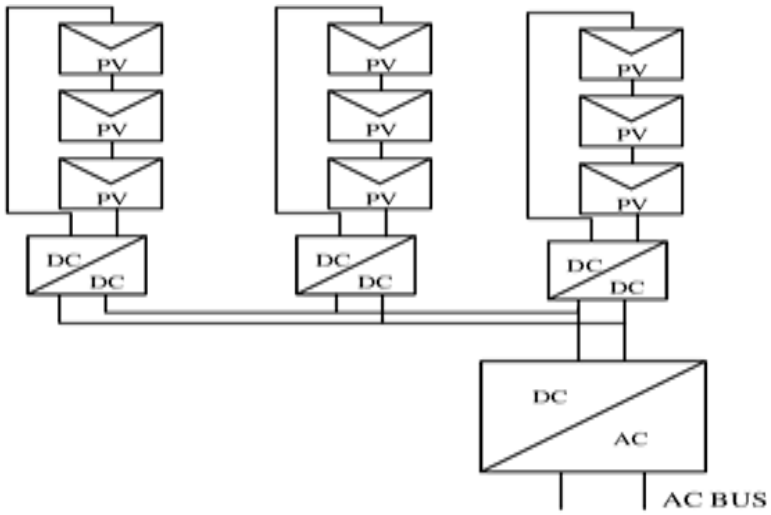

Figure 2.6. Multi-String inverters.

2.3.4. Micro-Inverters

Individual PV systems grids connected through an inverter (Figure 2.7) symbolize both the present and the future of renewable technology. Because MPPT is performed for each panel, it achieves a better coefficient of performance to the string inverters [22]. By merging the PV system and the converter into a single system, the prospect of constructing a component “plug and play” device that can be used by anyone with no prior knowledge of electric equipment becomes possible [23].

In this setup, mismatch losses between PV modules are minimized and the converter to PV module may be tuned, providing for an individualized MPPT of each module. Large-scale manufacturing will be possible since there will be more demand for devices than in earlier designs, resulting in cheaper pricing. On the other hand, the input voltage will decline, demanding a high voltage amplifier, which will impair overall efficiency.

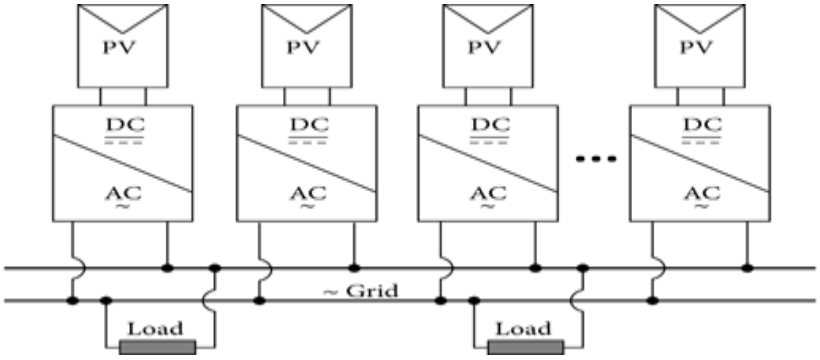

Figure 2.7. Micro inverters.

2.4. RELATED STUDIES

The literature contains numerous works related to grid-connected PV topology and its management strategies. In [24], the authors use a three-phase PV grid-tied, where the size of the PV system is 1.5 kW and consists of two stages. The first stage consists of a DC-DC boost converter utilizing P&O MPPT. The second stage consists of a DC-AC three-phase VSI. They use the controller in the Dubus voltage regulation loop of the DCC algorithm for the three-phase, grid-connected PV system. The suggested controller is called a fractional-order PI (FO-PI) controller. It is used to regulate the order of integration from integer to real value. The FO-PI controller may provide quick time of settling and withstands outside disturbances and variations of the parameter.

A three-phase PV grid-tied rated at 80 kW is studied in [25]. The system comprises a double stage. The primary stage is an isolated DC-DC forward converter and the secondary stage is a DC-AC, three-phase NPC multilevel inverter because it uses lower voltage stress and lower current harmonics on the other factors. The authors used the current controller to control the NPC inverter with PLL synchronizing the system with the grid voltage. The researchers used MATLAB/SIMULINK software.

El Malleh et al. [26] use a three-phase, PV grid-tied system, where the primary stage involves the DC-DC boost converter. To control the boost converter algorithm, an MPPT type incremental conductance was implemented. Another DC-bus controller is added in the boost control. They use two-level VSC and the LVRT method.

A three-phase, PV grid-connected inverter was studied in [27], where the investigators use a single-stage without a DC-DC converter and a three-phase, PV grid-connected inverter (SVPWM). The voltage is the outer loop in the double-loop control strategy, whereas the current is the inner loop. They use LCL and propose a detailed method for selection of the parameters of the LCL filter in addition to improved passive damping that results in lower loss and a more stable system.

Hui Zhang et al. [28] provide a study through the use of a three-phase SVPWM voltage-source inverter for a PV grid-connected system. They present a control diagram of the three-phase, current-controlled SVPWM inverter to rotate a synchronous match d-q with feed-forward recompense that uses many loop controls with the inverter inner loop's filter inductor current to accomplish a quick and dynamic response and the external loop to regulate the DC-bus voltage, which operates at the MPP. In the d-q reference frame, PLL is used to determine the voltage phase angle of the utility.

A topology of a single-phase, five-level PV inverter of a grid-tied PV solar system with a control scheme named PWM ia suggested in [29]. Two identical reference signals with offset equal to the amplitude of the triangular carrier signal is used to generate the PWM signals of the used switches. A type of digital proportional-integral current control algorithm is applied using DSP TMS320F2812 in order to maintain the current fed to the grid to obtain a high dynamic performance with quick-changing atmospheric circumstances. The proposed inverter provides much less overall harmonic alteration and it would operate at a near-unity power element. The suggested system is being confirmed during the imitation and is conducted in a prototype. The recorded practical findings are compared with the traditional single-phase, three-level grid-connected PWM inverter.

The researchers in [30] used a classical type DC-DC buck converter which is mainly responsible to step down or lower the voltage that results from various linked panels. Moreover, the buck converter also offers sinusoidal current connected to the main grid that is possible using hysteresis modulation. A type of CSI inverter including thyristors is cascaded with the DC-DC phase, and as a result, the AC voltage is obtained. The

level of the output voltage of the inverter is edited using a low-frequency transformer that is also used to feed galvanic isolation. The essential benefits of the suggested system are summarized by simplicity, a decrease in the harmonic content of the injected current, and low cost.

Another study conducted in [31] uses a novel fuzzy logic control method for the grid-tied solar system. The proposed system includes a DC-DC boost converter and a single-phase, full-bridge inverter tied to the main usefulness of the grid. The suggested control system depends on variable universe fuzzy logic in order to manage the MOSFET switch off both in the boost converter and the single-phase, full-bridge inverter linked to the grid. The novel fuzzy control may adjust the universe based on the input change. The recorded findings by simulation indicate that the output power of the PV inverter is characterized by good quality and it can provide energy, a high power element and low harmonics.

The study in [32] presents the researchers' design of a single-phase voltage source inverter on two levels to connect the solar cell system to the grid. The grid current and PowerPoint control the maximum level of a single control system. This is based on the principle of repetitive control.

In [33], a method to control a VSI with a solar cell system is proposed. The proposed method is based on a VSC control using control decoupling for each component. The research aims to control the power factor in the grid and improve the efficiency of power transmission from the solar cells to the grid and reducing deform the source voltage current. The researchers used the MATLAB/SIMULINK program to represent the system.

The authors of [34] designed a three-phase variant of the solar cell system where it is connected to the network with the power of the modulator being approximately 100 kW. One of the features of this modulator is the reliance on the fuzzy logic control scheme to have the MPP and DC-DC converter dispensed within this system.

In [35], the researchers use the voltage source modulator of the solar cell system as a synchronous static compensator during the night. The modulator is the main part of the STATCOM system. Therefore, the system is used as a synchronous static compensator during the idle time of the cells. The system is modeled using the MATLAB/SIMULINK environment. The reported results demonstrate that the system is operative in treating voltage disturbances as well as provide power factor improvement.

The difference between the use of a DC-DC modulator converter Cuk and boost modulator in a tracker circuit of the maximum capacity of the PV system connected to the network is examined in [36]. The first type of modulator has fewer losses than the second type and current is continuous at both input and the output to Cuk changer. It uses an algorithm known as Incremental Conductance for the time being and it obtains the maximum PowerPoint followed by using the DC-AC inverter to connect with the system. To control this modulator, they use the controlling method DC line voltage (constant voltage).

In [37], the authors use a VSI single-stage as an active filter to improve power quality, reasoning that their proposition by conventional inverters usually require a higher voltage difference on the DC side than the potential difference on both ends of the source of alternating current. Therefore, DC-DC converters are often used as they require high inductances to store energy during the switching process. The proposed system is represented by a triple 1.5 kW load phase, as the proposed system is three-phase, and the control circuit is designed to allow the current source inverter to work for the solar cell system with a voltage difference on the DC side that is less than the voltage difference on the AC side. The system efficiency is within 94% as compared to the conventional inverter, whose efficiency does not exceed 90%.

A useful way to remove or lower harmonics and imaginary current from an electrical network to which a PV system is linked is presented in [38]. The suggested approach is based on trigonometric functions. According to experts, this approach may be used to identify imaginary harmonics and currents and determine the control signals for the modulator market linked to the electrical grid and the solar cell system. The system is

designed as a three-phase system with a DC-DC converter and is implemented using dSPACE-II03. The recorded results of the representation and implementation for the proposed system demonstrate the effectiveness of the technique being used and that the electrical power quality is within acceptable limits.

The importance of power modifiers for solar cell systems that are linked to the electrical grid without transformers, with and without the use of adapters, is raised in [39]. Yin-Ming Chen et al. [40] designed a three-phase, three-level VSI with a PD PWM control on the inverter. Due to its lower seepage current and lower voltage stress when compared to two-level inverters, a type of three-level neutral point clamped inverter can be always invested in a transformer-less photovoltaic grid-connected system. Both reliability and efficiency are important factors in a transformer-less grid-connected PV inverter system. Due to the lack of isolation, the common-mode voltage of the inverter must be low in order to avoid any negative effects from the leakage current. To achieve high efficiency, the switching loss must be low. The researchers use a strategy of low switching loss PWM with a low common-mode voltage on a three-level, grid-connected inverter.

A single-stage three-phase PV grid-connected system implementing double closed-loop control is proposed in [41]. The control system consists of an inner current loop and an outer voltage loop as well as an outer voltage loop. By using a PI controller in conjunction with the inverter control and synchronous rotating coordinate transformation, it was possible to complete the active power and reactive power decoupling controlling tasks. This approach accomplished an elastic and quick grid-connected system with the highest power per factor while also reducing the cost of the grid-connected system and improving the quality of power. Moreover, it decreased the grid-connected cost while simultaneously improving the quality of power.

In [42], the authors used a three-phase PV system containing a two-stage system in which the first stage consists of a DC-DC boost converter followed by using the adaptive fuzzy turned PID voltage controller in order to preserve the DC-bus voltage. They used linear loads and nonlinear loads. The entire system was authenticated with

MATLAB/SIMULINK software under many transient circumstances, such as steady-state, load variation, and dynamic load circumstances.

MPPT algorithms are important for PV applications due to the variance of the MPP of a solar panel with sterilization and temperature. In the current study, Perturbation and Observation (P&O) is the method being utilized. They also use three-phase VSI, with "instantaneous reactive power theory" (P-Q theory) being used for a grid-connected PV system control strategy and the hysteresis band control technique being used for inverter output current control [43].

In [44], the authors used a three-phase, three-level DCMLI and the modulation technique with SPWM to offer a gating pulse to the three-level inverter. The entire system is evaluated depending on the inverter current, the grid current, and the overall inverter performance. The efficiency of the control system is investigated, and the findings are analyzed in terms of THD. The simulation work was performed using the MATLAB/SIMULINK software.

MPC relies on MPPT to achieve high accuracy and quick dynamic responses. Combining the two approaches increases the tracking capacity of the underlying algorithm. A three-phase grid-connected inverter powered by a PV panel group is used to evaluate the suggested control method. The MPC algorithm is utilized to create the switching signals of the inverter. The Perturb and Observe MPPT technique computes the reference current of the MPC algorithm. Consequently, the power flow is managed by the MPC algorithm, which is based on the MPPT technique. The power flow, MPPT effectiveness, and THD analyses were explored in a simulation using MATLAB/Simulink software [45].

The transformer-less inverter PV grid-connected has been popular recently because it is smaller in size and more efficient [46]. Despite this, the parasitic capacitance causes a significant seepage current value between the PV system and the main grid. Several converting topology and modulation approaches have lately been offered as solutions to this issue. However, because of the low modulation index, they result in higher costs and inefficiency despite enhancing common behavior. A revolutionary three-phase

transformer-less architecture eliminates the need for expensive components and difficult modulation procedures. The suggested topology is described in terms of operational and common-mode (CM) performance. Simulation findings are used to validate the analysis and performance.

The inverter in [47] has excellent static and dynamic characteristics. A nonlinear control approach called Passivity-Based Control (PBC) was applied depending on the present model since the mathematical model of the inverter is nonlinear. First, the conventional Euler-Lagrange (EL) current mode of the inverter is established; it shows strictly passive. The system energy may be redistributed based on the inverter's passivity. Moreover, it can use tactics such as injecting dampening and decoupling to optimize system performance.

Reference [48] proposes a modified IncCond MPPT algorithm that efficiently follows the optimized PowerPoint for irradiation variation in order to prevent losing the MPPT. The improved approach is used to remove the steady-state oscillations. However, additional calculations are performed inside the algorithms, which slows the tracker's reaction time.

The study in [49] suggests a customized IncCond MPPT optimization technique for fine-tuning the switching frequency of the DC-DC converter to eliminate the deviation from MPP that occurs in the traditional IncCond approach under fast-changing irradiation circumstances. This method improves the system's tracking efficiency from 91.39% to 96.40%. To increase system performance under rapidly changing irradiance, the modified IncCond approach is presented. However, with uniform irradiation, the MPPT behaves no unlike a traditional IncCond, slowing the algorithm response.

The revised kernel least mean square (KLMS) control approach was invested in a double-stage, grid-connected PV system at the common coupling point (CCP) to improve power quality. This suggests that the control method offers fewer oscillations, rapid resolution, fast response, and high steady-state performance. A control approach is utilized to extract the basic current source component of a load and create a standard

power flow for a bridge rectifier. Multiple power quality problems, including the unity power factor, harmonic suppression and load balancing, are addressed by the proposed improved control KLMS. The suggested system's dynamic performance is proven in the MATLAB Simulink environment [50].

PART 3

MODELING OF THREE-PHASE PV GRID-CONNECTED SYSTEM

3.1. INTRODUCTION

PV arrays and DC-DC boost converter, inverter, linear and nonlinear load, and grid are the components comprising the system analyzed by this research work. Figure 3.1 shows how these components are stacked together to generate the system required for our study. To begin, a quick rundown of each block is given to act as a basis for the final design. The modeling approach for each block is then discussed in depth. Finally, a two-stage, PV system grid-connected switching system MATLAB model is created.

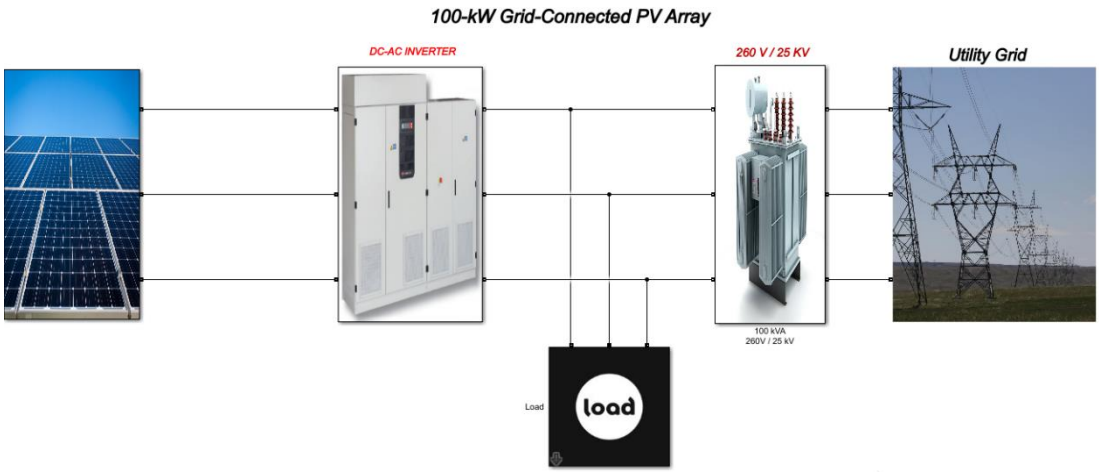

Figure 3.1. Block Diagram of PV Grid-Connected Model.

The modeled system is built in two steps: DC-DC converter and DC-AC converter, with both processes occurring at the same time. In this situation, the boost circuit is connected to the solar PV system's output and serves two purposes: maximizing the power output of the PV source and subsequently raising and stabilizing the PV source's

DC output voltage. The boost converter's DC output is converted to AC at the DC-AC conversion stage, which is subsequently sent into the power grid. A filter connected between the inverter and the grid removes higher frequency harmonics from the inverter output.

3.2. PV ARRAY MODELLING

In many solar cell models, a current source and an anti-parallel diode are included. Through a series resistor, the output is connected to them in parallel. The current produced by the ability to obtain is directed straight to the connections in the most basic form [51]. The series resistance there at the cell's terminal is used to depict the voltage drop. The parallel resistance is employed to account for current leakage that is proportional to the terminal voltage of the device [52]. Figure 3.2 shows the solar cell's equivalent circuit with parallel and series resistors.

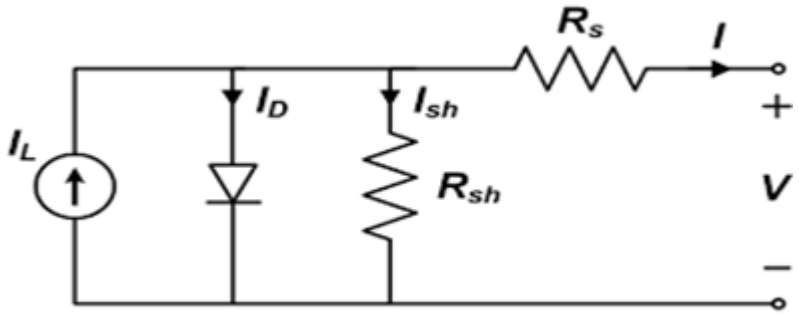

Figure 3.2. The Solar Cell's Equivalent Circuit.

The I-V characteristics of the relevant photovoltaic cells circuit may be computed using the calculations below [53].

$$I = I_L - I_D - I_{Sh} \tag{3.1}$$

$$I = [I_{SC} + K_i(\text{T-298})]\frac{G}{1000} - I_S\left\{\exp\left[\frac{e}{mkT}(V + IR_s)\right] - 1\right\} - \frac{V+IR_S}{R_{sh}} \tag{3.2}$$

Equation (3.3) defines the photocurrent of a solar PV cell.

$$I_L = [I_{SC} + K_i(\text{T-298})]\frac{G}{1000} \tag{3.3}$$

The current flowing through the diode is calculated as follows:

$$I_D = I_o \left\{\exp\left[\frac{e}{mkT}(V + IR_s)\right] - 1\right\} \tag{3.4}$$

The current flowing via parallel resistance is calculated as follows:

$$I_{Sh} = \frac{V + IR_s}{R_{Sh}} \tag{3.5}$$

Table 3.1 shows the manufacturer's specifications for such SPR-315 components. For modifying the solar irradiance, the photovoltaic modules block only has one input (input 1 in W/m2). A Signal Building component linked toward the Pv system inputs determines the irradiance profile.

Table 3.1. SPR-315 solar module characteristics.

The amount of cells in each module	96
Voltage in the open circuit Voc (V)	64.2
the current Isc in a short circuit (A)	6.14
the voltage Vmp at the maximum power point (V)	54.7
Maximum power point current Imp (A)	5.75
The Voc temperature factor (V/°C)	-0.177
The Vmp factor of temperature (V/°C)	-0.2727
The Imp's temperature factor (A/°C)	-0.061743

Figure 3.3 depicts the current and voltage characteristics of a single solar unit, as well as a power and voltage diagram at different temperature ranges and radiation intensity of 1000 W/m^2 (clear sky). An array of 80 solar modules, consisting of 20 strings of four series-connected 315.072 W modules linked in parallel, had current and voltage characteristics, as well as power and voltage characteristics, as shown in Figure 3.4. When the intensity of solar radiation remains constant at 1000 W/m^2, the influence of

module temperature variation on the current and power characteristics of the array of solar modules is obvious. Using the Simulink MATLAB software, Figure 3.5 depicts the current, voltage, power, and voltage characteristics of the array of solar units, as well as the effect of altering the intensity of solar radiation on the array's current and power at the temperature of constant 25 ºC.

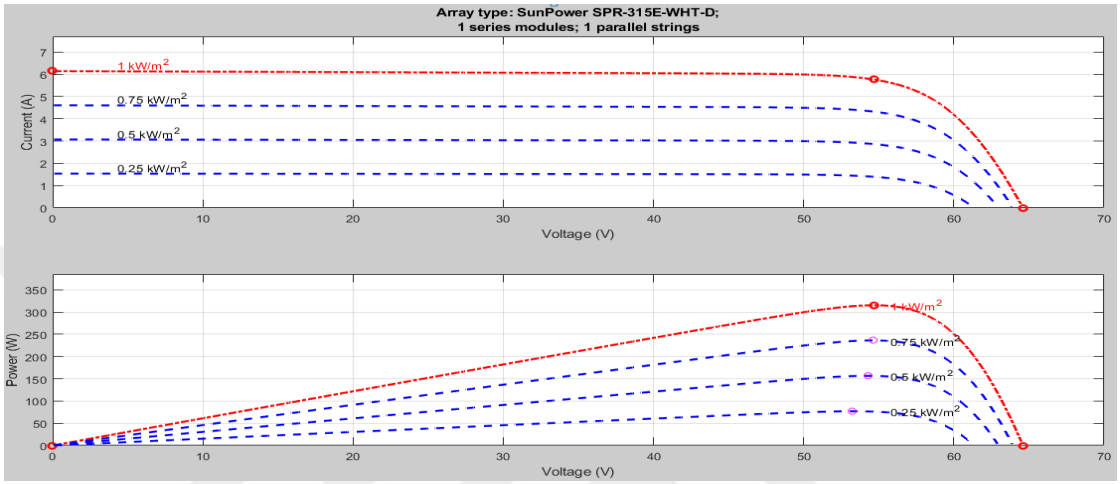

Figure 3.3. P-V and I-V curve of a single solar module at different irradiance intensities.

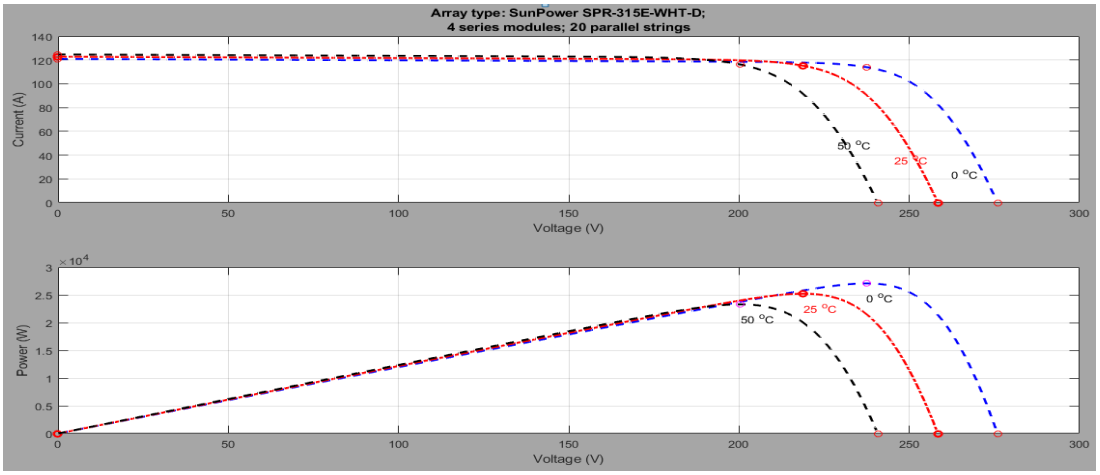

Figure 3.4. Characteristics curves of the 80-module array at 1000 W/m2.

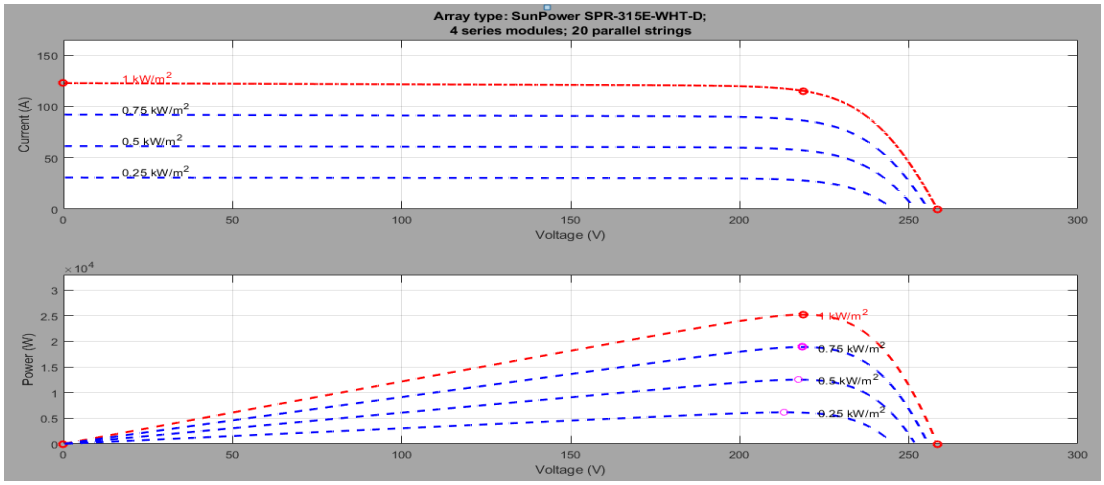

Figure 3.5. PV array characteristics at 25°C and various irradiation levels.

Atmospheric variables, which fluctuate throughout the year and sometimes within a short time, impact temperature and irradiance [54]. As a result of rapidly changing conditions such as clouds, they might alter swiftly. From the above-simulated characteristics, it can be observed that as the solar PV module temperature increases the productivity of the solar array decreases. also, as the solar irradiance increases the productivity of the solar array increases influenced by the increase in voltage and current of the solar cell. As a consequence, the MPP differs continually depending on irradiance and temperature circumstances. If the operating point is not near the Maximum PowerPoint, there are significant power losses. As a result, monitoring the highest PowerPoint under any scenario is crucial for ensuring that the PV panel delivers the maximum amount of power possible. In current solar power converters, the MPPT algorithms are in charge of this duty.

3.3. BOOST CONVERTER

A boost converter is often utilized in renewable power applications in solar and wind. Because solar and wind power generation is inherently intermittent, it is critical for increasing the overall efficiency of the system to account for the impact of its intermittent nature. A converter aids in improving the system's overall efficiency. A boost converter is a device that converts a low-voltage DC supply into a high-voltage DC supply. It also regulates the quantity of energy extracted from the solar panel and applies a steady voltage towards the terminating output [55].

A constant current input in the DC-link, which would be the boost converter's outputs capacitor, is required for the two-stage PV system that is grid-connected. Constant current injection maintains a constant DC-link voltage and minimizes output voltage variations [56]. As a consequence, the inverter will have a steady DC voltage supply, that will help it function better and save energy. A dc-dc converter is also less expensive than other types of converters. Figure 3.6 shows a basic boost converter with Vin also as a voltage source and Vo as the output voltage [57].

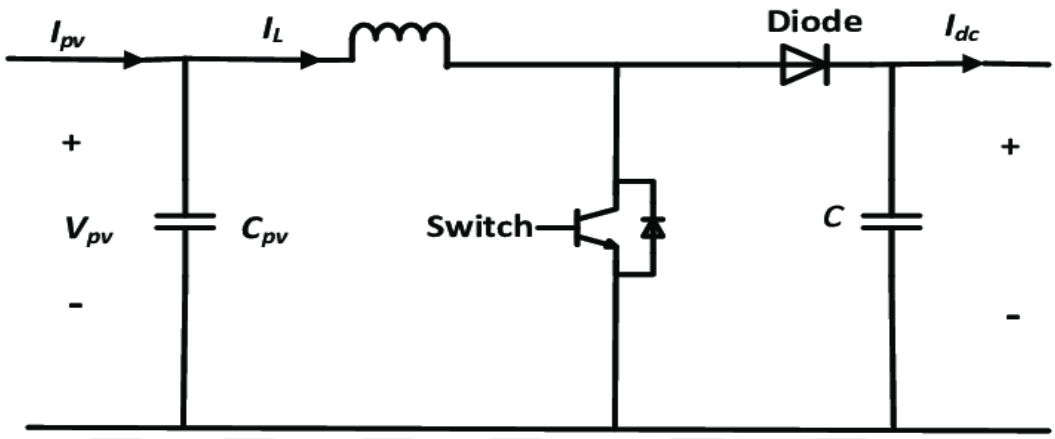

Figure 3.6. Equivalent Circuit of the Boost converter.

Because a diode will be reverse biased during switching, the current will be identical to the current in the inductor. The voltage applied during the on-interval is proportional to the output voltage. The capacitance should always be big enough to keep the voltage over the load steady. The inductance discharges inside an opposite direction during the off-interval, forward prejudicing the diode. The difference between input and output voltages is represented by the voltage throughout the inductor. The volt-sec balance across the inductor may be used to identify the relationship between the parameters and output voltages. The steady-state voltage across the inductor for one cycle is zero, according to the volt-sec balance.

$$V_O = \frac{1}{1-D} V_{in} \tag{3.6}$$

D = Ton / Tswitch is indeed the duty ratio with the duration divided by the switching period. A boost converter's DC input and output voltages are V_{in} and V_O, respectively.

In the same way, assuming there are no losses in the circuit, the relationship between the input current Iin and the output current Io may be established, as shown in (3.7).

$$I_o = \frac{1}{1 - D} I_{in} \tag{3.7}$$

A boost can also be designed to operate in either continuous conduction mode (CCM) or discontinuous conduction mode (DCM). The inductor current in CCM is non-zero, whereas in DCM it is zero, with zero inductance interlaced timing at period Δt.
The selection of inductor and capacitor is critical in boost converter design. The proportions of inductance and capacitance are influenced by a variety of circumstances. The L equation governs the selection of inductors for a boost converter design.

$$L_{boost} = \frac{D\,(1-D)V_{dc}}{f_{sw}\ \Delta I_L} \tag{3.8}$$

A capacitor is used between the PV and the DC-DC circuit to minimize harmonics in frequency (C_{pv}) which is given in Equation (3.9) [58].

$$C_{pv} = \frac{DV_{PV}}{4\Delta V\ F_{SW}^2\ L} \tag{3.9}$$

3.3.1. DC-Link

An electrolytic capacitor is typically used for the DC-link capacitor, also known as power decoupling. Electrolytic capacitors have been widely employed in inverter designs as bus connection capacitors. For many years, electrolytic capacitors have been the workhorse method for hard switched inverter bus link capacitors. Electrolytic capacitor technology has stayed relatively consistent throughout the years. Electrolytic capacitors have been attractive because of their low cost per farad [59]. The DC-link capacitor is crucial to the converter's lifetime; hence it should be maintained and replaced with film capacitors wherever possible. The inverter DC-link capacitance has been reduced by replacing electrolytic capacitors with more dependable, but also more

expensive and bigger film capacitors. The distinction between an electrolytic and a film capacitor is that an electrolytic capacitor's life is influenced by its temperature. Film capacitors are an obvious choice due to their extended lifespan and wide working temperature range. Since film capacitors are substantially more expensive per farad than electrolytic capacitors, the capacitance must be reduced to make the capacitor's price fair. A lesser capacitance, on the other hand, limits the DC-link capacity to decouple power, which might cause DC-link voltage swings, which distort the inverter's output current to the grid. The power input flowing into the DC-link capacitor rapidly increases/decreases, which causes the transient DC fluctuation. An extremely quick current controller can be used to eliminate this. When constructing a VSI for solar applications, DC fluctuation is not an important aspect to consider. The grid-side double-line frequency ripple power is responsible for the second component, known as AC fluctuation of the DC-link voltage-current reference signal can be severely skewed because such a double-cause vibration component can connect across the DC voltage control loop. In DC to AC inverters The capacitance of the bus connection is used to remove inductance influences from the DC voltage source to the energy bridge. The capacitor for the bus link also aids in lowering the inverter power bridge's leakage inductance Eq. (3.10)

$$C_{dc} = \frac{p_{out}}{2\pi f \, \Delta v_{dc} \, v_{dc}} \tag{3.10}$$

3.4. MAXIMUM POWER POINT TRACKING

Many MPPT techniques, including fuzzy control, neural network-based, incremental conductance, and P&O, have just been reported. These technologies have been used successfully in both off-grid and solar energy systems with grid connectivity, and they perform well in generally slow and smooth weather fluctuations. These strategies, however, are challenging to directly apply to transportable Pv systems due to restricted monitoring rates or sophisticated implementations. Recently, a technique of MPPT for Photovoltaic systems running in partially shaded situations and employing a dc-dc converter to monitor global high points was proposed and evaluated [60]. Although this technique is intended for high-power PV modules with numerous cells connected

in series and also has a significant quick pace (usually a few seconds), it is challenging to directly use in transportable PV systems. This is due to the fact that the energy produced by partly shaded cells is unusable, and the found significant effect is insufficient for many applications where shading conditions might change extremely fast (e.g., in a tenth of a second) [61]. The MPP of a single cell, on the other hand, is rather easy to calculate since it is so close to a given (temperature-dependent) operating voltage [62]. Using this very well phenomenon, the MPPT approach for regulating the voltage level of solar panels was developed and created for series-connected systems decades ago. It is simple to set up and provides quick changes in a creative manner in illumination. However, for this technique to work, uniform illumination is required for series-connected cells; shaded cells would impede the operation by lowering the necessary working voltage. As a result, if the PV modules are coupled in series, this technology can be applied in portable applications directly.

3.4.1. Incremental Conductance (IncCond)

In addition to the P&O technique, an incremental conductance method exists. It has the benefit of being able to compute the MPP and then cease perturbing the duty cycle of the converter once the MPP is captured. To collect the necessary measurements, the approach employs both voltage and current sensors. The approach then computes dI and dV, which are the differences between the most recent measurement point and the previous closest point, and may be approximated to dI and dV. These values are calculated because the algorithm analyses how a change in voltage affects a change in current (thus the name incremental conductance), and it makes use of the fact that dP/dV = 0 at the MPP to determine when to stop. If dP/dV is negative, the MPPT operating point will be to the right of the MPP. As shown in figure 3.7, the MPPT setpoint will be positive to the left of the MPP [63]. A change in voltage involves a shift in current, which is monitored and used to assess if the converter's operating voltage should be altered. The approach employs the following computations using these computations:

$$\frac{dP}{dV} = \frac{d(VI)}{dV} = I\frac{dV}{dV} + V\frac{dI}{dV} = I + V\frac{dI}{dV} \tag{3.11}$$

If $\frac{dP}{dV} = 0$ as this case MPP is :

$$\frac{dI}{dV} = -\frac{I}{V} \tag{3.12}$$

As a result, the MPP conditions are dP/dV = 0 and dI/dV = -I/V. The link between dI/dV and I/V is utilized to correctly control the duty cycle. The rationale is summarized as follows:

$\frac{dI}{dV} = -\frac{I}{V}$ at the MPP.

$\frac{dI}{dv} > -\frac{I}{V}$ left of the MPP.

$\frac{dI}{dV} < -\frac{I}{V}$ right of the MPP.

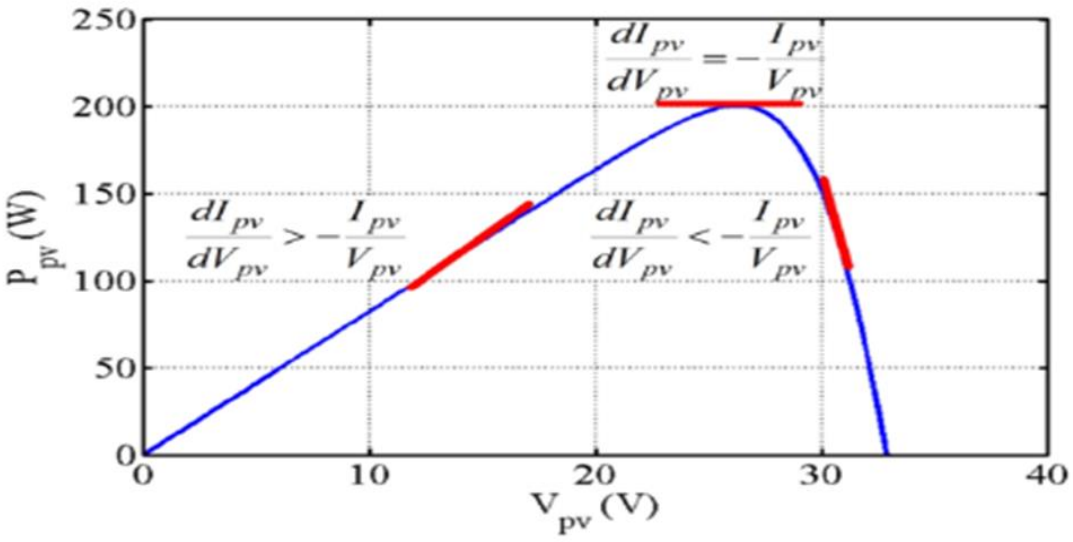

Figure 3.7 Incremental conductance concept

The algorithm implementation is depicted in Figure 3.8 is a logic flow chart. In this reasoning, consider a point to the left of the MPP. The algorithm calculates dV and dI after determining V and I. The dI/dV ratio is then compared to the - I/V ratio. The result shows that dp/dv > I/V, suggesting that the point is outside the MPP and that the duty cycle must be raised to get a higher voltage. The algorithm will halt and wait for the MPP operating point to shift to dI/dV-I/V when dI/dV= -I/V. The example also highlights the large number of computations needed to accomplish the MPPT

assignment. Incremental conductance needs more computing resources and is consequently more expensive to construct than perturb and observe, but it can locate the genuine MPP.

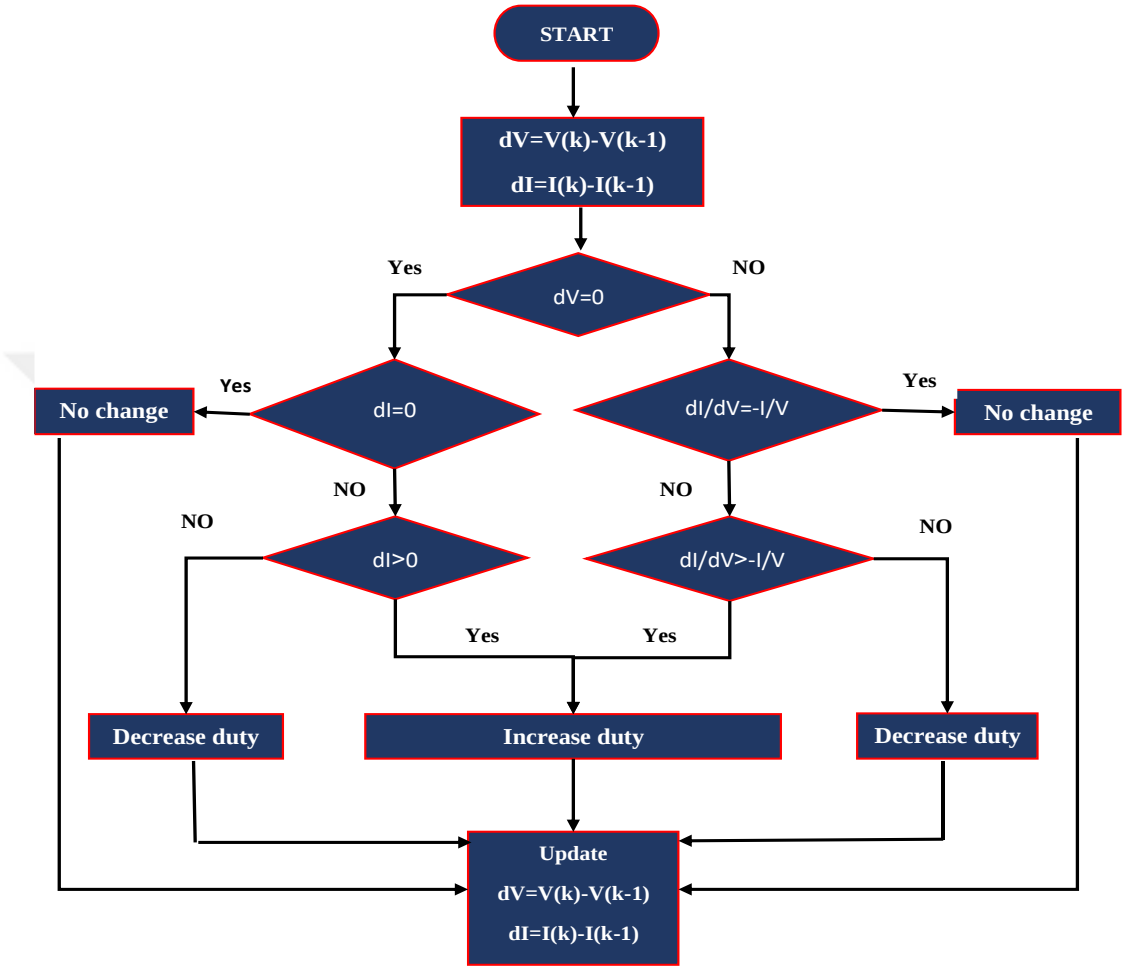

Figure 3.8. Methodology for the Incremental Conductance technique

3.5. INVERTER

DC-AC Switch Mode inverters use pulse width modulation to create sinusoidal alternating current from a direct current input (PWM). The AC output of the inverter may be adjusted in both amplitude and frequency. Inverters having a DC voltage source input are referred to as voltage source inverters (VSIs). The three types of inverters that are offered are square wave inverters, single-phase inverters and PWM inverters with voltage cancelation [64]. The most common inverter used in solar systems is a PWM inverter, which changes the DC link current to maintain the constant

voltage DC-link. Both the control signal as well as the output voltage waveform must be sinusoidal to create a sinusoidal output waveform voltage with the requisite frequency. And the waveform of the signal to which it is just being compared is triangular. The waveform frequency determines the switching frequency, which is usually kept constant. A more complete explanation of DC-AC Switch Mode Inverters can be found in the literature [65]. Multi-level inverters have several advantages, including lower filter requirements at the same duty ratio, lower voltages or harmonic currents, and fewer electromagnetic fields [66]. Multi-level inverters are now easy to regulate because of recent advancements in microprocessor technology. They've grown in popularity, particularly in high-power situations. Modern inverters, on the other hand, necessitate the use of additional features including switching devices, capacitors, and gate controllers, as well as more sophisticated circuit topologies [67]. The ability to achieve high voltage and power levels is another advantage of multi-level inverters. The flying capacitor (FC) inverter, The NPC inverter, and the cascaded H-bridge (CHB) inverter are all examples of multi-level inverters [68]. The complexity of comparing two capacitor voltages in an NPC inverter, the FC topology's bigger capacitor demand and larger size, and the CHB topology's isolated voltage requirement is all benefits and drawbacks of these topologies NPC inverters can also be utilized to eliminate the necessity for a DC voltage source that is separated. In the last decade, commercially available switching components with one leg of an NPC inverter have made NPC inverter formulation and construction easier. In NPC, a clamped diode is used, and the system supplies additional voltage, as illustrated in Figure 3.9. For N output phase voltage, every phase requires (N-1) capacitance, 2(N-1) switches, and (N-1) (N-2) clamping diodes. S1, S2, S3, and S4 are complimentary switching pairs.

Table 3.2. Inverter One Leg Output Voltages Based On Switches Status

Switch Position	S1	S2	S3	S4	Output voltage
P (Positive)	1	1	0	0	1/2V
O (Medium)	0	1	1	0	0
N (Negative)	0	0	1	1	-1/2V

Figure 3.9 depicts a general schematic of the NPC inverter.

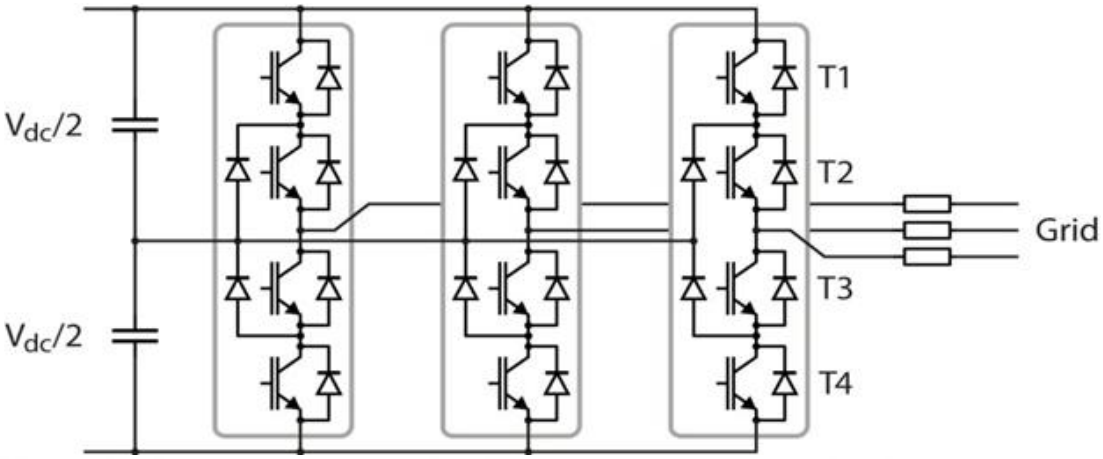

Figure 3.9. Three-phase NPC inverter.

3.5.1. Phase Locked Loop (PLL)

The phase-locked loop's function is to resolve the grid voltage abc components and supply the rotational frequency, direct, and quadrature voltage parts at the point of common connection (PCC). This information is used by various control frames in the PV system to control their production control signal. To eliminate cross-coupling in the active and reactive power terms, the PLL quantifies the grid voltage vector's rotation frequency by first translating it to the dq reference frame and then forcing the voltage amplitude portion to zero [69]. Figure 3.10 shows how a proportional-integral (PI) controller is used to accomplish this task. To obtain a rapid settling time, the controller's proportional (Kp) and integral (Ki) gains were consecutively tuned.

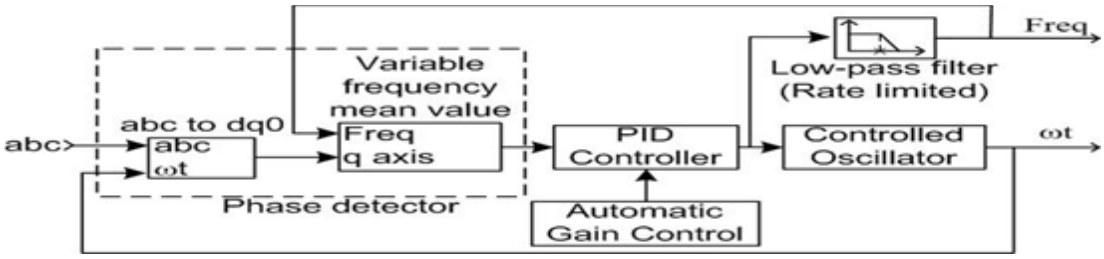

Figure 3.10. The phase-locked loop is depicted in this diagram

The PI controller outputs the rotational frequency in radians per second. Integrating this term yields the angular position in radians.

3.5.2. Control of Inverter

The basic purpose of the grid-tied control scheme would be to maintain a sinusoidal output current in phase with the output voltage, resulting in a power factor of about unity; hence, a voltage-oriented control (VOC) scheme using a controller PI is detailed for the PV system grid-tied. A method, also known as indirect power management, is based on the Stationary reference concept, in which three-phase abc currents and voltages are converted to a two-phase dq system, which would be the synchronized revolving frame (SRF), which lags 90 ° behind grid source voltage and so Vq =0. This type of metamorphosis is known as Park's transformation. In this control technique, there have been two loops: an interior control current loop and an outward control voltage loop. To keep the power factor near unity, the q-axis current is adjusted to zero. The following are the three-phase line voltage and phase current equations for a grid-connected inverter:

$$Va = Vm\ \cos wt \tag{3.13}$$

$$Vb = Vm\ \cos(wt - 2\pi/3) \tag{3.14}$$

$$Vc = Vm\ \cos(wt + 2\pi/3) \tag{3.15}$$

and

$$Ia = Im\ \cos wt \tag{3.16}$$

$$Ib = Im\ \cos(wt - 2\pi/3) \tag{3.17}$$

$$Ic = Im\ \cos(wt + 2\pi/3) \tag{3.18}$$

The voltages at the inverter end of the grid-tied inverter with LC filter are Va, Vb, and Vc, whereas the voltages at the grid end are Ua, Ub, and Uc. As a guide, use Kirchhoff's law:

$$V_a = L\frac{dI_a}{dt} + U_a \tag{3.19}$$

$$V_b = L\frac{dI_b}{dt} + U_b \tag{3.20}$$

$$V_c = L\frac{dI_c}{dt} + U_c \tag{3.21}$$

Where L denotes the filter's inductance and Ia, Ib, and Ic denote current values. Three-phase current (Iabc) and voltages (Vabc) are converted into a two-phase synchronized rotational frames (SRF) dq0 system using Park's transformation (Vdq0 and Idq0). This shift is denoted by the following:

$$\begin{bmatrix} d \\ q \\ 0 \end{bmatrix} = \begin{bmatrix} \cos wt & \cos(wt - 2\pi/3) & \cos(wt + 2\pi/3) \\ -\sin wt & -\sin(wt - 2\pi/3) & -\sin(wt + 2\pi/3) \\ 0 & 0 & 0 \end{bmatrix} \tag{3.22}$$

A dq transform equation for transforming these three-phase voltage data is as follows:

$$Vd = L\frac{dI_d}{dt}dt + Ud - wL\, I_q \tag{3.23}$$

$$Vq = L\frac{dI_q}{dt}dt + Uq + wL\, I_d \tag{3.24}$$

The voltage and current equations for the dq axis may be expressed as,

$$Vdq = Vd + jVq \tag{3.25}$$

$$Idq = Id + jIq \tag{3.26}$$

Apparent power may also be expressed as,

$$S = \frac{3}{2}(Vdq\ Idq\ *) \tag{3.27}$$

Where Idq* denotes Idq complex conjugate.

As a result, the grid is provided with the following active and reactive powers:

$$P = \frac{3}{2}(Vd\ Id + Vq\ Iq) \tag{3.28}$$

$$Q = \frac{3}{2}(-Vd\ Iq + Vq\ Id) \tag{3.29}$$

Vq=0 because the grid is synchronized and the system is in a steady-state condition. The following is how the equation may be represented:

$$P = \frac{3}{2}(Vd\ Id) \tag{3.30}$$

$$Q = \frac{3}{2}(-Vd\ Iq) \tag{3.31}$$

Reactive power has a negative sign, indicating that it can move in either route, of the grid to the inverter or vice versa. The outer voltage loop, which controls the dc-link voltage to a reference signal, which would be a stop signal, is controlled by a PI controller, while an inner current control loop wants to regulate real and reactive currents in the dq0 reference frame, which is aligned to the grid's voltage vector, is controlled by a PI controller. Monitoring three-phase grid voltages using a PLL allows you to calculate the angle between grid voltage and current. Controlling the production of active energy, Id* and Iq* results are calculated to record Id and Iq. As illustrated in Figure 3.11, to produce comparative d-axis and q-axis voltages, two PI controllers are utilised. (Vd*, Vq*) depending on d-axis current Id and q-axis current Iq.

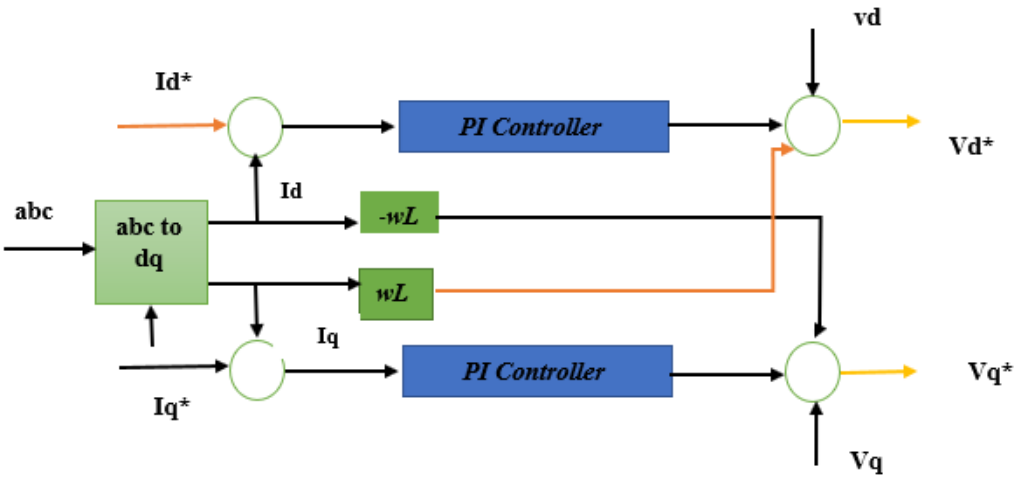

Figure 3.11. Vd* and Vq* were generated by PI controllers

Finally, the dq0 axis is transformed into the abc reference axis using an inverse of Park's transform. A PWM-based modulation approach employing abc reference frame voltages is employed to create switching pulses for the inverter.

3.6. INVERTER FILTER DESIGN

Solar PV electricity is often converted utilizing a VSI system before even being pumped into the grid, as previously stated. The harmonics inherent in the inverter's output voltage may be reduced by placing an appropriate filter between the VSI system and the network, thereby protecting the grid operator power quality. The L-filter, LC-filter, and LCL-filter are the most common filters, each with its own set of benefits and drawbacks.

3.6.1. LC Filter

In a grid-connected solar PV system, the filter's effectiveness and type affect how so many harmonic components are attenuated. Among the several types of filters listed above, the first-order filter with just an inductor linked in series with mains is the most widely used in recent years [70]. This is due to the fact that it is simple, inexpensive, and free of the resonance concerns that two and three filters have. Despite the fact that such a filter has a significant disadvantage because it needs a big filter to provide effective harmonics reduction, this is still a feasible alternative. A VSI system model's high-frequency switching scheme is perfect for this filter.

In VSI applications, the LC filter is a second-order filter that decreases harmonic components at the inverter's output voltage. The illustrated LC filter is used in both grid-connected and off-grid PV power systems. This type of filter's resonance frequency varies with the grid's including the values, which is a significant disadvantage. As just a result, its export LC-filter must be constructed in such a way that it reduces inverter harmonics while still ensuring that clean power is delivered to the grid. The filter parameters Lf and Cf are calculated by utilizing equations 3.32 and 3.33 to supply the inductance ripple current and voltage values, respectively.

$$L_f = \frac{V_{dc}}{4 f_s \Delta_i} \tag{3.32}$$

$$C_f = \frac{\Delta_i}{8 f_s \Delta V_O} \tag{3.33}$$

3.7. LOADS

The simulated grid-tied PV system includes two types of loads: nonlinear and linear. The sine waves of current and voltage are represented by a waveform. Consider a waveform that represents the voltage and current as smooth, pure 60 Hz sine waves. When a linear load is present the current seems to be the same as the voltage in their waveforms. Non-linear loads have an impedance that varies when the voltage is applied. Because of the change in impedance, the current will not be sinusoidal. Harmonic properties in these non-sinusoidal currents cause voltage distortion in the power system and the equipment linked to it [71]. Some home and industrial non-linear loads are examined for THD analysis in this study. The non-linear loads for home and industrial applications, as well as precise requirements, are discussed. Lighting units related to discharge lamps and then discontinuous current connected with power electronic equipment are instances of non-linear loads that use continuous current. Power electronics devices are used in the most challenging Non-Linear Loads. Other examples include phase-controlled thyristor bridges, enclosed bipolar transistors (IGBTs), and diodes (as in an uncontrolled bridge). Harmonic current distortion is produced by all of these devices, which alters the applied AC voltage waveform.

Table 3.3. Parameters of the proposed system

Parameter	Value
Capacitance of PV capacitor (Cpv)	100 µf
The inductance of PV reactor (Lboost)	5 mH
Boost converter switching frequency (Fs)	5 KHz
Capacitance of DC link capacitor (Cdc)	24 mH
Series Resistance	0.005 Ω
Dc-Bus voltage	500 V
Current PI controller gains	Kp =0.3, Ki =20
Dc-Bus voltage controller gains	Kp=7, Ki=800
Non-linear load	7 kW
Linear load	45 kW
Reactive power in linear load	3 kVAR

3.8. THE UTILITY GRID

The grid is a network of interconnected power-producing and consumption units that transports energy from the point of generation to the point of consumption. The grid is meant to keep active and reactive electricity flowing while maintaining the balance of power generation and consumption, often known as supply and demand. At all times, the system's frequency must be kept at or near its nominal frequency. However, because various nations function differently, this number varies according to the standard [72]. The system operator must respond quickly to any major deviation from the ideal operating frequency. Because there is too much load in the system, load shedding or increased power output is required when the frequency falls below the usual frequency. Whenever the outset the nominal frequency, the load must be increased or the production must be reduced. This indicates that the amount of power generated now exceeds the amount used. As a result, in order to sustain the nominal frequency, the power produced and used must be kept constant.

Table 3.4. Parameters of three phase grid connected PV systems.

Parameter	Value
Grid phase voltage (RMS)	25 kV
Grid frequency	60 HZ
Transformation ratio	25 KV /260 V
Feeder	5 km

The asynchronous generator is shown powering a three-phase voltage source with a phase-to-phase RMS voltage of 25 kV, and one grid-connected transformers [73]. Because the grid frequency is normally 60 Hz, synchronization is possible if the solar system's frequency is slightly higher (0.1 to 0.5) than the grid frequency, but not lower. One of the most crucial elements to consider is voltage matching. The voltage levels in both systems should be the same [74]. As the capability of Solar PV rises, the impact of PV systems on the public grid must be considered. Grid-connected PV systems have the potential to destabilize the grid by generating additional harmonics and reducing grid stability. This problem can become critical when a large-scale PV component is

connected to the grid where table 3.4 shows the Utility Grid details. Voltage and current instabilities, as well as poor power system performance, are caused by current harmonics [75].

PART 4

SIMULATION RESULTS AND DISCUSSION

4.1. INTRODUCTION

This chapter focuses mostly on the simulation findings and analysis. In the MATLAB/Simulink environment, a grid-connected PV system is modeled and simulated. There are many cases that we used to obtain the results in the case of linear and non-linear loads, where in the first case the solar system operates at the maximum power and thus provides the loads with the required energy. As for the rest of the energy, it is injected into the network. In the second case, the solar system produces a capacity that supplies the loads only without Any increase in the capacity to go to the grid, but in the third case, the solar system gives less capacity than the required capacity of the loads, so the network participates in supplying the rest of the demand for loads. In the fourth case, the solar system does not work in the case of night or clouds, so the network works to supply the loads with the required energy.

4.2. SIMULATION OF DC-BUS MODEL

MATLAB/Simulink software was used to design and simulate the PV system. The grid-connected solar energy system consists of four sub-arrays of solar panels, each group providing 25 kW of rated power, whereas the four sub-systems comprise 100 kW of nominal capacity. Each group of modules has a DC-DC boost converter, as shown in Figure 4.1.

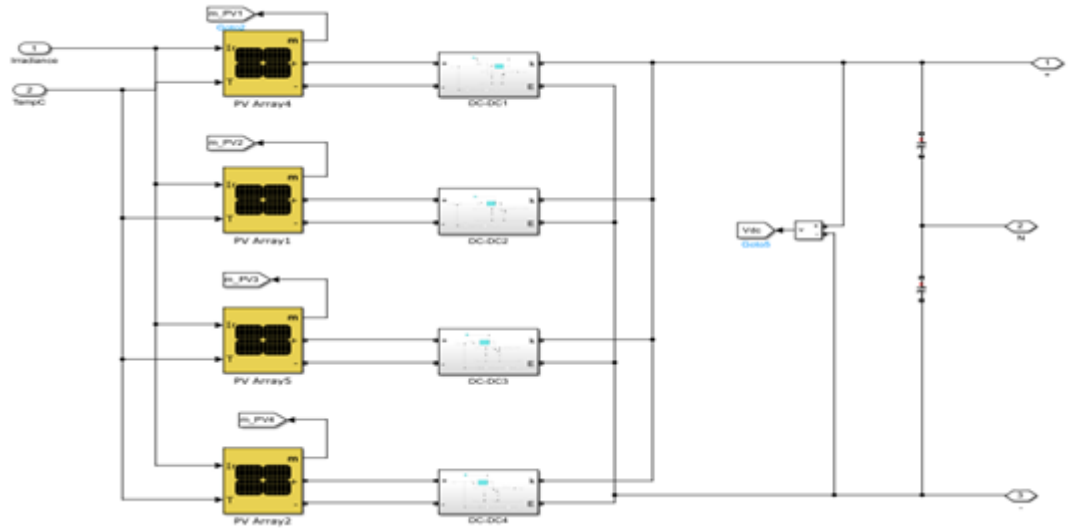

Figure 4.1. Simulated four PV sub-systems and associated DC-DC converter.

The SunPower (SPR-315) 25 kW PV sub-array is composed of 20 strings of four series-connected 315.072 W modules which are linked in parallel. Figure 4.2 depicts the equivalent circuit of a solar cell with parallel and series resistors using a Simulink environment.

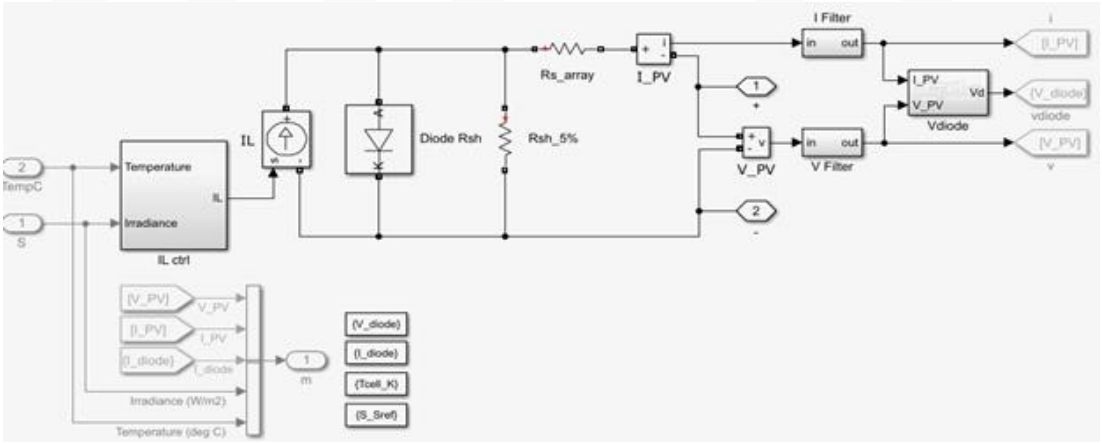

Figure 4.2. Equivalent circuit of the solar cell considering non-idealities

On the other hand, Figure 4.3 depicts the schematic design for the boost converter utilized in this study to increase the PV output voltage to a higher level acceptable for the inverter that is linked to the utility grid.

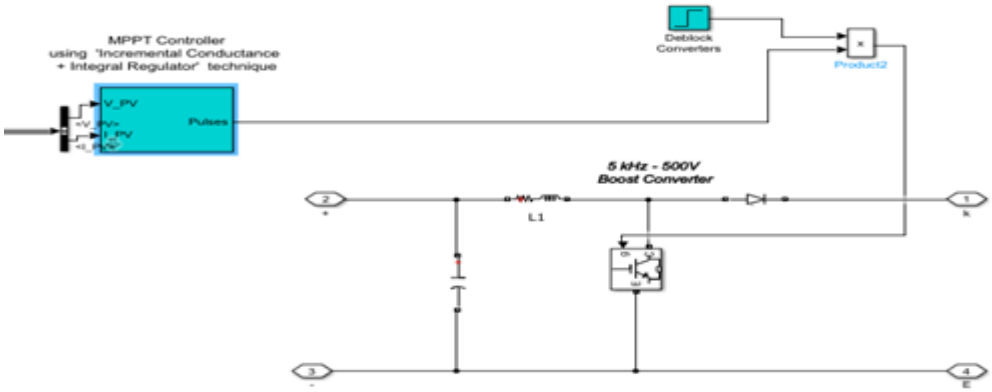

Figure 4.3. Simulation block for the DC-DC boost converter

Solar technology has advanced in recent years. This has resulted in the incorporation of several systems that will easily track the peak energy point of the PV panel throughout the operation. Incremental conductance, parasitic capacitance, current-based peak power tracking, and perturbation and observation approaches are some examples of such algorithms. The incremental conductance approach was utilized in this research study, as shown in Figure 4.4. Essentially, the incremental conductance algorithm is used to calculate and compare incremental conductance and conductance. Both are accomplished by computing the product of current and voltage. One notable advantage of this approach is its ability to track maximum power with trivial problems related to control in the MATLAB/Simulink environment.

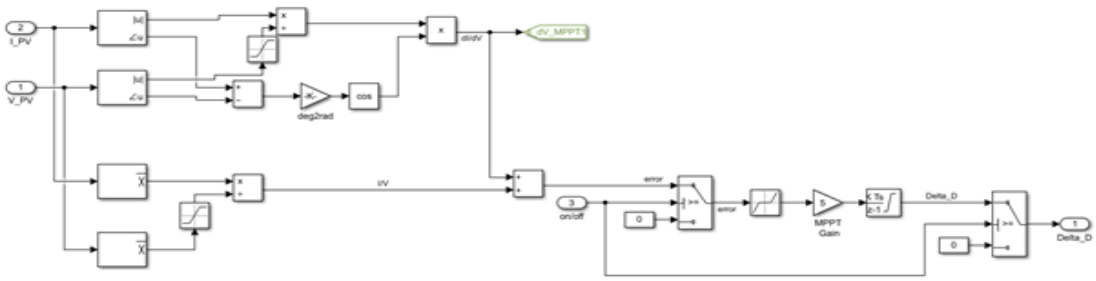

Figure 4.4. Simulink model of the modified Incremental Conductance (IncCond) MPPT algorithm

4.3. SIMULATION OF AC-BUS MODEL

While the DC-DC boost converter converts DC voltage to a higher DC voltage level, the inverter converts the DC voltage obtained from the solar PV system to an AC

voltage that is sufficient for coupling with the grid at an appropriate power factor. As shown in Figure 4.5, the delta modulation index of the PWM determines this.

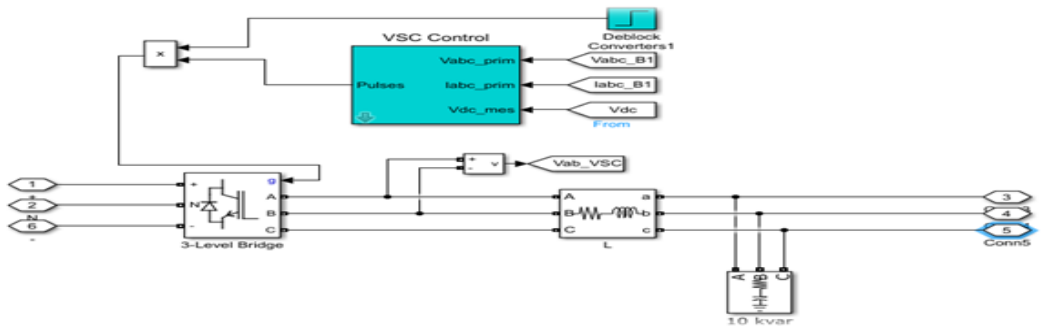

Figure 4.5. DC-AC converter with VSC control

The controlling process is divided into two loops: an inside control loop which maintains the Id and Iq grid currents (real and reactive power current elements), and an exterior control device that maintains the inverter's DC voltage using the Id compensating current as of the DC voltage controller's output. To keep the PF at unity, the Iq reference current is set to zero. On the other hand, the Vq and Vd voltage outputs of the current regulator are transformed into three-modulating signals (Uref abc), which are employed by the PWM three-level pulse generator.

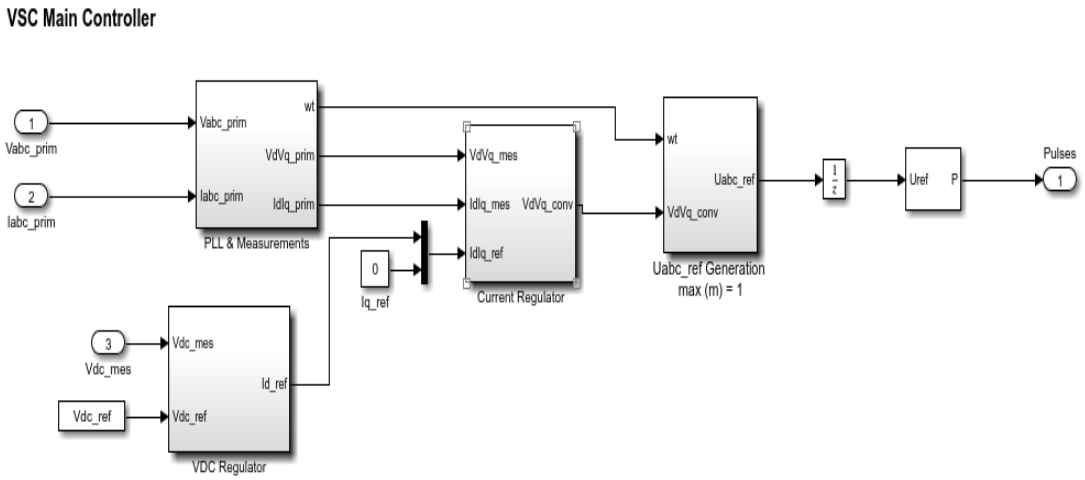

Figure 4.6. VSC controller

It should be reminded that the inverter's AC output voltage must be synchronized with the linked transmission grid, which necessitates PLL control. Phase voltages on the

grid are measured and transformed into a space vector quantity. When the spinning reference frame synchronizes with the grid voltage, Vq equals zero. As a result, Vq is set to zero by the PI controller. The grid measurements (V and I) in the d-q axis, as well as the PLL block diagram, are presented in Figure 4.7.

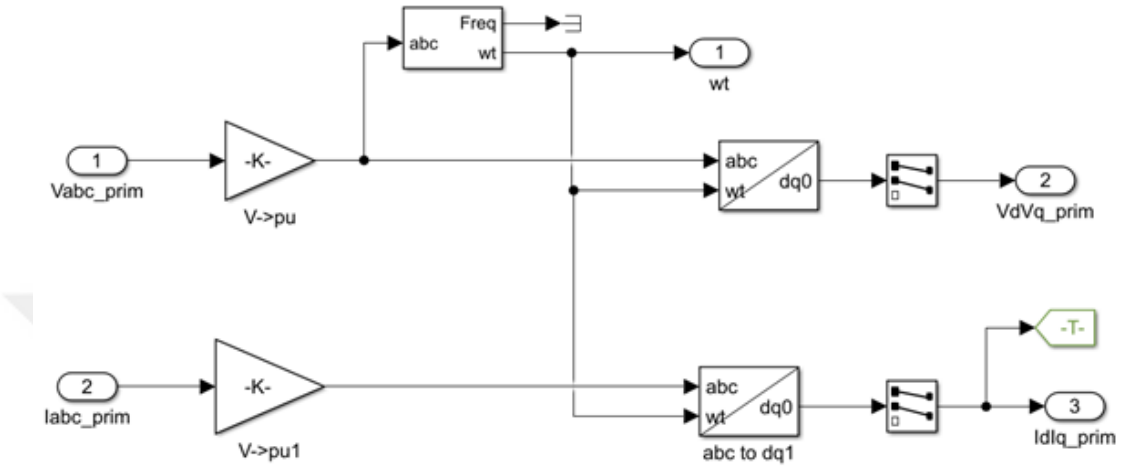

Figure 4.7. Phased Locked Loop and grid measurements in d-q axes.

Furthermore, Figure 4.8 presents the DC voltage control loop for the three-phase inverter.

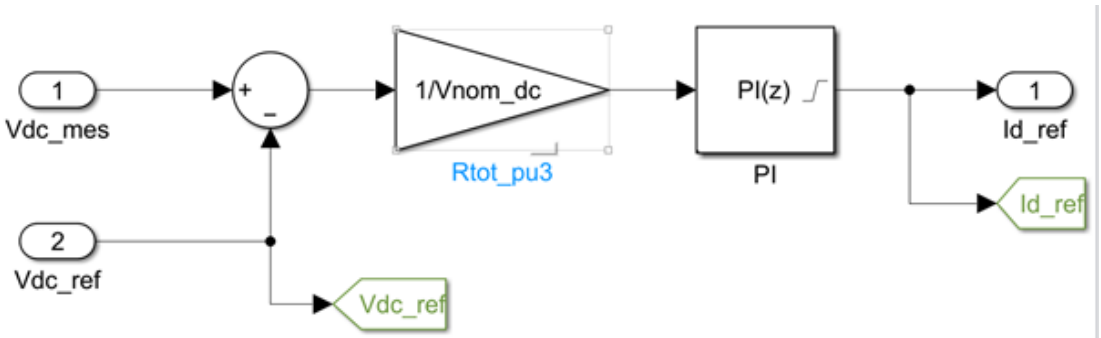

Figure 4.8. The DC voltage control loop for the 3-phase inverter.

The term "current control" refers to the process of regulating the active and reactive power that is commanded. As shown in Figure 4.9, the typical PI controller is utilized to change the current loops on the q and d axes.

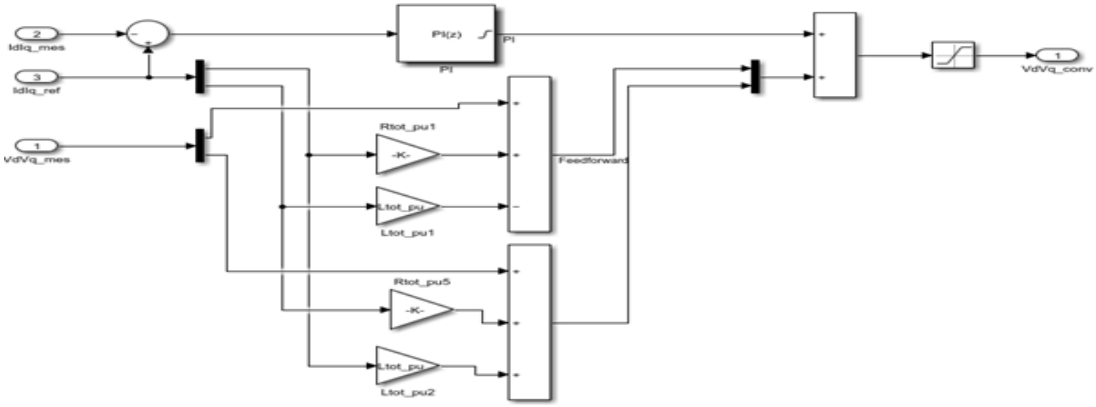

Figure 4.9. Current controller block diagram.

As displayed in Figure 4.10, the PWM three-level pulse generator is utilized to transform the current regulator's Vq and Vd voltage outputs into three modulating signals (Uref abc).

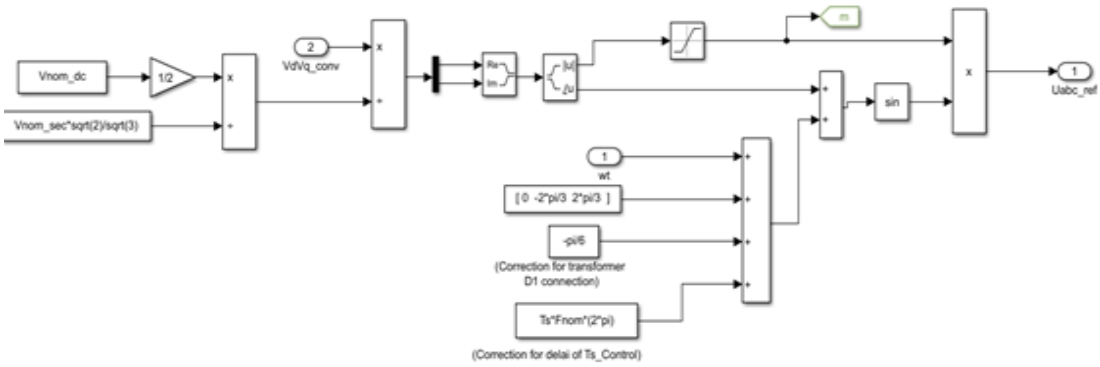

Figure 4.10. The 3-level PWM pulse generator.

The grid is represented as a synchronous generator driving a three-phase voltage source with a phase-to-phase RMS voltage of 25 kV, linked to the grid, as illustrated in Figure 4.11.

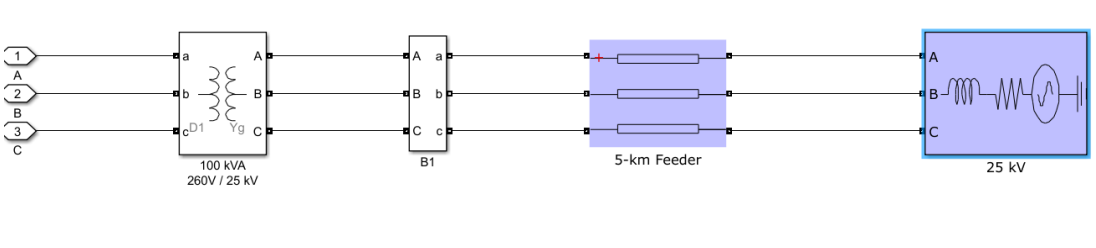

Figure 4.11. The unity grid at 25 kV.

4.4. SIMULATION RESULTS OF PV SYSTEM

The aforementioned specified PV system that was chosen was modeled to ensure that the design was proper and also to examine and evaluate its performance. In this regard, two PV systems were simulated, each with a different power rating. Figure 4.12 exhibits the first PV system, which has a power capacity of 25.205 kW, an output current of 115.2 A, and a boosted generated voltage of 218.8 Vdc. The other PV system contains four parallel PV arrays with the same features and quality as the first. In other words, four identical PV systems are interconnected in parallel, resulting in a total power capacity of 100.82 KW., a total output current of 460.2 A, and a voltage of 218.8 Vdc, as shown in Figure 4.13. From Figure 4.13 it is evident that the MPPT controller works efficiently, tracking the maximum voltage and fixing it at all encountered irradiation conditions. It is also obvious that the system delivers its rated power at the standard condition i.e., 1000 W/m^2 and 25 ℃.

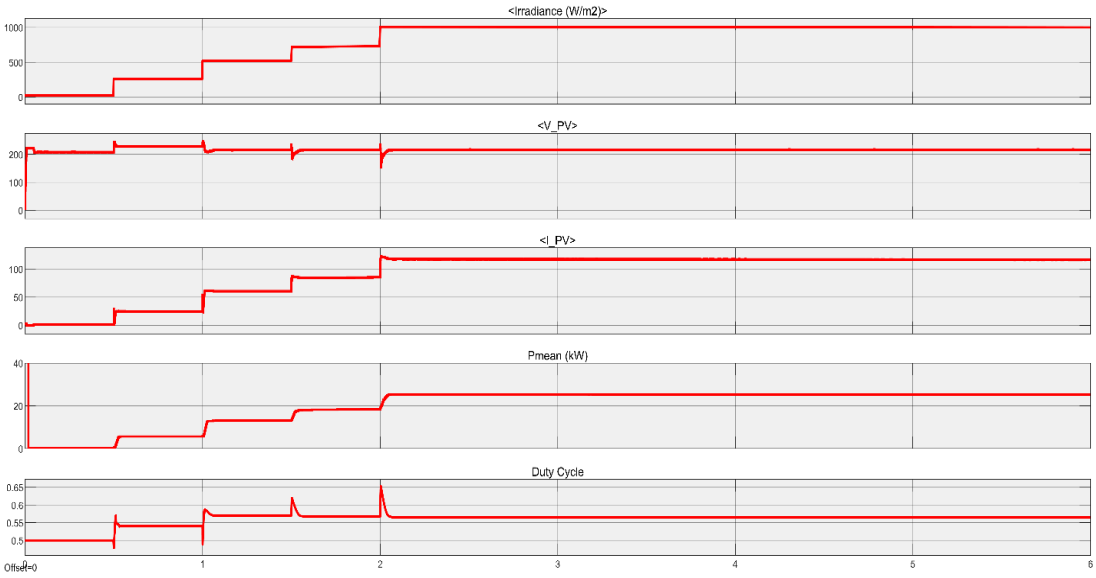

Figure 4.12. Output parameters for the 25 kW PV sub-system

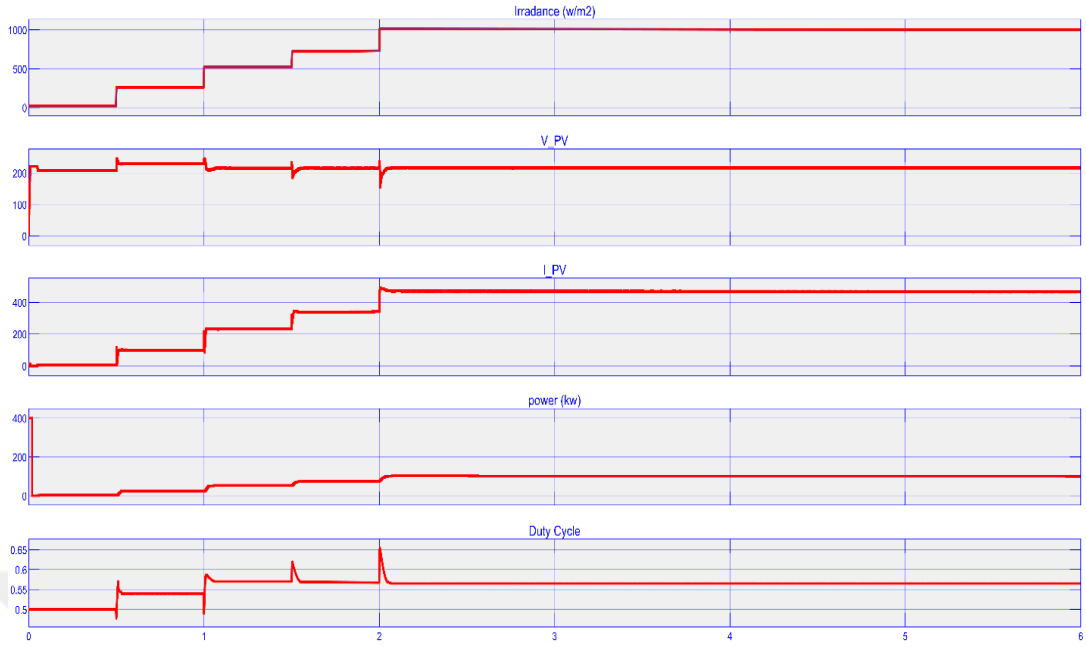

Figure 4.13. Output parameters for the 100 kW PV sub-system

4.5. SIMULATION RESULTS OF THE INVERTER BEFORE THE LC-FILTER

Based on the approach described in chapter three, the output voltage waveforms of the inverter are given in Figure 4.14. Va is labled by the black waveform, Vb represents the blue waveform, and Vc represents the red waveform. In Figure 4.14, the output of the Vabc voltages at the output terminal of the inverter which are measured directly before the LC filter. The Vab line to line 500 V (before the LC filter) is depicted in Figure 4.15.

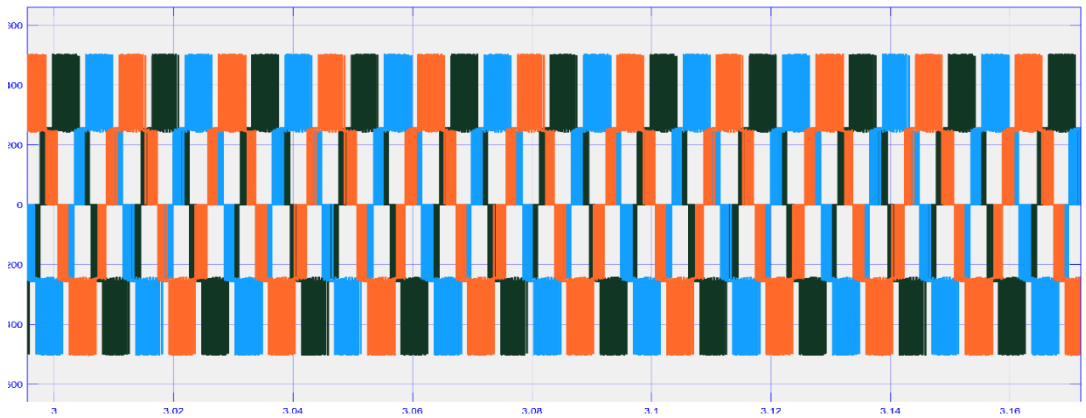

Figure 4.14. The output voltage of the inverter before the LC filter

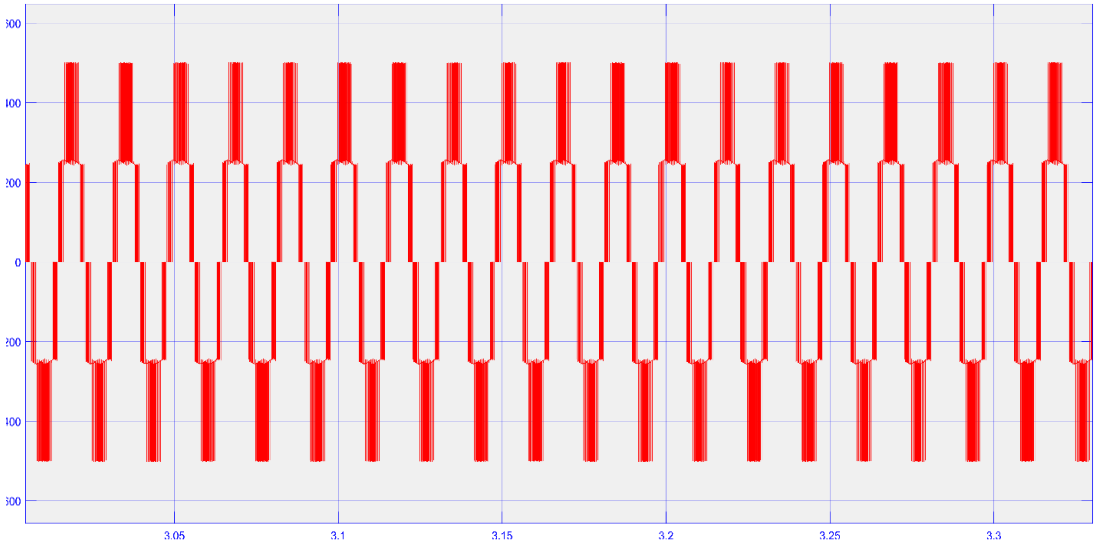

Figure 4.15. The line output voltage Vab of the inverter before the LC filter

Iabc represents the inverter output current waveforms, where Ia represents the black waveform, Ib is distinguished by the blue waveform, and Ic represents the red waveform. In Figure 4.16, the output of the Iabc voltages at the inverter's output terminal is measured immediately before implementing the LC filter, and the Iab before the LC filter is presented in Figure 4.17. The presence of harmonics is clear in both figures and this necessitates treatment.

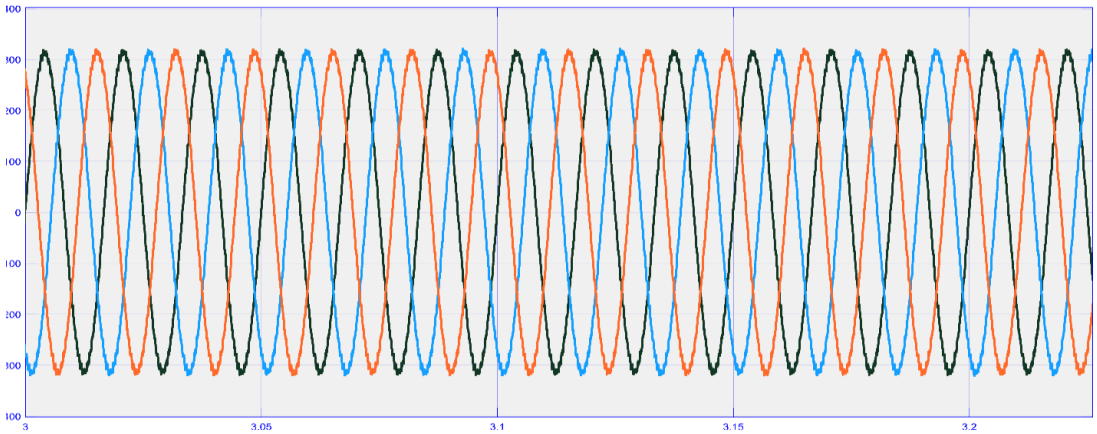

Figure 4.16. The output current of the inverter before the LC filter

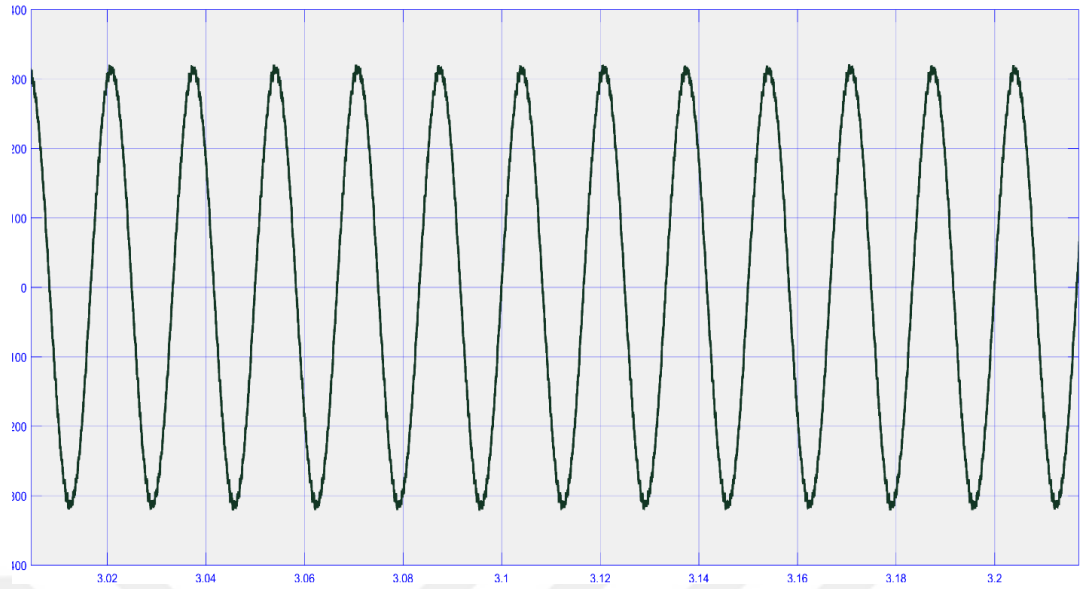

Figure 4.17. The per-phase output current of the inverter before the LC-filter

4.6. SIMULATION RESULTS OF THE INVERTER WITH THE IMPLEMENTATION OF THE LC-FILTER

The relatively high harmonic components causing ripples on the output voltage have been reduced and removed by the LC filter following the inverter. As a result, only fundamental lower-order harmonics are left over. Figure 4.18 depicts the Vabc waveform, and Figure 4.19 depicts the Vab after the inclusion of the LC-filter.

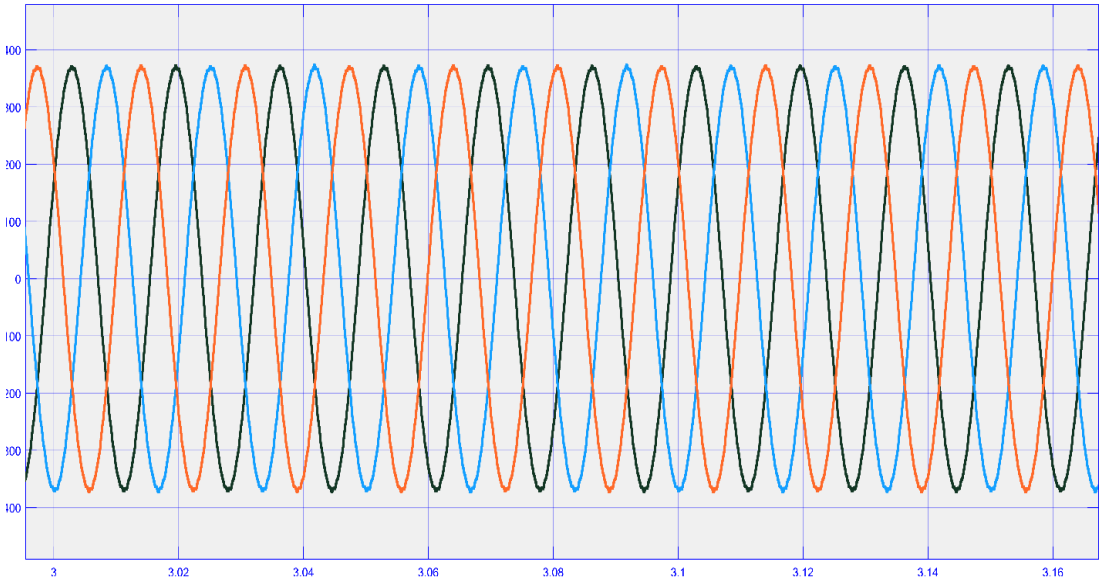

Figure 4.18. The output voltage of the inverter after the LC-filter

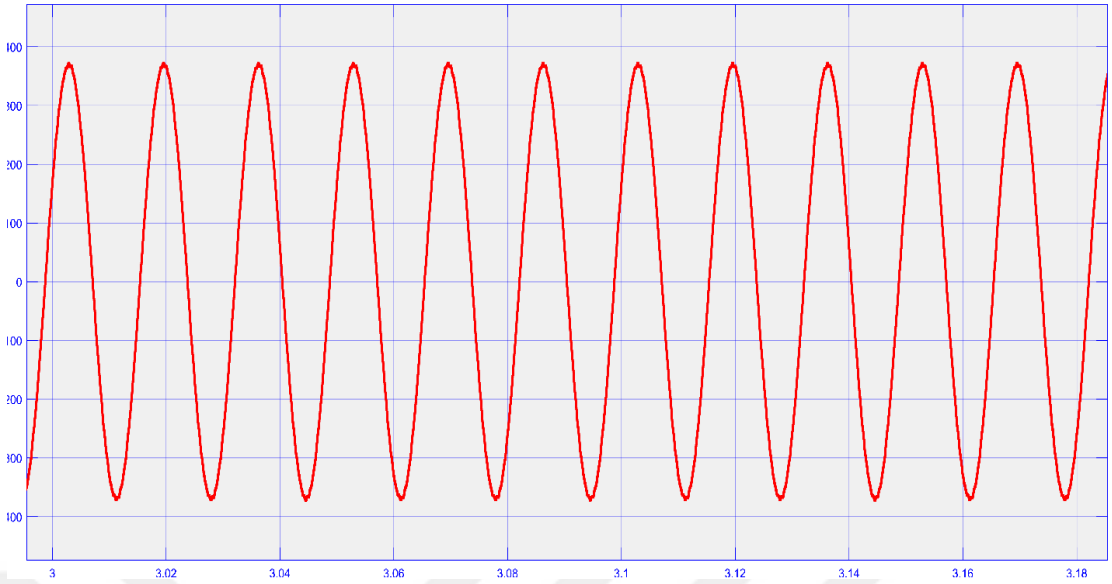

Figure 4.19. The per-phase output voltage of the inverter after the LC filter

The output three phase currents Iabc at the output terminal of the inverter in Figure 4.20 is measured immediately after the LC filter and shown in Figure 4.21 is the line current Iab after the intervention of LC filter.

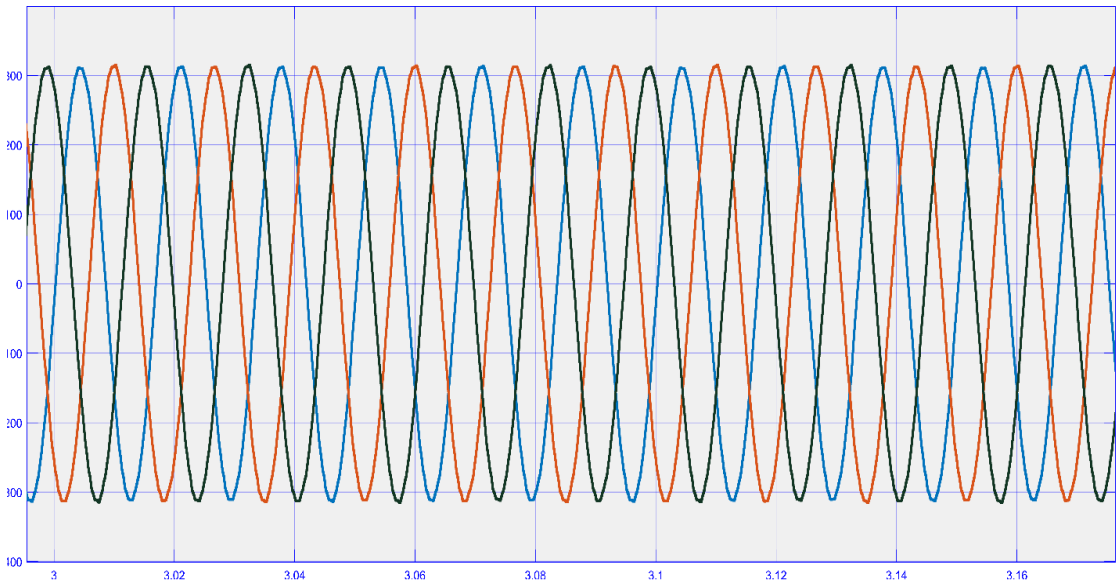

Figure 4.20. The output current Iabc of the inverter after the LC-filter

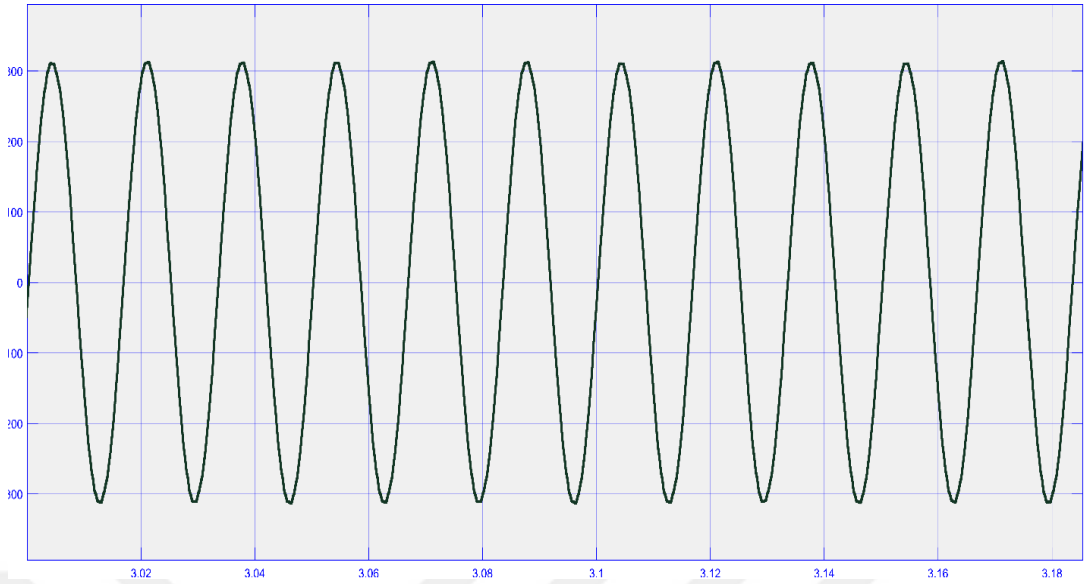

Figure 4.21. The per-phase output current Iab of the inverter after the LC filter

4.7. SIMULATION RESULTS OF THE LOADS

In this section, simulation results of two loads (linear and non-linear) are presented, where the linear load is 45 kW and the non-linear load amounts to 7 kW. The PV system operating temperature was fixed at 25 ^{o}C, and the load current and grid were analyzed for each of the previous cases.

4.7.1. Linear Load

In the first scenario, the amount of the real power supplied by the solar PV system is made greater than the corresponding amount required for the load, and in this case, the excess power is to be injected into the public grid when the value of solar radiation is at 1000 W/m^2. Figure 4.22 shows the power export from the solar system when the PV generator produces 100.67 kW; part of it satisfies the load (45 kW) while the rest is injected (54.25 KW) into the public grid. Figure 4.23, on the other hand, shows all the waveforms of the load current, the grid current, and the grid voltage. In addition, the spectral analysis of the linear load current is pictured in Figure 4.24 which appears as 0.36% for the THD. Figure 4.25 also shows the spectral analysis of the grid current which is found to be 1.35 %.

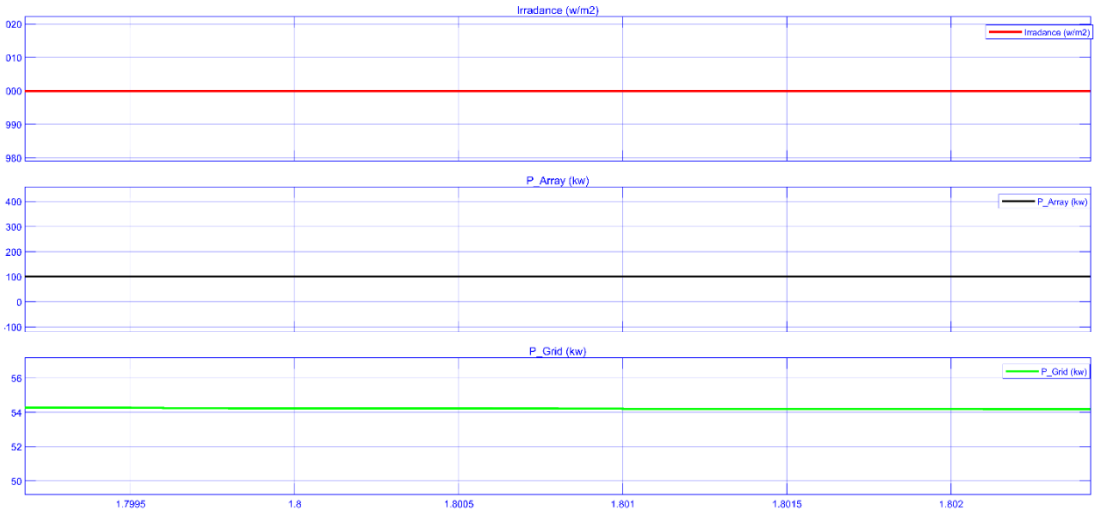

Figure 4.22. The active power from the solar panels and the power injected into the grid.

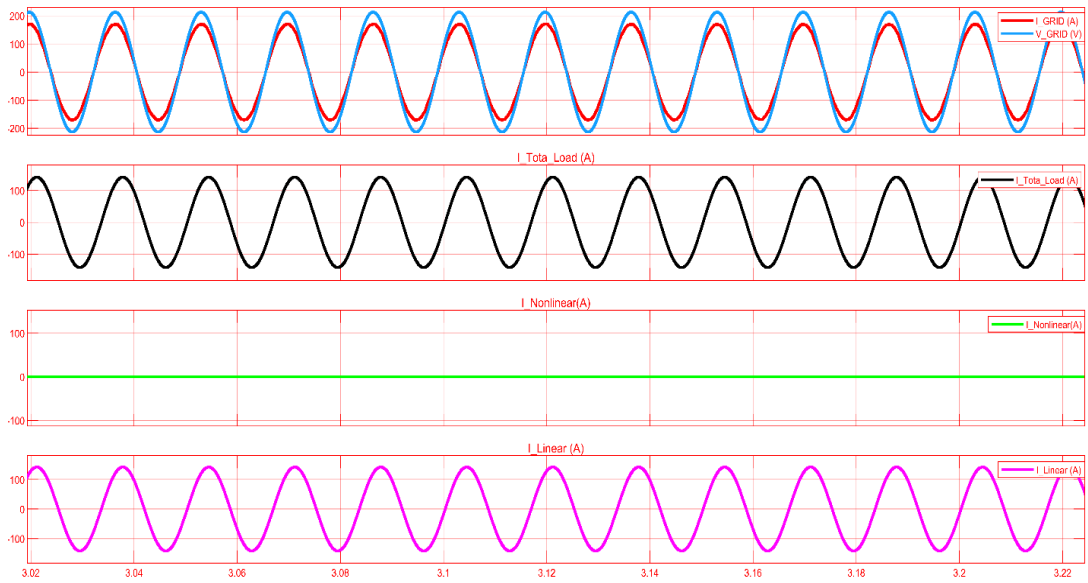

Figure 4.23. Waveforms of grid voltage (Vg), grid current (Ig), and Linear load current (ILL) at 1000 W/m^2.

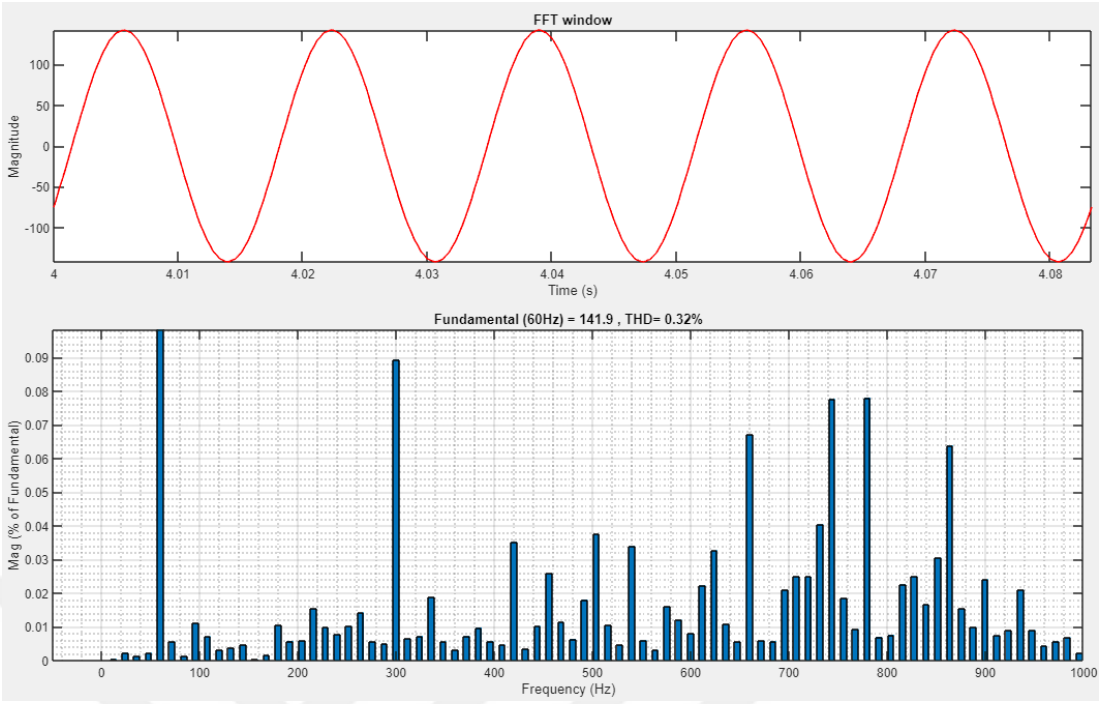

Figure 4.24. THD analysis linear load current (ILL) at 1000 W/m^2

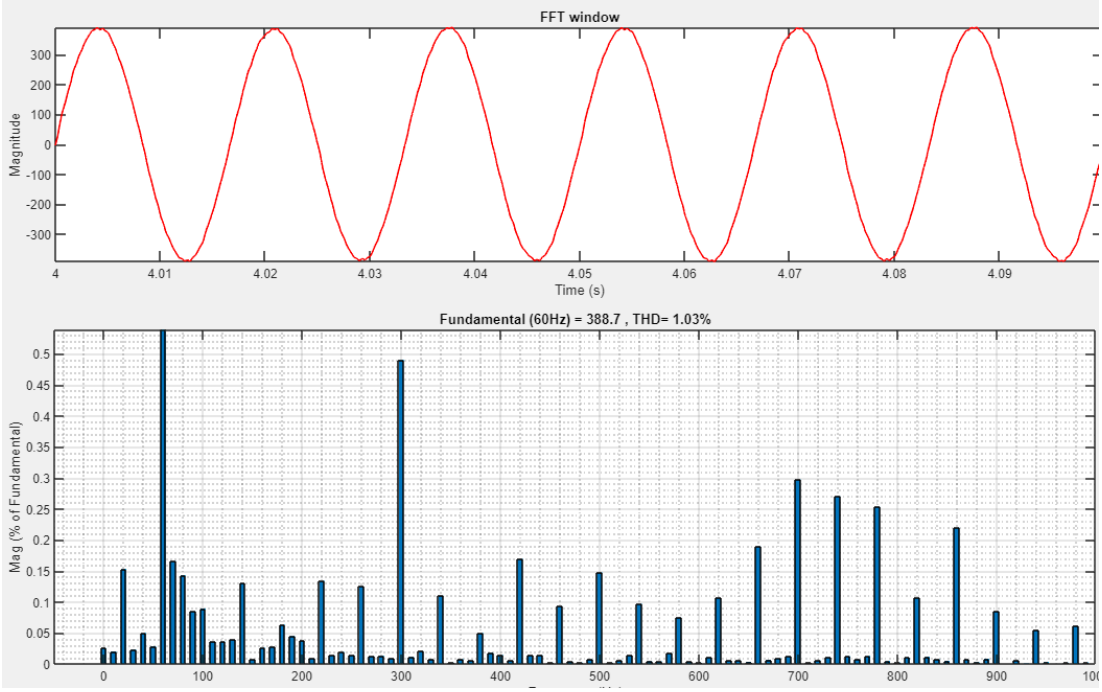

Figure 4.25. THD analysis for linear grid current (Ig) at 1000 W/m^2

In a second scenario, the value of the real power supplied by the solar system is equal to the amount of the linear load (45.67 kW), and power from or injected into the grid is zero, as shown in Figure 4.26 when the value of solar radiation reaches 457 W/m^2.

Figure 4.27 shows all the waveforms of the load current, the grid current, and the grid voltage; the grid current is observed to be negligible. Also, Figure 4.28 shows the spectral analysis of the linear load current which is found to be 0.32%.

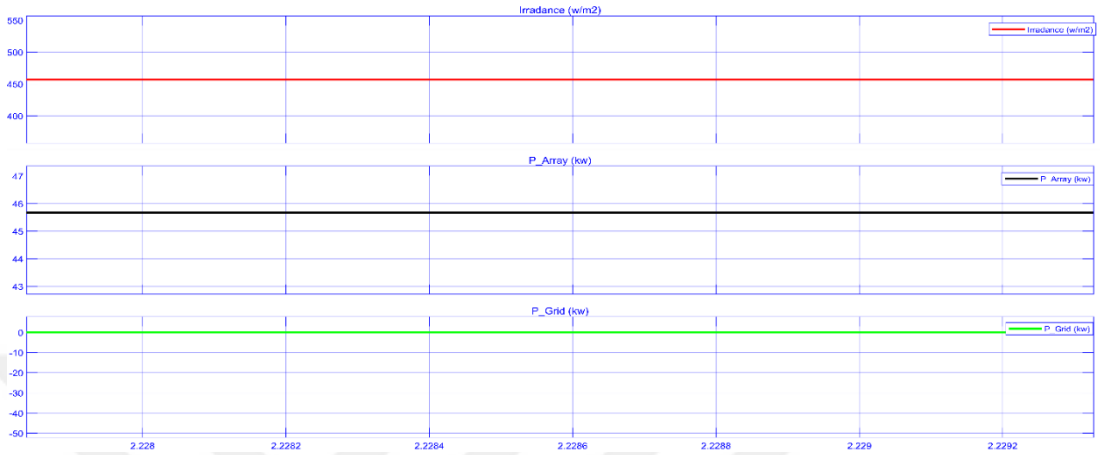

Figure 4.26. The active power from the solar panels and the power grid at an irradiance level of 457 W/m^2

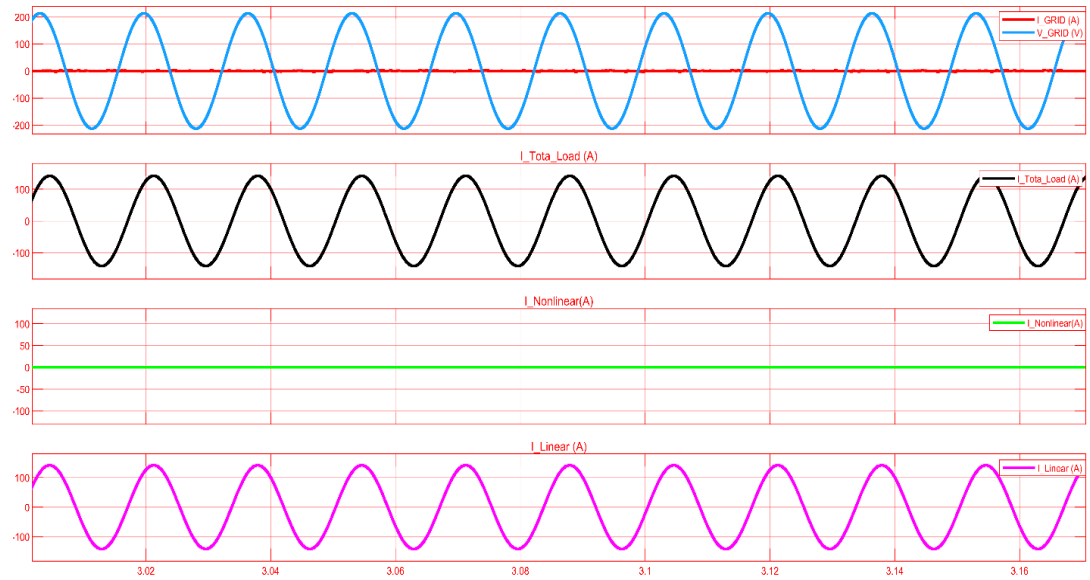

Figure 4.27. Grid voltage (Vg), grid current (Ig), and Linear load current (ILL) at 457 W/m^2

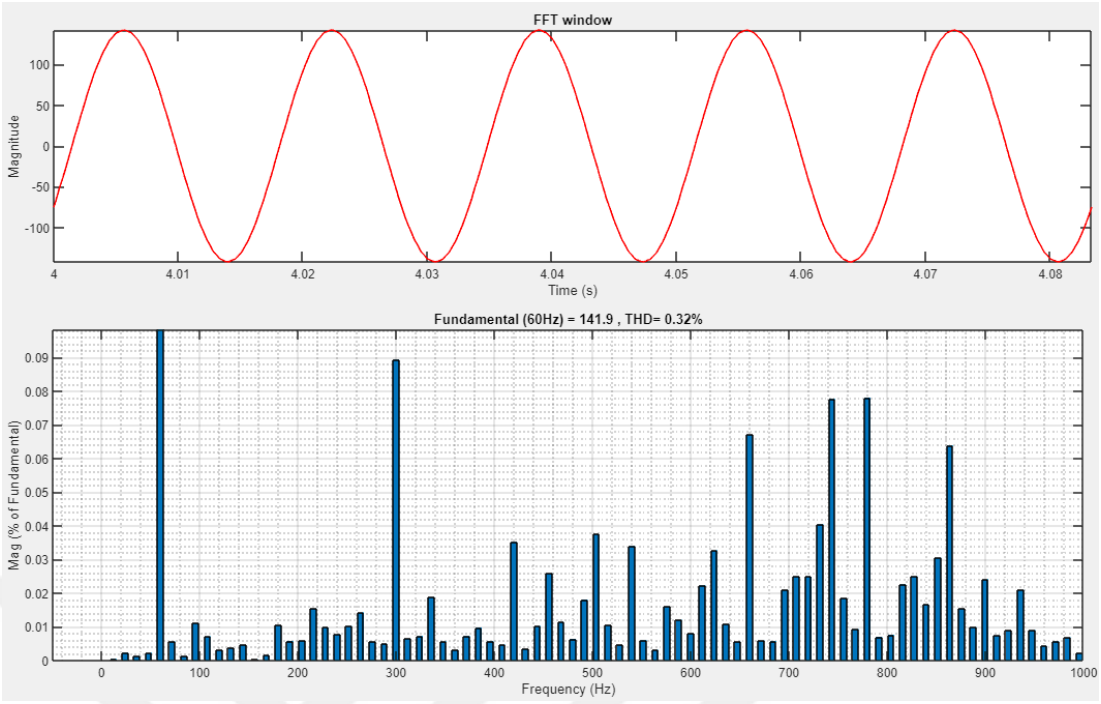

Figure 4.28. THD analysis for the linear load current (ILL) at 457 W/m^2.

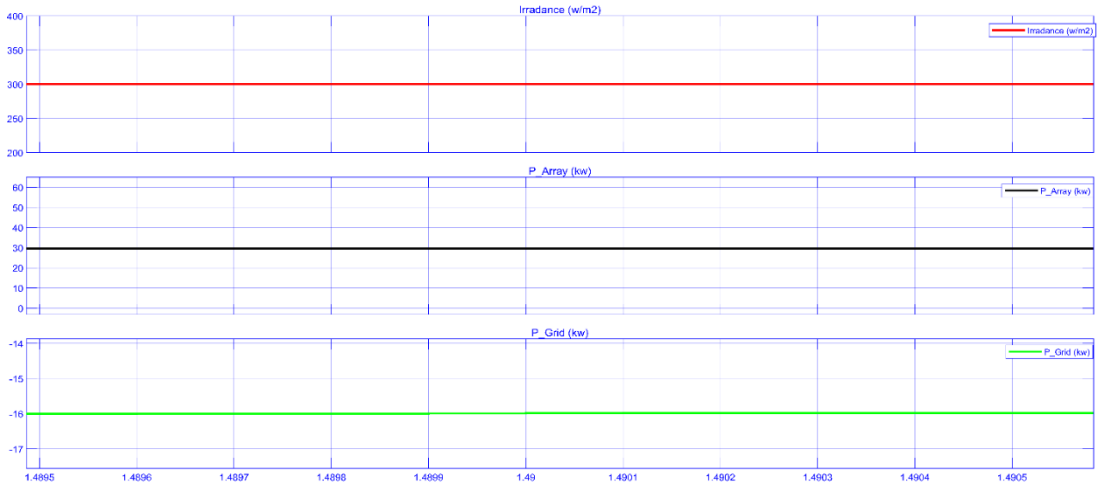

Figure 4.29. The active power from the solar panels and the power grid at 300 W/m^2.

In a third scenario, the solar system can supply real power of 29.56 kW, which is less than the value of the real power required for the load, so the grid complements the power that is required from the load (-16.05 kw), as visualized in Figure 4.29. This occurs when the value of solar radiation is 300 W/m^2. Figure 4.30 shows all the waveforms of the load current, the grid current, and the grid voltage. Similarly, In addition, the spectral analysis of the linear load current is pictured in Figure 4.31 which

appears as 0.32% for the THD. Figure 4.32 also shows the spectral analysis of the grid current which is found to be 3.47 %.

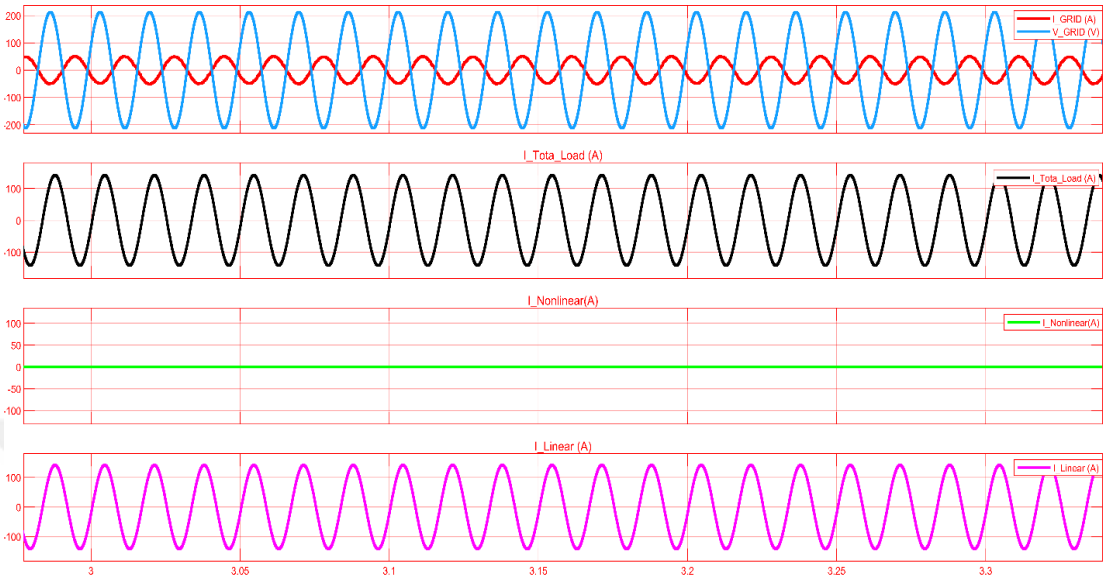

Figure 4.30. Waveforms for grid voltage (Vg), grid current (Ig), and Linear load current (ILL) at 30 W/m^2

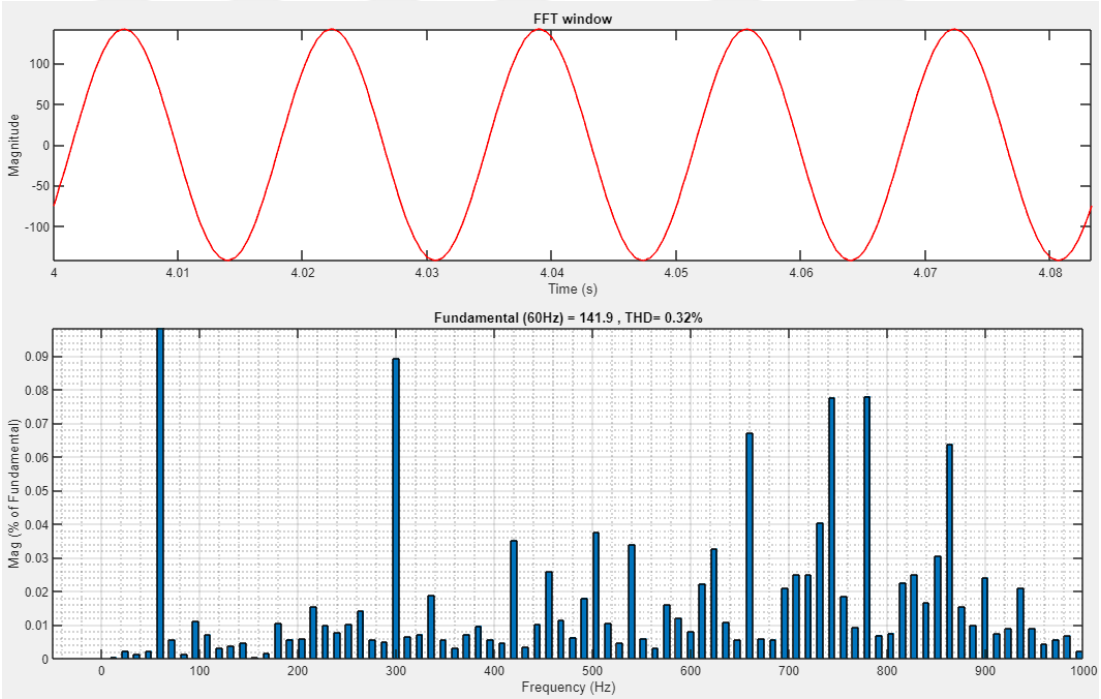

Figure 4.31. THD analysis for the linear load current (ILL) at 300 W/m^2

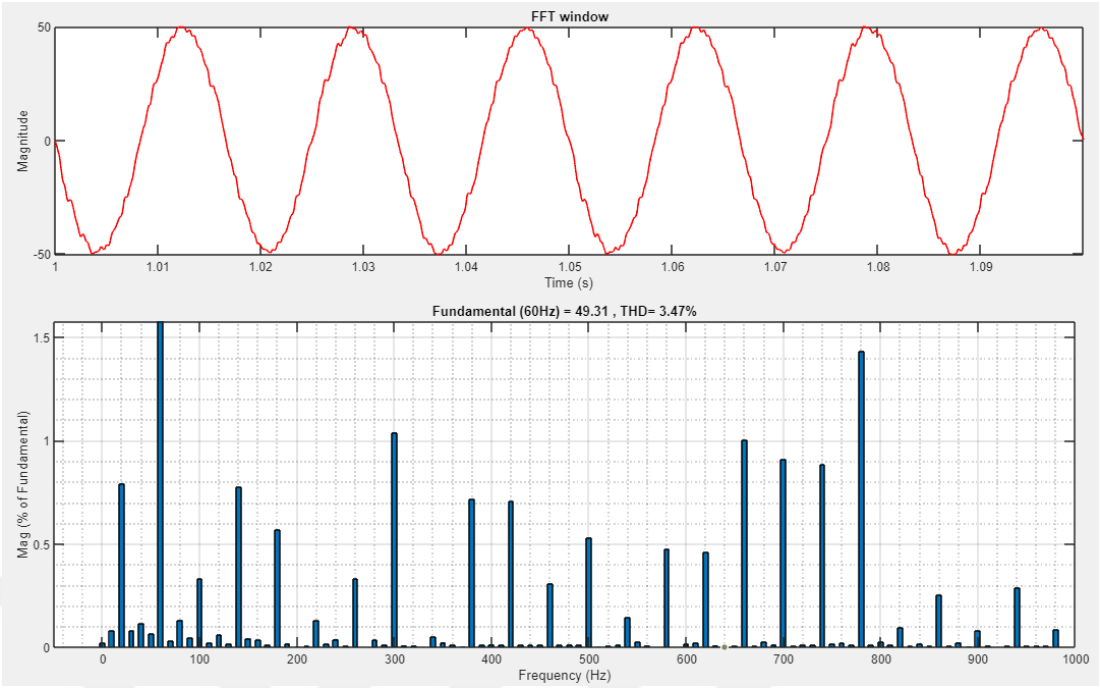

Figure 4.32. THD analysis for the linear grid current (Ig) at 300 W/m^2

In a forth simulated scenario, the solar PV system is unable to fulfil the real power of the load and the grid substitutes the active power to the load (-45.51 KW), as exhibited in Figure 4.33. The value of solar radiation coincides 0 W/m^2 at this condition. Figure 4.34 shows all the waveforms of the load current, the grid current, and the grid voltage. Also, Figure 4.35 shows the spectral analysis of the linear load current (0.27 %) while Figure 4.36 shows the spectral analysis of the grid current (found to be 0.99 %). The system exhibits good behavior via flexible dealing with changes in both the load and the intensity of the radiation, as the power factor is related to the alternating source current in all of the six examples indicated in table 4.1.

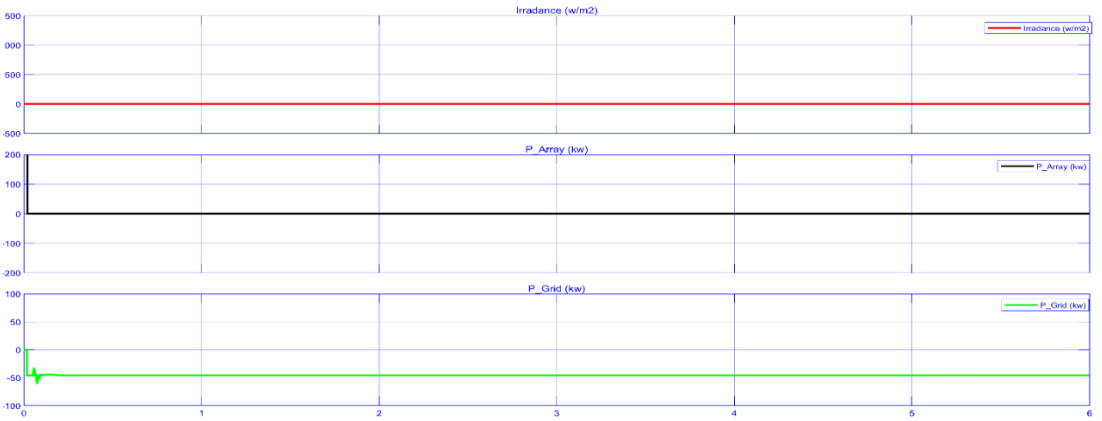

Figure 4.33. The active power from the solar PV generator and the power grid at 0 W/m^2

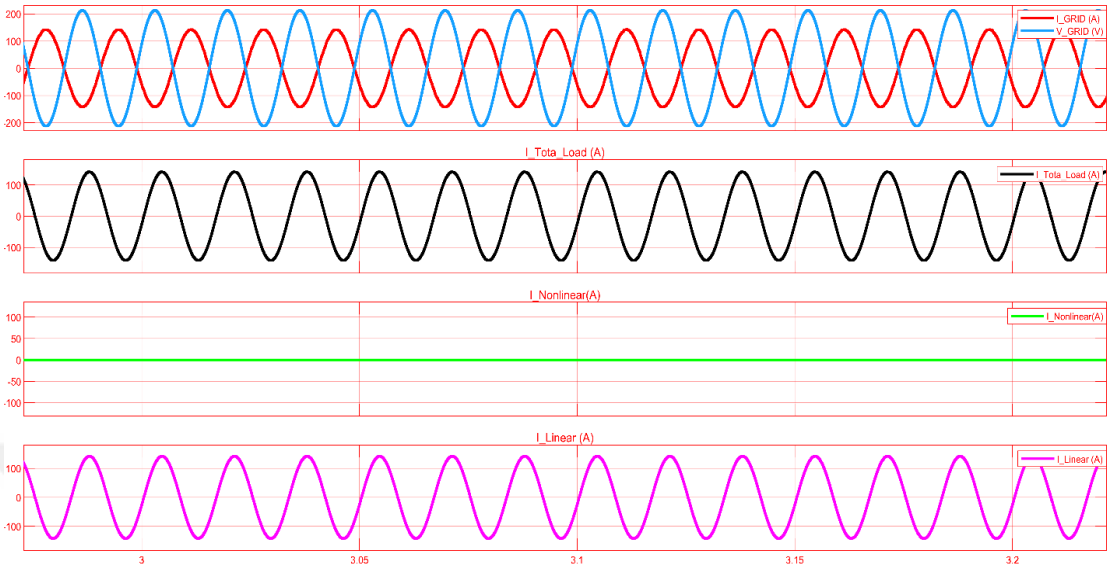

Figure 4.34. Grid voltage waveform (Vg), grid current (Ig), and linear load current (ILL) at 0 W/m^2

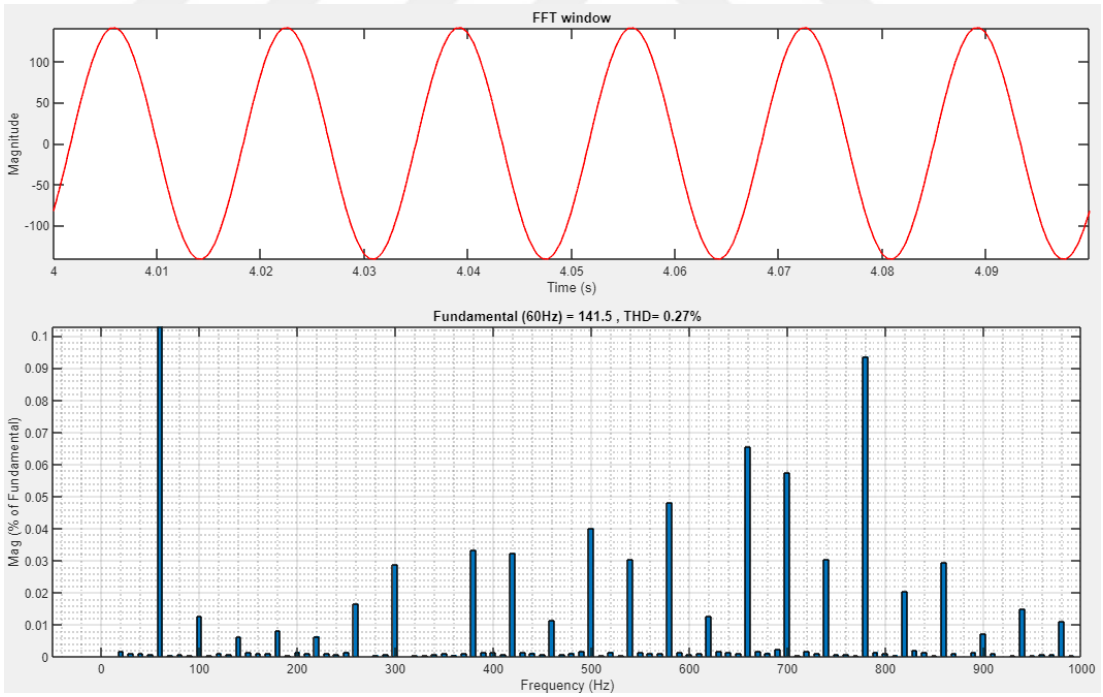

Figure 4.35. THD analysis for the(ILL) at 0 W/m^2

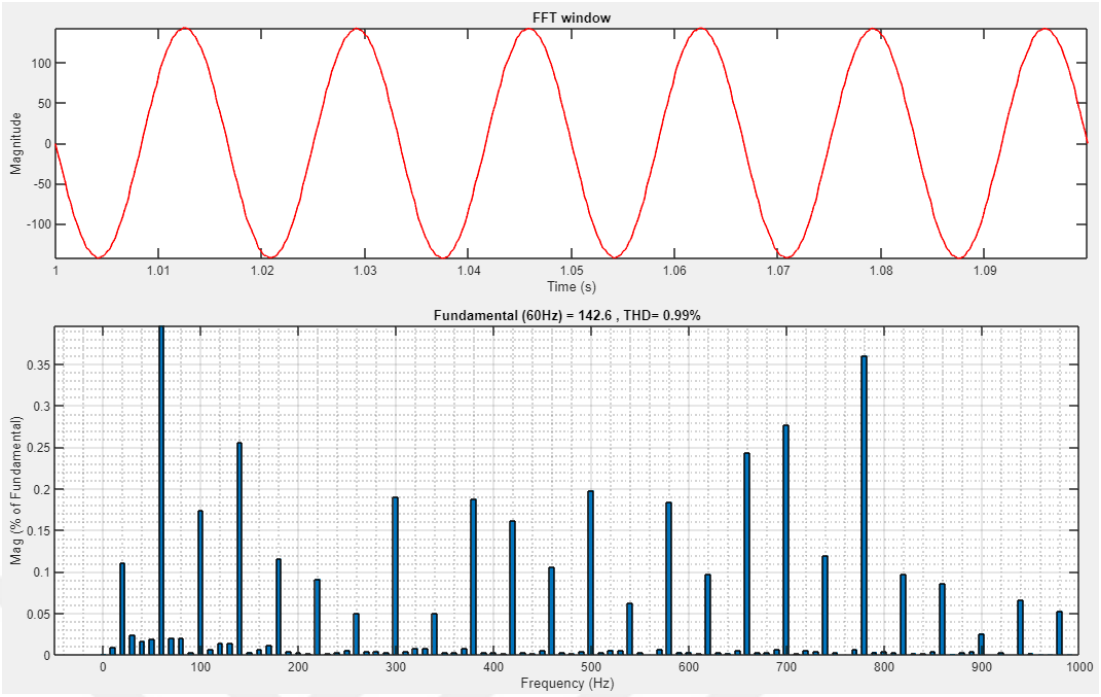

Figure 4.36. THD analysis for the linear grid current (Ig) at 0 W/m^2

Table 4.1. P.F for load and grid in the for many cases of linear load

Irradiace	1000	800	600	400	200	0
P.F_Grid	0.999	0.999	0.999	-0.999	-0.999	-0.999
P.F_Load	0.85	0.85	0.85	0.85	0.85	0.85

4.7.2. Non-Linear Load

At 1000 W/m^2 the value of the real power supplied by the solar system is greater than the value of the power delivered to the load, and in this case, the excess power is directly injected into the public grid. Figure 4.37 displays the power from the solar system where the panels generates (100.68 kW), part of it flows to the load (7 kW) while the rest is injected (92.79 kW) into the public grid. Figure 4.38 shows all the waveforms of the load current, the grid current, and the grid voltage. Figure 4.39 presents the spectral analysis of the linear load current, whilst figure 4.40 shows the spectral analysis of the grid current and also Figure 4.39 exhibits the spectral analysis

of the non-linear load current (0.76 %). Additionally, Figure 4.40 shows the spectral analysis of the grid current which has a THD of 1.21 %.

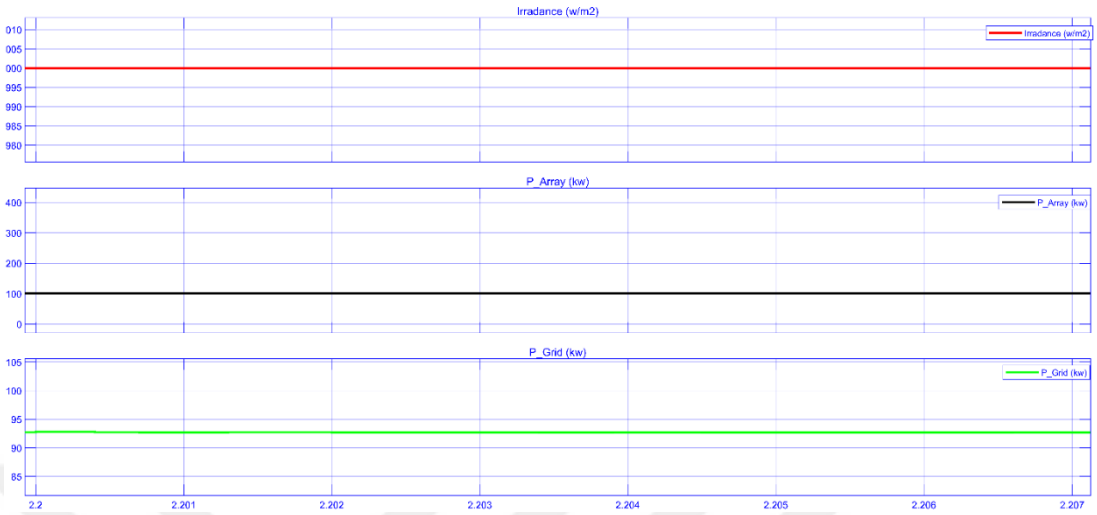

Figure 4.37. The active power from the solar panels and the power grid at 1000 W/m^2

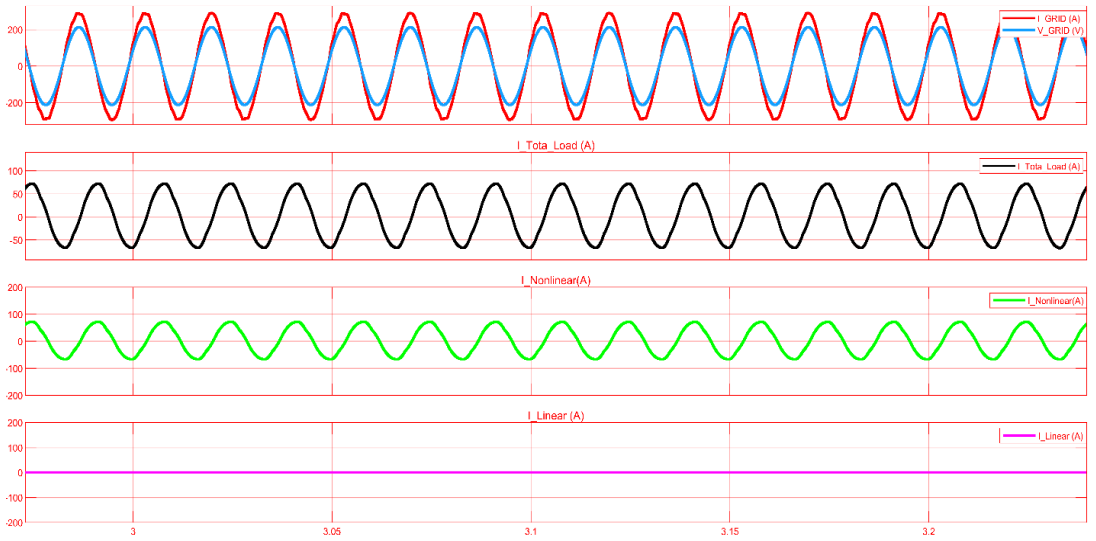

Figure 4.38. Grid voltage (Vg), grid current (Ig), and Non-Linear load current (INL) at 1000 W/m^2

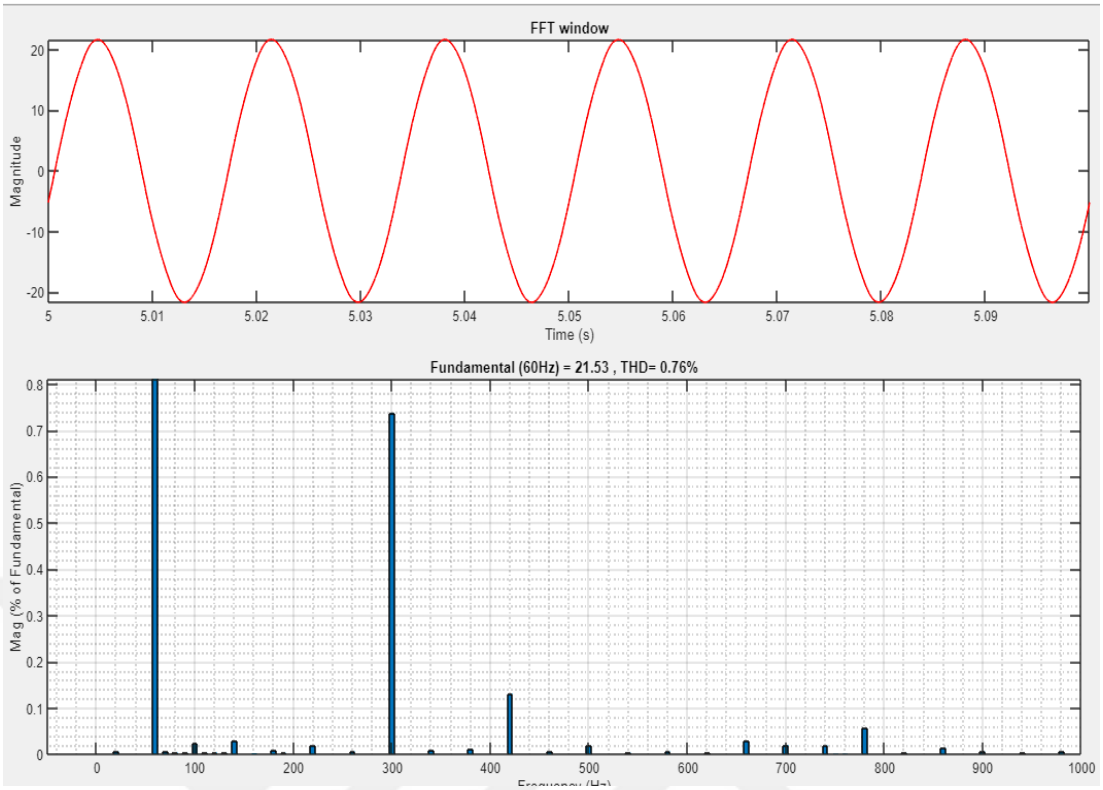

Figure 4.39. THD analysis for the Non-linear load current (INL) at 1000 W/m^2.

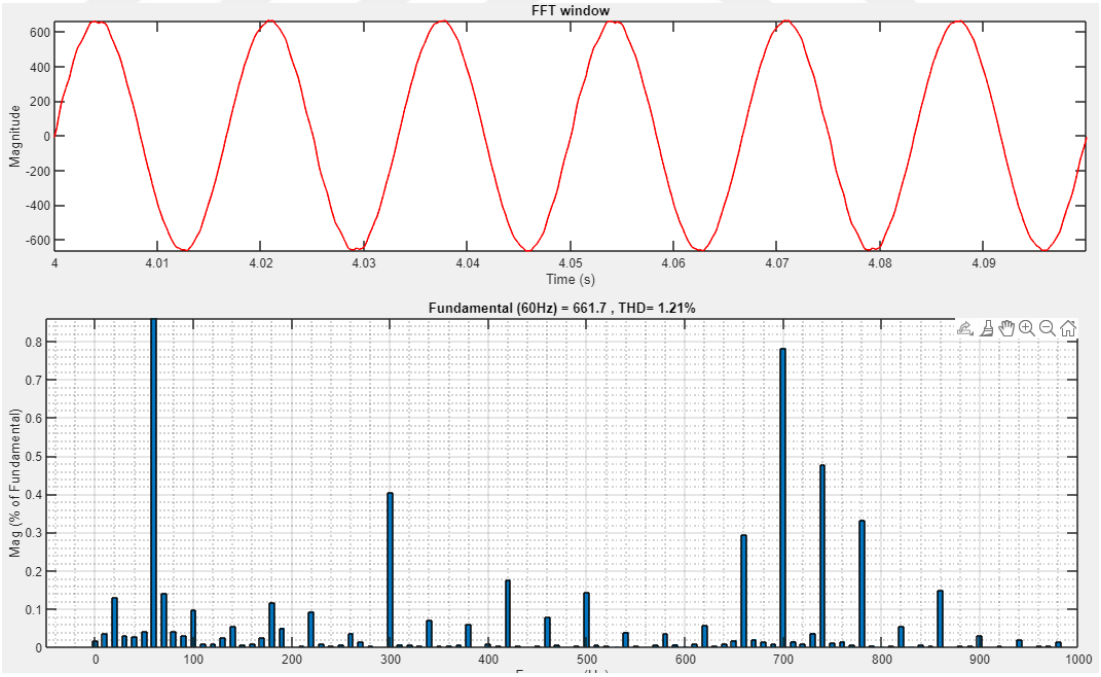

Figure 4.40. THD analysis for the Non-linear grid current (Ig) at 1000 W/m^2.

At 500 W/m^2, the solar PV system provides 50.05 kW, where part of the power goes to the non-linear load and the rest of the generated power (42.79 kW) is injected into

the utility grid, as seen in Figure 4.41. In Figure 4.42, shown is the waveforms of the load current, the grid current, and the grid voltage. Likewise, this corresponds to a solar radiation level of 500 W/m^2. Figure 4.43 exhibits the spectral analysis of the non-linear load current (0.79 %). Additionally, Figure 4.44 shows the spectral analysis of the grid current which has a THD of 1.73 %.

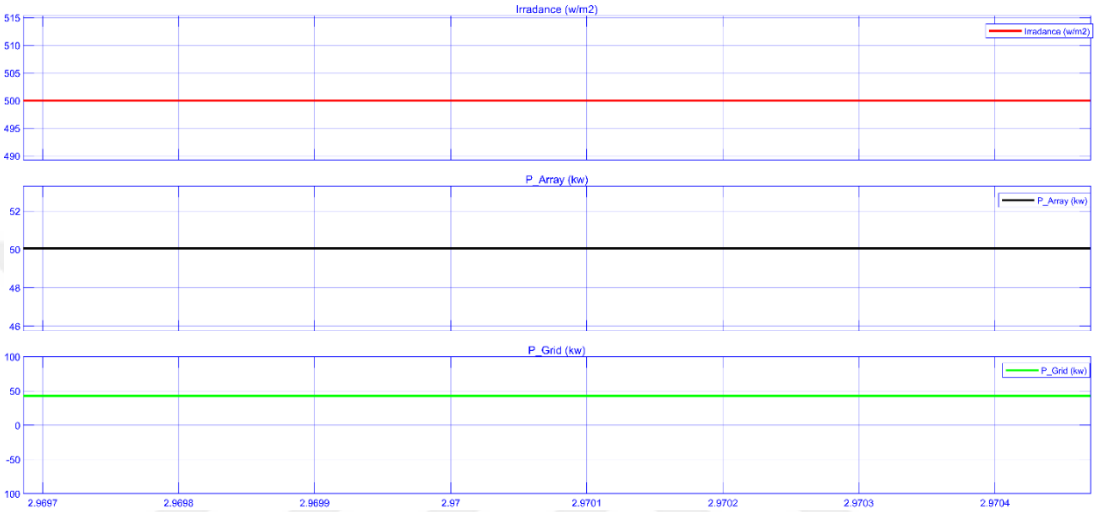

Figure 4.41. The active power from the solar panels and the power grid at 500 W/m^2.

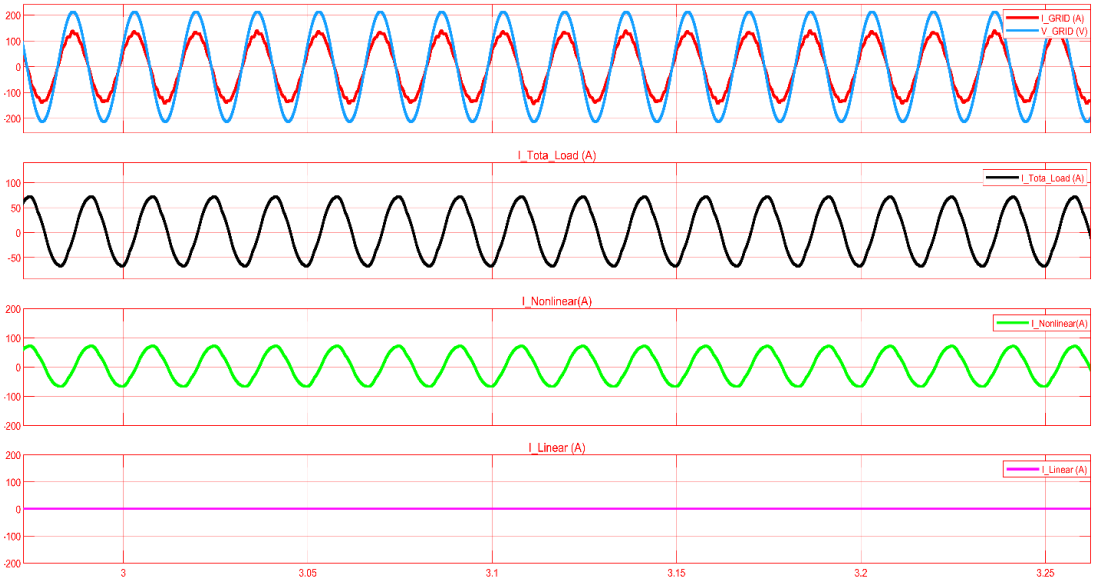

Figure 4.42. Grid voltage (Vg), grid current (Ig), and non-linear load current (INL) at 500 W/m^2.

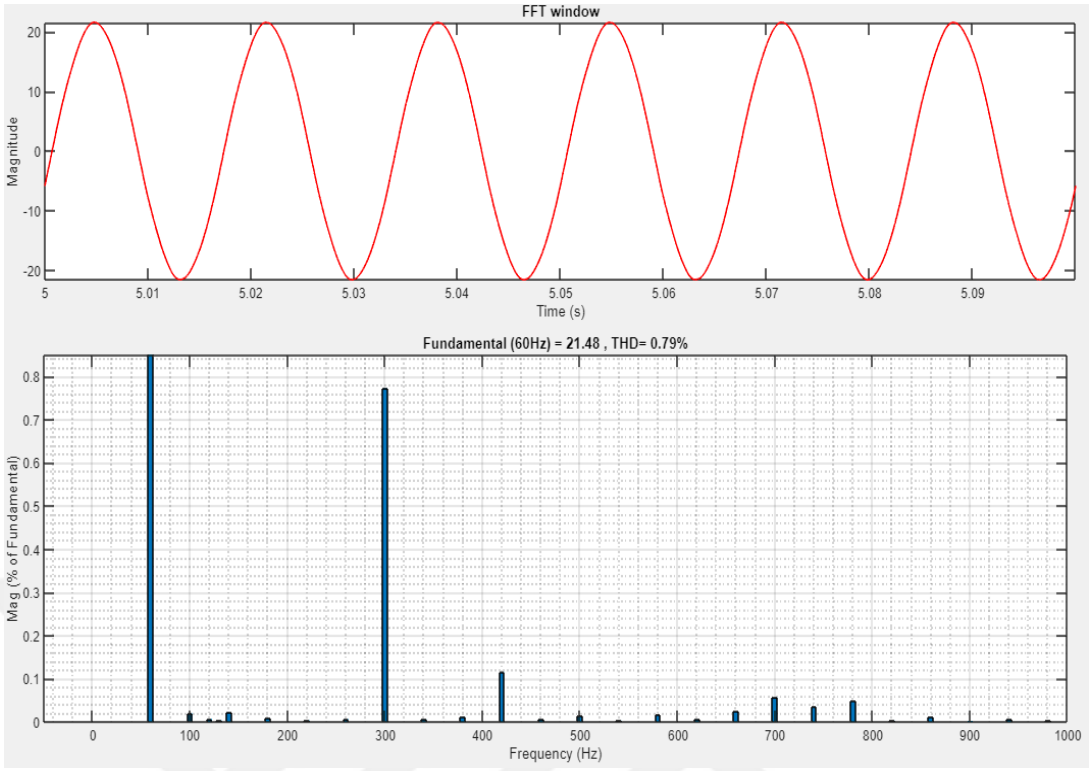

Figure 4.43. THD analysis for the non-linear load current (INL) at 500 W/m^2.

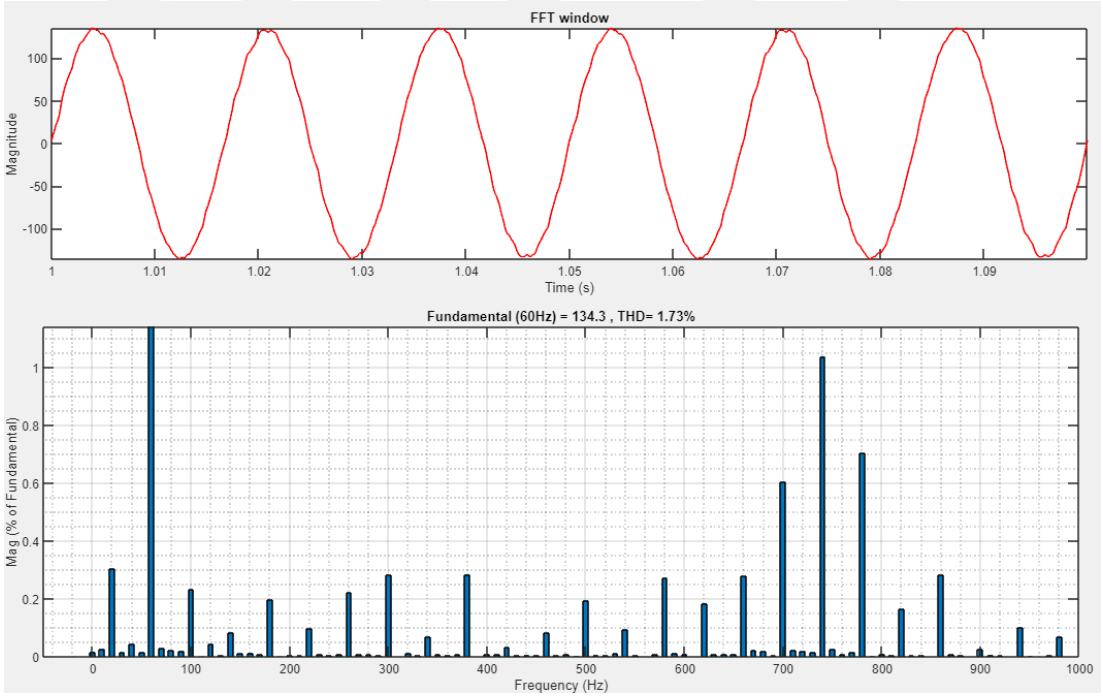

Figure 4.44. THD analysis for the non-linear grid current (Ig) at 500 W/m^2.

In another case, the solar system can supply real power amounts to 29.56 kW, where part of the power goes to the non-linear load (7.14 kW) and the remaining (22.45 kW)

is pushed into the utility grid, as drawn in Figure 4.45. This corresponds to a solar radiation level of 300 W/m^2. Figure 4.46 shows all the waveforms and Figure 4.47 exhibits the spectral analysis of the non-linear load current (0.78 %). Additionally, Figure 4.48 shows the spectral analysis of the grid current which has a THD of 3.51 %.

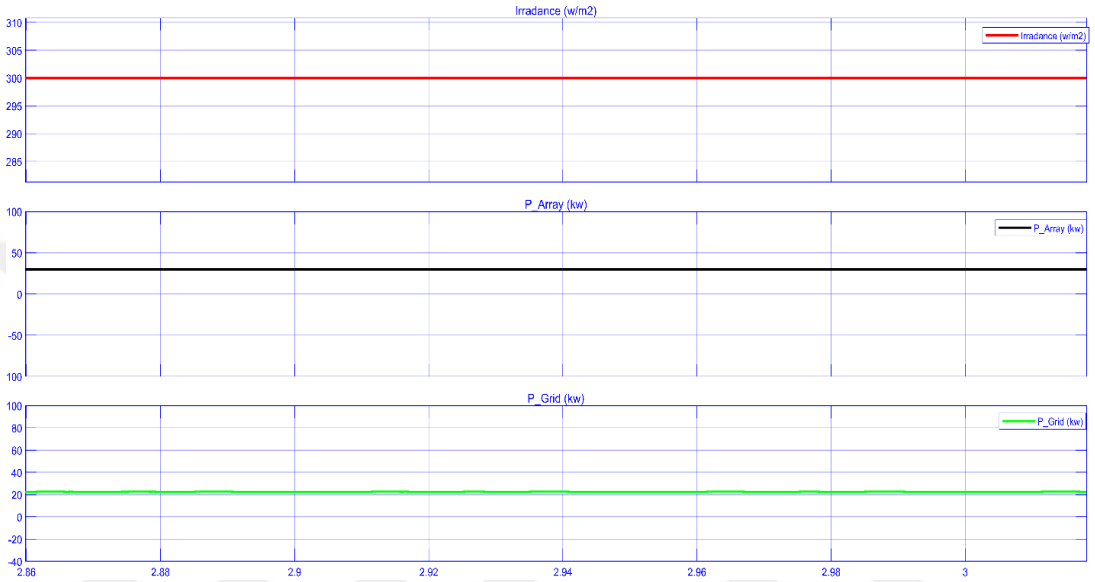

Figure 4.45. The active power from the solar panels and the power grid at 300 W/m^2.

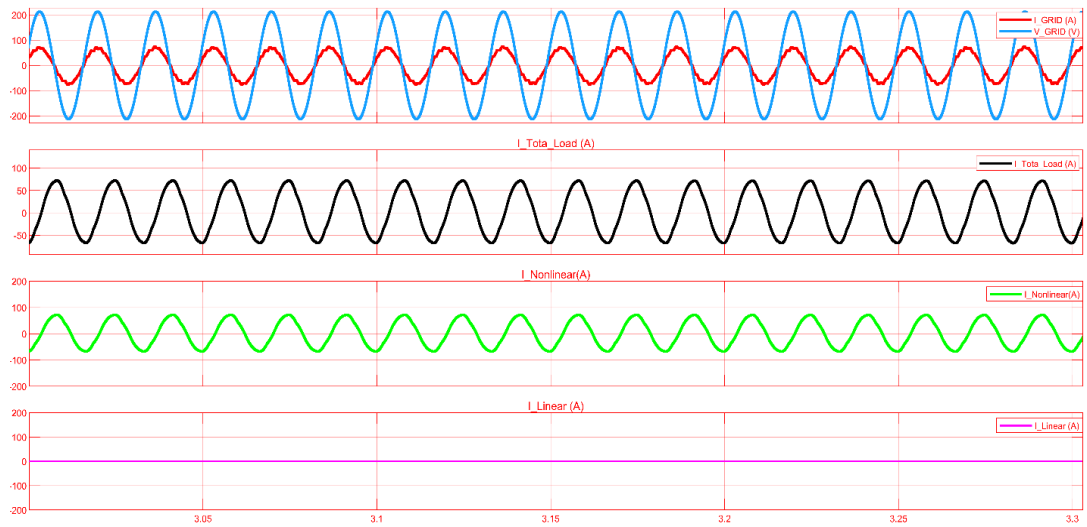

Figure 4.46. Grid voltage (Vg), grid current (Ig), and non-linear load current (INL) at 300 W/m^2.

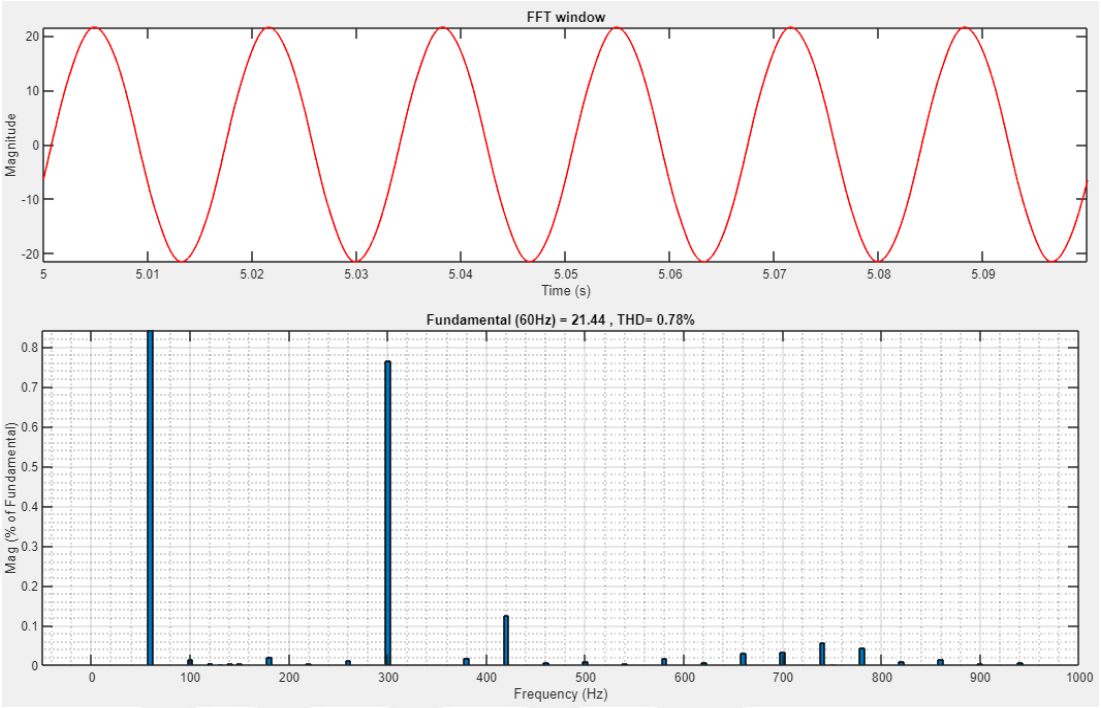

Figure 4.47. THD analysis for the non-linear load current (INL) at 300 W/m^2.

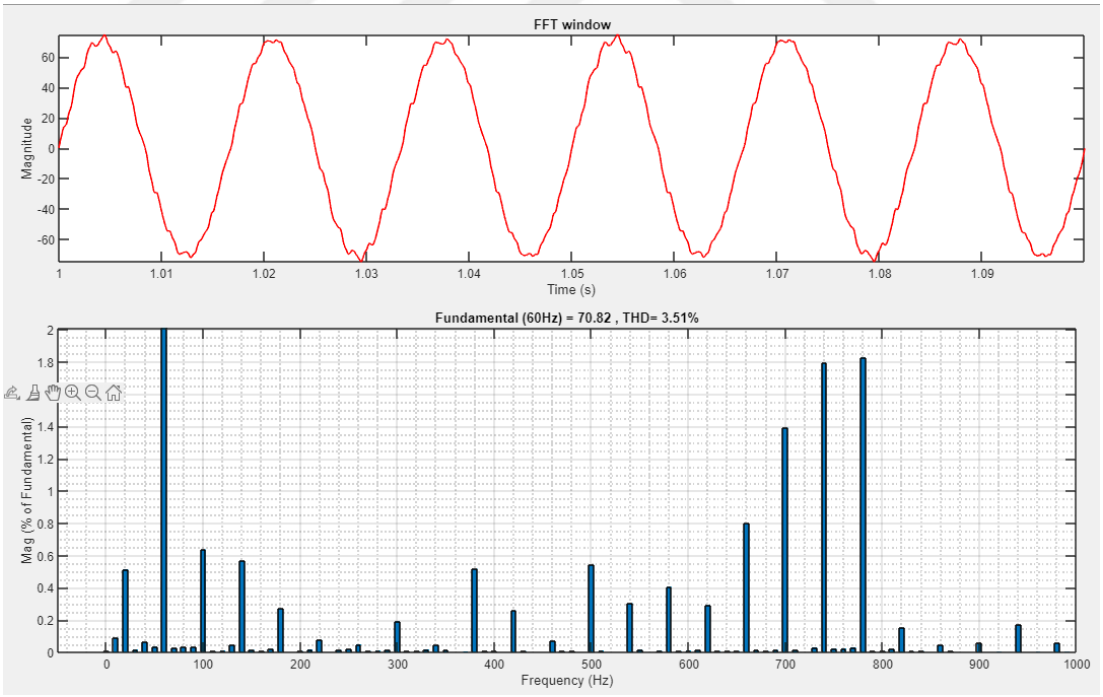

Figure 4.48. THD analysis for the non-linear grid current (Ig) at 300 W/m^2.

In a different scenario, the amount of real power supplied by the solar system is zero. The non-linear load imports power from the grid (7.01 kW), as elaborated in Figure 4.49. This coincides a solar radiation of 0 W/m^2. Figure 4.50 shows all the waveforms of the load current, the grid current, and the grid voltage. In addition, the spectral analysis of the non-linear load current is pictured in Figure 4.51 which appears as 0.36% for the THD.

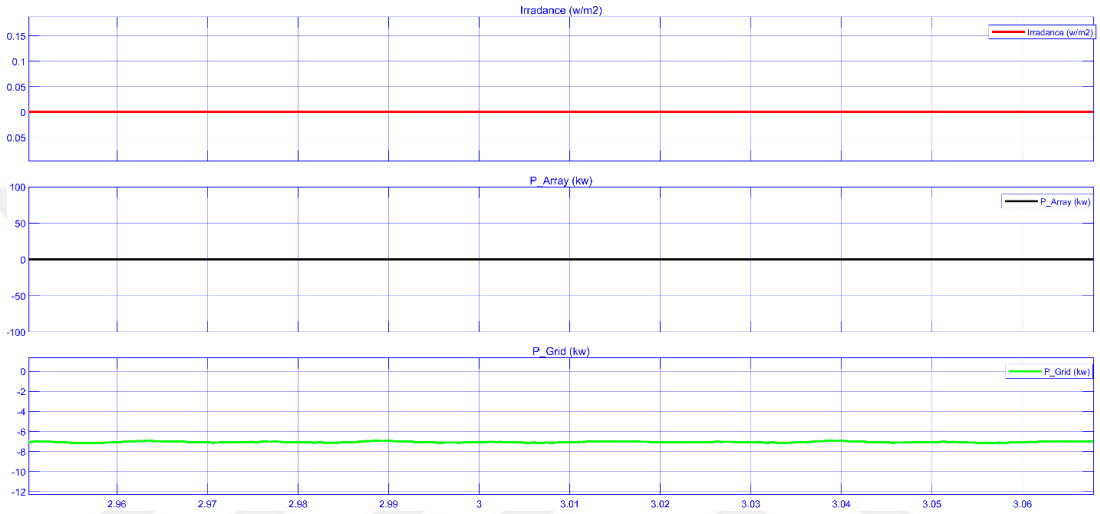

Figure 4.49. The active power from the solar panels and the power grid at 0 W/m^2.

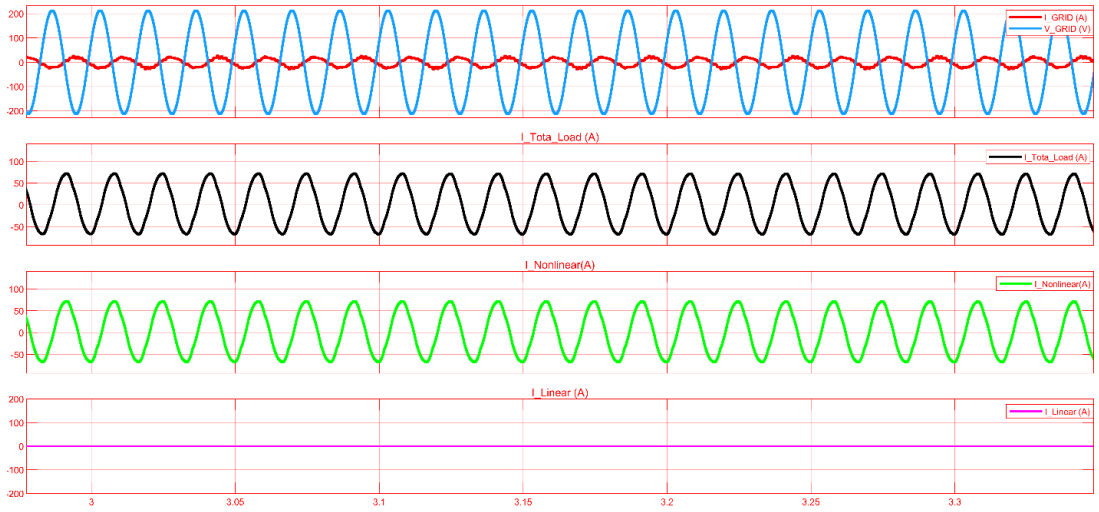

Figure 4.50. Grid voltage(Vg), grid current(Ig), and non-Linear load current (INL) at 0 W/m^2.

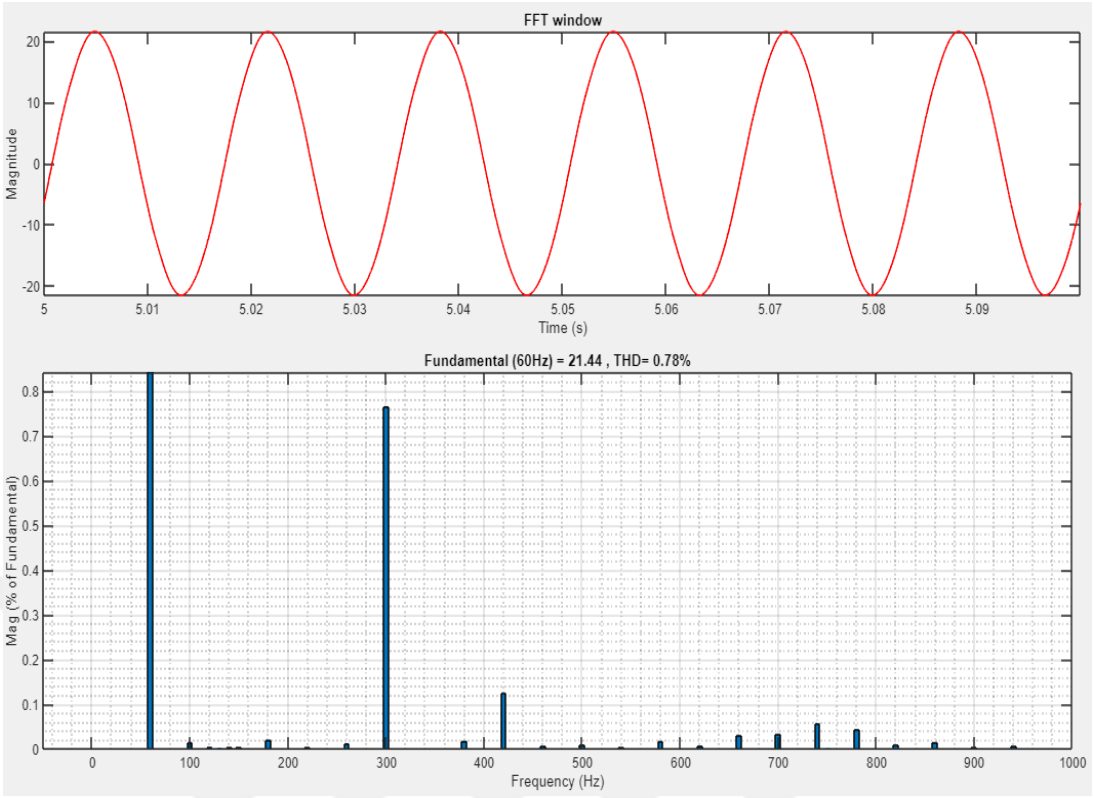

Figure 4.51. THD analysis for the non-linear load current at 0 W/m^2.

By observing the results of the representation, it turns out that the system shows a good behavior through flexible handling with the change of both the load and the intensity of the radiation, as the power factor is relative to the AC current in all the size cases that were represented as shown in the table 4.2.

Table 4.2. P.F for load and grid in the for many cases of non-linear load

Irradiace	1000	800	600	400	200	0
P.F_Grid	0.999	0.999	0.999	0.999	0.999	-0.999
P.F_Load	0.85	0.85	0.85	0.85	0.85	0.85

PART 5

CONCLUSION AND FUTURE WORKS

This chapter presents the most important conclusions that have been reached by studying the exploitation of the smart modulator of the solar cell system to enhance the source of alternating current. It also presents the ideas that crystallized after completing the thesis, which could be future works that could be accomplished by subsequent researchers based on the idea of this thesis.

5.1. CONCLUSION

Through the results that we obtained from the system using the Matlab program and the cases that we dealt with through the change of load, as well as through the cases we imposed from the change in the intensity of solar radiation, as the distortion rate in the source stream was less than 5%, as well as the distortion rate in the source current for linear load and load linear.

The first PV system, seen in Figure 4.12, has a power capacity of 25.205 kW, an output current of 115.2 A, and a boosted produced voltage of 218.8 Vdc. The second PV system is made up of four parallel PV arrays with the same features and quality as the first. In other words, four identical PV systems are linked in parallel to provide a total power capacity of 100.82 KW, a total output current of 460.2 A, and a voltage of 218.8 Vdc, as illustrated in Figure 4.13. Figure 4.13 shows that the MPPT controller functions efficiently, tracking the maximum voltage and fixing it under all irradiation circumstances encountered. It is also obvious that the system delivers its rated power at the standard condition i.e., 1000 W/m^2 and 25 ℃.

In the case of a linear load, and when the value of the solar radiation falling on the panels is 1000 W/m^2, where we notice from the Figure 4.22 that the solar panels

operate at the highest energy, producing 100.67 kW, where 45.42 kW of them go to the load, and the rest 54.25 kW is injected into the public network also note in the figure that the spectral analysis of the source current and the load current, where their value is less than 5%. In the other case of linear load, note that the solar system provides the load only with the real power, as it produces only 45.67 kW when the solar radiation is 457 W/m^2, as shown in Figure 4.26 and in this Figure 4.28, notice that the distortion rate in the load current is less than 5% and the grid current is zero. In the following Figure 4.29, the solar energy system and the grid share in supplying the load with energy, as the first supplies 29.56 kW and the second supplies the rest of the load's needs -16.05 kW in this case, the value of solar radiation is 300 W/m^2.In the case when the solar system is unable to produce energy when the solar radiation is 0 W/m^2, where the grid works to supply the load with energy as shown in Figure 4.33.

In the case of a non-linear load, when the intensity of solar radiation is 1000 W/m^2, 500 W/$m^{2,}$ and 300 W/m^2, where the solar system operates at maximum power, where the solar system supplies the load with energy, and the remainder is injected into the public grid as shown in the Figure 4.37, Figure 4.41, and Figure 4.45. In another case, the solar system is unable to produce energy when the intensity of solar radiation is 0 W/m^2, so the grid supplies the load with energy. Also, the distortion of the sine waves of the load current and the source current is less than 5% as shown in Figure 4.39, Figure 4.40, Figure 4.43, Figure 4.44, Figure 4.47, and Figure 4.48. In the case of linear load as shown in the Table 4.1, the value of the power factor for the source current in all the case is 0.999 and the load current is not less than 0.85. In the case of linear load as shown in the Table 4.2, the value of the power factor for the source current in all the case is 0.999 and the load current is not less than 0.85.

5.2. FUTURE WORKS

There is a set of future work for researchers that can be carried out in the field of exploiting the solar cell system to enhance the source of alternating current, based on the idea of this thesis, which is:

1. The possibility of addressing the imbalance of loads to maintain the stability of the electrical network.
2. Developing the system to deal with the instantaneous disturbance in the voltage due to the sudden change of the loads.
3. Study the behavior of the proposed system in the event of a fault in the electrical network system.
4. The possibility of using other new energies, such as wind energy, for example.
5. Using a Cuk DC-DC converter instead of Boost to gain maximum power point in the solar cell system.
6. Use a multi-level inverter to match network and transmission line voltages, such as 9-level, for example.

REFERENCES

1. Simonsen, S. O., "Development of a Grid Connected PV System for Laboratory Use", ***Master's thesis, Institute for Elkraftteknikk,*** 22-27 (2009).

2. Almaktar, M., & Shaaban, M., "Prospects of renewable energy as a non-rivalry energy alternative in Libya", ***Renewable and Sustainable Energy Reviews,*** 143: 110852. (2021). https://doi.org/10.1016/j.rser.2021.110852

3. Rajab, Z., Almaktar, M., Al-Naily, N., Saad, S. M., & Mohamed, F. A., "Modeling approach to evaluate wind turbine performance: Case study for a single wind turbine of 1.65 MW in Dernah Libya", ***In 2017 8th International Renewable Energy Congress (IREC),*** Jordan, 1-5 (2017).

4. Villalva, M. G., Gazoli, J. R., & Ruppert Filho, E.M, "Comprehensive approach to modeling and simulation of photovoltaic arrays", ***IEEE Transactions on Power Electronics,*** 24(5): 1198-1208 (2009).

5. Almaktar, M., Hussein, T., Rahman, H. A., & Albreki, A. M., "Advantages of Utilizing the Solar Water Heating Technology in Reducing Total Electricity Consumption and Improving Grid Efficiency: A Case Study of Benghazi, Libya", ***In 2020 11th International Renewable Energy Congress (IREC),*** Jordan, 1-5 (2020).

6. Ishaque, K., & Salam, Z., "A review of maximum power point tracking techniques of PV system for uniform insolation and partial shading condition", ***Renewable and Sustainable Energy Reviews,*** 1(9): 475-488 (2013).

7. Wang, J., Mu, X., & Li, Q. K., "Study of passivity-based decoupling control of T-NPC PV grid-connected inverter", ***IEEE Transactions on Industrial Electronics,*** 64(9): 7542-7551 (2017).

8. Yazdani, A., & Dash, P. P., "A control methodology and characterization of dynamics for a photovoltaic (PV) system interfaced with a distribution network", ***IEEE Transactions on Power Delivery,*** 24(3): 1538-1551 (2009).

9. De Oliveira, F. M., da Silva, S. A. O., Durand, F. R., Sampaio, L. P., Bacon, V. D., & Campanhol, L. B., "Grid-tied photovoltaic system based on PSO MPPT technique with active power line conditioning", ***IET Power Electronics,*** 9(6): 1180-1191 (2016).

10. Soni, M. K. & Soni, N., "Review of Causes and Effect if Harmonics on Power System", ***International Journal of Science, Engineering and Technology Research,*** 3(2): 214-220 (2014).

11. Bhagyashri, S. & Patil, V. S. “Power Quality Effects on Non Linear Loads”, ***International Research Journal of Engineering and Technology,*** 4 (6): 3244-3247 (2017).

12. Saha, S., Das, S., & Nandi, C., “Harmonics analysis of power electronics loads”, ***International Journal of Computer Applications,*** 92(10): 231-241 (2014).

13. Duryea, S., Islam, S., & Lawrance, W., “A battery management system for standalone photovoltaic energy systems”, ***In Conference Record of the 1999 IEEE Industry Applications Conference. Thirty-Forth IAS Annual Meeting, 4***(2): 2649-2654 (1999).

14. Almaktar, M., Elbreki, A. M., & Shaaban, M., “Revitalizing operational reliability of the electrical energy system in Libya: Feasibility analysis of solar generation in local communities”, ***Journal of Cleaner Production,*** 279: 123647 (2021). https://doi.org/10.1016/j.jclepro.2020.123647

15. Almaktar, M., Albreki, A. M., Mohamed, F. A., Yahya, K., & Hussein, T., “Performance evaluation of different solar photovoltaic technologies in Libya”, ***In 2020 11th International Renewable Energy Congress (IREC),*** Tunisia, 1-5 (2020).

16. Storage, E., “Draft Guide for Array and Battery 2 Sizing in Stand-Alone Photovoltaic 3 (PV) Systems”, IEEE ***Transactions on Power Delivery,*** 7(5): 431-451 (2018).

17. Almaktar, M. A., “Towards an extensive exploitation of solar PV technology in Libya: Legislative, economic and environmental considerations”, ***Libyan Journal of Science & Technology,*** *7*(2): 103-113 (2018).

18. Kjaer, S. B., Pedersen, J. K., & Blaabjerg, F., “A review of single-phase grid-connected inverters for photovoltaic modules”, ***IEEE Transactions on Industry Applications,*** 41(5): 1292-1306 (2005).

19. Almaktar, M., Abdurahim Aweys, Rahman, H., & Hassan, M. Y., “Economic and Environmental Analysis of a Grid-connected Solar Photovoltaic System in Malaysia”, ***Indian Journal of Advanced in Electrical Engineering,*** 1(1): 11-32 (2013).

20. Muresan, V. A., “Control of grid connected PV systems with grid support functions”, ***Doctoral dissertation, Master’s Thesis, Department of Energy Technology-Pontoppidanstræde, Aalborg University,*** Denmark, 23-34 (2012).

21. Rakotomananandro, F. F., “Study of photovoltaic system”, ***Doctoral Dissertation, The Ohio State University***, 45-57 (2011).

22. Council, C. E., “Tech Info Energy Efficient and Renewable Energy Bulletin”, ***John Wiley & Sons,*** New York, 23-43 (2012).

23. Evju, S. E., “Fundamentals of grid connected photo-voltaic power electronic converter design”, ***Master's Thesis, NTNU University,*** Norway, 23-55 (2007).

24. Afghoul, H., Krim, F., Chikouche, D., & Beddar, A., “Fractional order direct current control algorithm for three-phase grid-connected PV system”, ***In 2015 3rd International Conference on Control, Engineering & Information Technology,*** Algeria, 1-6 (2015).

25. Rahman, M. M., Hossain, S., & Rezwan, S., “Dispatched power and unbalanced operation of a three-phase NPC based double-stage grid connected PV system”, ***In 2019 4th International Conference on Electrical Information and Communication Technology (EICT),*** Bangladesh, 1-6 (2019).

26. Dhia, C., & Lassaad, S., “LVRT control strategy for three-phase grid connected PV systems”, ***In 2017 International Conference on Green Energy Conversion Systems (GECS)***, Tunisia, 1-7 (2017).

27. Yin, W., & Ma, Y., “Research on three-phase PV grid-connected inverter based on LCL filter”, ***In 2013 IEEE 8th Conference on Industrial Electronics and Applications (ICIEA),*** Australia, 1279-1283 (2013).

28. Zhang, H., Zhou, H., Ren, J., Liu, W., Ruan, S., & Gao, Y., “Three-phase grid-connected photovoltaic system with SVPWM current controller”, ***In 2009 IEEE 6th International Power Electronics and Motion Control Conference***, Wuhan, 2161-2164 (2009).

29. Selvaraj, J., & Rahim, N. A., “Multilevel inverter for grid-connected PV system employing digital PI controller”, ***IEEE Transactions on Industrial Electronics,*** 56(1): 149-158 (2008).

30. Tofoli, F. L., Schönell, J. C., Gallo, C. A., & Sanhueza, S. M. R., “A low cost single-phase grid-connected photovoltaic system with reduced complexity”, ***In 2009 Brazilian Power Electronics Conference***, Brazil, 1033-1038 (2009).

31. Wang, Y., & Cao, F., “Implementation of a novel fuzzy controller for grid-connected photovoltaic system”, ***In 2009 Asia-Pacific Power and Energy Engineering Conference***, China, 1-4 (2009).

32. Zhou, X., Song, D., Ma, Y., & Cheng, D., “Grid-connected control and simulation of single-phase two-level photovoltaic power generation system based on Repetitive control”, ***In 2010 International Conference on Measuring Technology and Mechatronics Automation***, 2(3): 366-369 (2010).

33. Samerchur, S., Premrudeepreechacharn, S., Kumsuwun, Y., & Higuchi, K., "Power control of single-phase voltage source inverter for grid-connected photovoltaic systems", ***In 2011 IEEE/PES Power Systems Conference and Exposition,*** USA, 1-6 (2011).

34. Nagaraju, B., "A Fuzzy Logic MPPT Three-Phase Grid-Connected Inverter for Photovoltaic Applications", ***International Journal of Engineering Research and Applications (IJERA),*** *2*(1): 104-107 (2012).

35. Prasanthi, N. L., & Krishnarayalu, M. S., "Photovoltaic solar plant as a statcom during dark periods in a distribution network", ***International Journal of Engineering Research & Technology (IJERT),*** 1(9): 1-7 (2012).

36. Syam, M. S., & Kailas, T. S., "Grid connected PV system using Cuk converte", ***In 2013 Annual International Conference on Emerging Research Areas and 2013 International Conference on Microelectronics, Communications and Renewable Energy***, India, 1-6 (2013).

37. Mariappan, B., Fernandes, B. G., & Ramamoorty, M., "A novel single-stage solar inverter using hybrid active filter with power quality improvement", ***In IECON 2014-40th Annual Conference of the IEEE Industrial Electronics Society***, USA, 5443-5449 (2014).

38. Verma, A. K., & Singh, B., "Harmonics and reactive current detection in a grid interfaced PV distribution system", ***In 2016 IEEE 6th International Conference on Power Systems (ICPS)***, India, 1-6 (2016).

39. Schimpf, F., & Norum, L. E., "Grid connected converters for photovoltaic, state of the art, ideas for improvement of transformer less inverters", ***In Nordic Workshop on Power and Industrial Electronics (NORPIE/2008), University of Technology,*** Finland, 23-34 (2008).

40. Chen, Y. M., Chen, K. Y., Wei, C. L., & Dong, J. Q., "Three-level pwm for grid-connected pv inverter considering switching loss and common-mode voltage", ***In 2018 7th International Symposium on Next Generation Electronics (ISNE),*** Taiwan, 1-4 (2018).

41. Wu, X., & Xu, F., "Control and simulation on three-phase single-stage photovoltaic (PV) system as connecting with power grids", ***In 2014 IEEE Workshop on Electronics, Computer and Applications***, Canada, 190-193 (2014).

42. Babu, P. N., Babu, P. R., Chittibabu, B., & Panda, G., "Three-Phase Grid-tied Photovoltaic System with an Adaptive Current Control Scheme in Active Power Filter", ***In 2019 IEEE 1st International Conference on Energy, Systems and Information Processing (ICESIP)***, India, 1-6 (2019).

43. Jesadia, B. M., Balar, A. B., & Detroja, R. K., "Analysis of solar energy embeded to distribution grid for active & reactive power supply to grid", ***In 2017 International Conference on Inventive Systems and Control (ICISC)***, India, 1-5 (2017).

44. Matiyali, K., Goel, S. K., & Joshi, H., "Voltage Oriented Control of Grid-tied Solar PV System", ***In 2019 Women Institute of Technology Conference on Electrical and Computer Engineering (WITCON ECE)***, India, 28-34 (2019).

45. Güler, N., & Irmak, E., "MPPT based model predictive control of grid connected inverter for PV systems", ***In 2019 8th International Conference on Renewable Energy Research and Applications (ICRERA)***, Romania, 982-986 (2019).

46. Suan, F. T. K., Abd Rahim, N., & Ping, H. W., "Three-phase transformerless grid-connected photovoltaic inverter to reduce leakage currents", ***In 2013 IEEE Conference on Clean Energy and Technology (CEAT),*** Malaysia, 277-280 (2013).

47. Mu, K., Ma, X., Mu, X., & Zhu, D., "A new nonlinear control strategy for three-phase photovoltaic grid-connected inverter", ***In Proceedings of 2011 International Conference on Electronic & Mechanical Engineering and Information Technology***, 9(3): 4611-4614 (2011).

48. Tey, K. S., & Mekhilef, S., "Modified incremental conductance MPPT algorithm to mitigate inaccurate responses under fast-changing solar irradiation level", ***Solar Energy,*** 10(1): 333-342 (2014).

49. Belkaid, A., Colak, I., & Isik, O., "Photovoltaic maximum power point tracking under fast varying of solar radiation", ***Applied Energy,*** 17(9): 523-530 (2016).

50. Kumar, A., Singh, B., Jain, R., & Verma, A., "Multifunctional Grid-Tied PV System Using Modified KLMS Control", ***In 2019 IEEE Energy Conversion Congress and Exposition (ECCE),*** USA, 4774-4780 (2019).

51. Almaktar, M., Abdul Rahman, H., Hassan, M. Y., & Saeh, I., "Artificial neural network-based photovoltaic module temperature estimation for tropical climate of Malaysia and its impact on photovoltaic system energy yield", ***Progress in Photovoltaics: Research and Applications,*** 23(3): 302-318. (2015). DOI: 10.1002/pip.2424

52. Izadian, A., Pourtaherian, A., & Motahari, S., "Basic model and governing equation of solar cells used in power and control applications", ***In 2012 IEEE Energy Conversion Congress and Exposition (ECCE)***, USA, 1483-1488 (2012).

53. Almaktar, M. A., Mahmoud, H. Y., Daoud, E. Y., & Hasan, Z. R., "Meteorological Parameters in Malaysia: An Investigation Between Real Measurements and NASA Database", ***Adv. Electr. Electron. Eng. Sci. J,*** 1(2): 1-6 (2017).

54. Villalva, M. G., Gazoli, J. R., & Ruppert Filho, E., "Comprehensive approach to modeling and simulation of photovoltaic arrays", ***IEEE Transactions on Power Electronics,*** 24(5): 1198-1208 (2009).

55. Mohan, N., Undeland, T. M., & Robbins, W. P., "Power electronics: converters, applications, and design", ***John Wiley & Sons,*** New York, 23-34 (2003).

56. Walker, G. R., & Sernia, P. C., "Cascaded DC-DC converter connection of photovoltaic modules", ***IEEE Transactions on Power Electronics,*** 19(4): 1130-1139 (2004).

57. Mattingly, D., "Designing stable compensation networks for single phase voltage mode buck regulators", ***Intersil Technical Brief,*** USA, 1-10 (2003).

58. Zeb, K., Khan, I., Uddin, W., Khan, M. A., Sathishkumar, P., Busarello, T. D. C. & Kim, H. J., "A review on recent advances and future trends of transformer less inverter structures for single-phase grid-connected photovoltaic systems", ***Energies,*** 11(8): 19-68 (2018).

59. Salcone, M., & Bond, J., "Selecting film bus link capacitors for high performance inverter applications", ***In 2009 IEEE International Electric Machines and Drives Conference,*** USA, 1692-1699 (2009).

60. Coelho, R. F., Concer, F., & Martins, D. C., "A study of the basic DC-DC converters applied in maximum power point tracking", ***In 2009 Brazilian Power Electronics Conference***, Brazil, 673-678 (2009).

61. Patel, H., & Agarwal, V., "Maximum power point tracking scheme for PV systems operating under partially shaded conditions", ***IEEE Transactions On Industrial Electronics,*** *55*(4): 1689-1698 (2008).

62. Saleih, B. E. A., & Teich, M. C., "Fundamentals of Photonics", ***Wiley,*** New York, 123-145 (1991).

63. Almaktar, M., Abdul Rahman, H., & Hassan, M. Y., "Economic analysis using net present value and payback period: case study of a 9kWp grid-connected PV system at UTM, Johor Bahru Campus", ***In Applied Mechanics and Materials,*** 818: 119-123 (2016). doi:10.4028/www.scientific.net/AMM.818.119

64. Putri, R. I., Wibowo, S., & Rifa'i, M., "Maximum power point tracking for photovoltaic using incremental conductance method", ***Energy Procedia,*** 6(8): 22-30 (2015).

65. Milosevic, M., "Decoupling control of d and q current components in three-phase voltage source inverter", ***In Power Systems Conference and Exposition (PSCE),*** USA, 34-44 (2003).

66. Odeh, N., Grassie, T., Henderson, D., & Muneer, T., "Modelling of flow rate in a photovoltaic-driven roof slate-based solar ventilation air preheating system", ***Energy Conversion and Management,*** 47(8): 909-925 (2006).

67. Vickers, N. J., “Animal communication: when I’m calling you, will you answer too”, ***Current Biology,*** 27(14): 713-715 (2017).

68. Arribas, J. R., & Gonzalez, C. V., “Optimal vector control of pumping and ventilation induction motor drives”, ***IEEE Transactions on Industrial Electronics,*** 49(4): 889-895 (2002).

69. Kroutikova, N., Hernandez-Aramburo, C. A., & Green, T. C., “State-space model of grid-connected inverters under current control mode”, ***IET Electric Power Applications***, 1(3): 329-338 (2007).

70. Kim, H., Yu, T., & Choi, S., “Indirect current control algorithm for utility interactive inverters in distributed generation systems”, ***IEEE Transactions on Power Electronics***, 23(3): 1342-1347 (2008).

71. Ko, A., Swe, W., & Zeya, A., “Analysis of harmonic distortion in non-linear loads”, ***International Journal of the Computer, the Internet and Management,*** 19(1): 661-666 (2011).

72. Almaktar, M., Muftah, S., Shuaib, S., & Naily, N., “Economic Study on the Implementation of Feed in Tariff for Photovoltaic Technology in Libya”, ***Libyan International Conference on Electrical Engineering and Technologies (LICEET2018)***, Tripoli, LICEET13732018, 1-5 (2018).

73. Benaissa, O. M., Hadjeri, S., & Zidi, S. A. (2017). Modeling and simulation of grid connected PV generation system using Matlab/Simulink. ***International journal of power electronics and drive systems***, *8*(1), 392.

74. Hamrouni, N., & Chérif, A., “Modelling and control of a grid connected photovoltaic system”, ***Revue des Energies Renouvelables,*** 10(3): 335-344 (2007).

75. Malek, H., “Control of grid-connected photovoltaic systems using fractional order operators”, ***Doctor of Philosophy in Electrical Engineering, Utah State University,*** USA, 12-34 (2014).

RESUME

Mustafa Hashim Muttaleb MUTTALEB finished primary, intermediate, and high school in this city. After finishing school, he joined the College of Engineering, Department of Electrical at Tikrit University in 2012. Then in 2020, he started at Karabuk University Electrical and Electronics Engineering to complete his M. Sc. education.